Full title: Mealtime alters daily rhythm in nuclear O-GlcNAc proteome to regulate hepatic gene expression

Short title: Nuclear O-GlcNAc proteome regulates hepatic transcriptome

Xianhui Liu[1,2,3]†, Yao D Cai[2]†, Chunyan Hou[4], Xu Liu[1], Youcheng Luo[1], Aron Judd P. Mendiola[5], Xuehan Xu[2], Yige Luo[6], Haiyan Zheng[7], Caifeng Zhao[7], Ching-Hsuan Chen[2], Yong Zhang[1], Yang K. Xiang[3], Junfeng Ma[4], and Joanna C. Chiu[2]*

[1]Cambridge-Suda Genomic Resource Center, The Fourth Affiliated Hospital, Suzhou Medical College, Soochow University, Suzhou 215123, Jiangsu, China.

[2]Department of Entomology and Nematology, University of California, Davis, CA 95616, USA.

[3]Department of Pharmacology, University of California, Davis, CA 95616, USA.

[4]Department of Oncology, Lombardi Comprehensive Cancer Center, Georgetown University Medical Center, Washington, DC 20007, USA.

[5]Department of Medical Microbiology and Immunology, University of California, Davis, CA 95616, USA.

[6]Department of Evolution and Ecology, University of California, Davis, CA 95616, USA.

[7]Biological Mass Spectrometry Facility, Robert Wood Johnson Medical School and Rutgers, the State University of New Jersey, Piscataway 08901, USA.

†These authors contributed equally to this work.

*Author for correspondence: Joanna C. Chiu (E-mail: jcchiu@ucdavis.edu)

Keywords: O-GlcNAcylation, phosphorylation, TMT quantitative proteomics, feeding-fasting cycle, metabolism, mouse liver, CLOCK

Abstract

The liver circadian clock and hepatic transcriptome are highly responsive to metabolic signals generated from feeding-fasting rhythm. Previous studies have identified a number of nutrient-sensitive signaling pathways that could interpret metabolic input to regulate rhythmic hepatic biology. Here, we investigated the role of O-GlcNAcylation, a nutrient-sensitive post-translational modification (PTM) in mediating metabolic regulation of rhythmic biology in the liver. We observe daily oscillation of global nuclear protein O-GlcNAcylation in the liver of mice subjected to night-restricted feeding (NRF) using label-free global O-GlcNAc proteomics. Additional site-specific O-GlcNAc analysis by tandem mass tag mass spectrometry further supports temporal differences in O-GlcNAcylation by revealing day-night differences. Proteins involved in gene expression are enriched among rhythmically O-GlcNAcylated proteins, suggesting rhythmic O-GlcNAcylation may directly regulate the daily rhythmicity of the hepatic transcriptome. We show that rhythmic O-GlcNAcylation can also indirectly modulate the hepatic transcriptome by interacting with phosphorylation. Several proteins harboring O-GlcNAcylation-phosphorylation interplay motif exhibit rhythmic O-GlcNAcylation and phosphorylation. Specifically, we show that O-GlcNAcylation occurs at a phospho-degron of a key circadian transcriptional activator, circadian locomotor output cycles kaput (CLOCK), thus regulating its stability and transcriptional output. Finally, we report that day-restricted feeding (DRF) in the nocturnal mouse significantly alters O-GlcNAcylation rhythm. Whereas global O-GlcNAcylation analysis indicates dampening of global O-GlcNAcylation rhythm in mice fed under DRF, site-specific analysis reveals differential responses of O-GlcNAc sites when timing of food intake is altered. Notably, a substantial number of O-GlcNAcylation sites exhibit inverted day-night profiles when mice are subjected to DRF. This suggests the dysregulation of daily nuclear protein O-GlcNAcylation rhythm may contribute to the disruption in liver transcriptomic rhythm previously observed in DRF condition. In summary, our results provide new mechanistic insights into metabolic regulation of daily hepatic transcriptomic rhythm via interplay between O-GlcNAcylation and phosphorylation and shed light on the deleterious effects of improper mealtimes.

Introduction

Circadian clocks are cell-autonomous, endogenous molecular timers that integrate environmental time cues and metabolic signals, enabling organisms to adapt to 24-hour environmental changes by exhibiting time-of-day specific physiology and behavior, such as sleep-wake cycles, feeding-fasting cycles, and metabolism [1,2]. Clock disruption is associated with a wide range of diseases, including cancer, diabetes, and heart disease [3–6]. At the molecular level, mammalian circadian clocks are composed of interlocked transcriptional-translational feedback loops. At the core loop, brain and muscle Arnt-like protein-1 (BMAL1) and circadian locomotor output cycles kaput (CLOCK) form heterodimers and activate the expression of a repertoire of genes [7]. Among these clock-regulated genes are core clock genes that encode PERIOD (PER1, PER2 and PER3) and CRYPTOCHROME (CRY1 and CRY2) proteins, which form repressor complexes to inhibit the activity of BMAL1 and CLOCK [7]. As PER and CRY proteins degrade, transcriptional repression is relieved to initiate the next circadian transcriptional cycle. This cell-autonomous molecular clock was first characterized in the suprachiasmatic nuclei (SCN) of the hypothalamus in mammalian brain; the SCN receive light/dark signals to regulate the pace of molecular clocks [8–10]. Follow-up investigations have established that almost all peripheral tissues harbor molecular clocks, and metabolic signals from daily feeding activity appear to be more potent than light as time cues in peripheral tissues [10–13].

Among all the peripheral organs that are synchronized by feeding-fasting cycles, the liver is one of the most nutrient-sensitive [11,13–15]. Feeding nocturnal mice during daytime can reverse the phase of clock gene expression in liver within a few days [14,15]. Indeed, many studies revealed the importance of metabolic regulation of the molecular clock [16]. Adenosine-monophosphate-activated protein kinase (AMPK), a nutrient sensor, phosphorylates and destabilizes CRY1 [17]. NAD^+ is essential for the activity of Poly [ADP-ribose] polymerase 1 (PARP1), which poly(ADP-ribosyl)ates CLOCK and reduces DNA-binding of CLOCK-BMAL1 complex [18]. Despite 10-20% of the rhythmic hepatic transcriptome is driven by liver intrinsic clocks [12,19], timing of food intake has actually been shown to be the dominant driver for rhythmic liver transcriptome. 70-80% of the oscillating liver transcripts lose their rhythmicity when rhythmic feeding is disrupted in mice by fasting paradigms [20] or arrhythmic feeding [21]. Moreover, in mice with ablated clocks, time-restricted feeding can partially restore rhythmic liver transcriptome [19,20,22]. Despite that several nutrient-sensitive pathways, such as those involving

87 CREB, AKT, mTOR, and ERK1/2, have been identified to modulate food-driven rhythmic
88 transcripts [20,21], our understanding on the molecular mechanisms by which nutrient input
89 regulate genome-wide rhythmic gene expression is far from complete.

90 O-linked-N-acetylglucosaminylation (O-GlcNAcylation) is a nutrient-sensitive post-
91 translational modification (PTM) that modifies thousands of proteins and regulates nearly all
92 aspects of cellular physiology, such as transcription, translation, cell signaling, immune response,
93 and cell cycle [23–26]. O-GlcNAcylation is nutrient-sensitive given the substrate for O-
94 GlcNAcylation, UDP-GlcNAc, is produced from the hexosamine biosynthetic pathway (HBP),
95 which integrates glucose, amino acid, lipid and nucleotide metabolism [23–25]. Indeed, nutrient
96 manipulation in cell media has been shown to alter cellular UDP-GlcNAc level and O-
97 GlcNAcylation in several mammalian cell lines [27,28]. More importantly, Durgan et al. [29] and
98 our previous study [30] showed that O-GlcNAcylation exhibits daily rhythmicity in mouse heart
99 and *Drosophila* tissues respectively, with the peak phase of O-GlcNAcylation rhythm closely
100 aligned with timing of food intake. A large body of work have previously demonstrated the role
101 of O-GlcNAcylation in regulating gene expression [23–25,31]. In the molecular clock, O-
102 GlcNAcylation regulates the stability of transcription factors BMAL1 and CLOCK in a time-of-
103 day manner [32]. Beyond the molecular clock, O-GlcNAcylation regulates gene expression by
104 modifying the function of other gene-specific transcription factors [33–36], general transcriptional
105 machineries [31,37–40], regulators of DNA methylation [41–44], histone modifiers and chromatin
106 remodelers [45–49], and components of RNA spliceosome [50–52]. Therefore, we hypothesize
107 that the hepatic nuclear proteome, especially proteins involved in orchestrating gene expression,
108 could be rhythmically modified and regulated by O-GlcNAcylation.

109 In addition to directly modifying substrate proteins, O-GlcNAcylation also regulates
110 protein functions by interacting with phosphorylation. O-GlcNAcylation and phosphorylation (G-
111 P) can target the same serine/threonine residues on substrate proteins [23,27,53]. For example, in
112 the molecular clock, competition of O-GlcNAcylation and phosphorylation at serine 662 (S662)
113 residue of PER2 modulates transcriptional repressor activity of PER2 [54]. O-GlcNAcylation of
114 histone H3 inhibits its mitosis-specific phosphorylation at S10, S28, and T32 to deter entry into
115 mitosis [47]. 5%-60% phosphoproteins have been shown to exhibit rhythmic phosphorylation over
116 a 24-hour period in liver tissue, and regulates many aspects of liver physiology, including gene
117 expression, metabolism, cell signaling, apoptosis, and autophagy [55–58]. Since there is extensive

118 interplay between O-GlcNAcylation and phosphorylation, it is possible that O-GlcNAcylation
119 indirectly regulates rhythmic liver physiology through modulating daily phosphoproteome.
120 In this study, we showed that hepatic nuclear proteins exhibit daily oscillation of O-
121 GlcNAcylation in liver of mice subjected to night-restricted feeding (NRF). We then performed
122 O-GlcNAc chemoenzymatic labeling in combination with label-free mass spectrometry (MS)
123 proteomics on mouse liver samples collected at 6 time-points over the day-night cycle to identify
124 O-GlcNAcylated nuclear proteins and observed that proteins involved in transcriptional regulation
125 were enriched in rhythmically O-GlcNAcylated proteins. To support our observation of time-of-
126 day differences in protein O-GlcNAcylation status, we also performed site-specific O-GlcNAc
127 analysis by tandem mass tag (TMT) quantitative proteomics at two time points (ZT11 and ZT23)
128 over the day-night cycle and identified 125 O-GlcNAc sites with day-night differences belonging
129 to 101 proteins. We then evaluated potential proteome-wide GlcNAcylation-phosphorylation (G-
130 P) crosstalk by performing TMT site-specific phosphoproteomic analysis using the same liver
131 samples we used for global O-GlcNAc proteomics. Potential rhythmic G-P crosstalk were
132 identified by close proximity of O-GlcNAc and phosphorylation sites as well as prediction by G-
133 P interplay motif analysis. We performed functional analysis on one such G-P interplay motif in
134 circadian locomotor output cycles kaput (CLOCK), a key circadian transcriptional activator, and
135 showed that G-P interplay regulates CLOCK transcriptional activity.
136 Finally, to determine if altering timing of food intake impacts daily O-GlcNAcylation
137 rhythm, we compared O-GlcNAcylation patterns in liver of mice fed under NRF and day-restricted
138 feeding (DRF). We observed dampening of global O-GlcNAcylation rhythm of liver nuclear
139 proteins in mice fed under DRF but site-specific O-GlcNAcylation analysis revealed differential
140 responses of O-GlcNAcylation sites when timing of food intake was altered. Our results suggest
141 that nutrient-sensitive O-GlcNAcylation regulates daily hepatic transcriptome and liver
142 physiology by modifying proteins at the post-translational level.
143
144 **Results**
145 **Hepatic nuclear protein O-GlcNAcylation exhibits robust daily oscillation**
146 We have previously reported that protein O-GlcNAcylation, a highly nutrient-sensitive
147 PTM, exhibits daily rhythmicity in *Drosophila* tissues, and this rhythm is altered when we
148 modified the timing of food intake [30]. Given the mammalian liver is a highly metabolically

149 responsive tissue [11,13–15], we hypothesize that protein O-GlcNAcylation could exhibit daily
150 rhythmicity in the liver and contribute to the regulation of daily rhythms in liver physiology. Liver
151 samples from C57BL/6 male mice were collected every 4 hours over a 24-hour period (12h:12h
152 light-dark (LD)). Since restricting timing of food intake to natural feeding window in *Drosophila*
153 has been shown to enhance daily O-GlcNAcylation rhythm [30], we subjected mice to night -
154 restricted feeding (NRF). To measure O-GlcNAcylation level, the O-GlcNAc moieties on nuclear
155 protein were biotinylated using GalT1-dependent chemoenzymatic labeling and detected using
156 streptavidin-HRP as previously described [30,59]. We only analyzed nuclear fractions, as our
157 primary goal for this study was to investigate nutrient-sensitive PTM mechanisms that regulate the
158 hepatic transcriptome. We observed that a group of nuclear proteins, ranging from 50KD to 250KD,
159 are O-GlcNAcylated (Fig 1A) and global nuclear proteins exhibit rhythmic O-GlcNAcylation over
160 a day-night cycle, as determined by Rhythmic Analysis Incorporating Nonparametric (RAIN) [60].
161 Nuclear protein O-GlcNAcylation peaks at zeitgeber time (ZT) 20 (calculated by RAIN), which is
162 eight hours after the beginning of feeding period (Fig 1A and B). To confirm that the detected
163 signals were indeed O-GlcNAcylated proteins, unlabeled samples were processed in parallel,
164 where GalT1 labeling enzyme is absent. As compared to labeled samples (Lane 3-4), almost no
165 signal was detected in the unlabeled samples (Lane 1-2), indicating the labeled signals are specific
166 for O-GlcNAcylated proteins (Fig S1).
167 It is possible that feeding-fasting cycles contribute to daily rhythmicity in protein O-
168 GlcNAcylation by rhythmically supplying UDP-GlcNAc as substrate via hexosamine biosynthetic
169 pathway (HBP). To investigate this possibility, we performed targeted metabolomics on HBP
170 metabolites from the same mouse livers used in the analysis of O-GlcNAcylation shown in Fig 1A.
171 We were able to detect UDP-GlcNAc, the immediate substrate of O-GlcNAcylation, despite many
172 of the metabolites in HBP were not detected using our current method (S1 File). Similar to what
173 we observed in flies [30], UDP-GlcNAc exhibited daily rhythm in mouse liver, with its peak
174 preceding daily protein O-GlcNAcylation (UDP-GlcNAc: ZT12; O-GlcNAcylation: ZT20, RAIN).
175 Furthermore, the timing of food intake occurred earlier than the rise of UDP-GlcNAc level
176 (feeding: ZT12-24; UDP-GlcNAc: ZT 3-7) (Fig 1C). Although mice were allowed to feed from
177 ZT12 to 24, the majority of feeding events are expected to occur earlier in the dark period [12,21]
178 Our data suggest that feeding-fasting cycles could drive the oscillation of UDP-GlcNAc, which

179 results in the oscillation of protein O-GlcNAcylation. The impact of meal timing on UDP-GlcNAc
180 and O-GlcNAcylation rhythms will be evaluated in later sections of the study.
181
182 **Label-free global and TMT site-specific O-GlcNAc proteomics identify daily changes of**
183 **nuclear protein O-GlcNAcylation**
184 O-GlcNAcylation modifies thousands of proteins involved in many fundamental cellular
185 processes [23–25,31]. As O-GlcNAcylation is shown to be rhythmic in liver nuclei, we
186 hypothesize that O-GlcNAcylation regulates rhythmic liver function by modifying nuclear
187 proteins in a time-of-day manner. To test our hypothesis, we performed daily label-free MS O-
188 GlcNAc proteomics using liver samples from C57BL/6 male mice that were collected every 4
189 hours over a 24-hour period (12h:12h LD). Biotinylated O-GlcNAc nuclear proteins were enriched
190 by affinity purification and then quantified using mass-spectrometry (Fig S2). To filter out non-
191 specific proteins, unlabeled samples were processed as described above and affinity purified (Fig
192 S2). To identify O-GlcNAcylated proteins, labeled and unlabeled samples were compared by
193 Student's t test with p value cutoff of 0.05. To identify proteins with rhythmic O-GlcNAcylation
194 with normalization to their protein expression, we performed TMT proteomic analysis to obtain
195 the expression level of each protein (see next section) (S2, S3 Files and Fig S2). We identified 449
196 O-GlcNAcylated proteins in total. Multivariate PLS-DA analysis showed that O-GlcNAc
197 proteome exhibits time-of-day variability (Fig 2A), which is further confirmed by pairwise
198 multivariate analysis distinguishing each time point from the rest of the dataset (Fig 2B).
199 Rhythmicity analysis was performed using JTK and RAIN with different q-value cutoffs ($q<0.1$,
200 0.2, 0.3 or 0.4) (Fig 2C). O-GlcNAcylated proteins with RAIN $q<0.2$ were used for further analysis.
201 Most of the protein O-GlcNAcylation were found to occur during the dark phase when mice are
202 active (Fig 2D and E). This is consistent with the overall O-GlcNAcylation profile measured by
203 streptavidin-HRP on Western blot (Fig 1A and B).
204 To identify the molecular pathways or processes that are rhythmically O-GlcNAcylated,
205 we performed functional enrichment analysis on the proteins that we found to be rhythmically
206 modified. We found that proteins related to gene expression were enriched (Fig S3). To further
207 dissect out the function of the rhythmically O-GlcNAcylated proteins, we classified these proteins
208 into protein complexes using the CORUM database [61] (S4 File). We highlighted the protein
209 complexes that regulate gene expression, such as transcriptional regulation, histone modification,

210 chromatin remodeling, and RNA processing, and plotted their daily O-GlcNAcylation levels (Fig
211 S4). We also included several proteins that do not belong to specific protein complex in CORUM
212 but were found to exhibit rhythmic O-GlcNAcylation. Consistent with previous studies [32],
213 CLOCK is rhythmically O-GlcNAcylated with the peak time at the end of the feeding time window
214 (Fig S4). It is important to note that in addition to gene-specific transcription factor complexes
215 (Bmal1-CLOCK-CRY1/2), general machineries that regulate gene expression are also
216 rhythmically O-GlcNAcylated. These include general transcription factors (mediator and Brd4-
217 TEFb complex), histone deacetylases (SP130), histone methyltransferases/demethylases (KDM6A,
218 SETD1A and SETD2), chromatin remodelers (Zipzap/p200-Srf-p49/STRAP-Nkx2.5 and NoRC
219 complex) and RNA processing enzymes (FUS and RBM33) (Fig S4). These data suggest rhythmic
220 O-GlcNAcylation may modulate hepatic gene expression at multiple layers.

221 To gain further insights into the temporal functions of O-GlcNAcylation, we next
222 performed quantitative site-specific analysis of protein O-GlcNAcylation. Based on our results
223 thus far, we collected mouse liver at ZT11 and ZT23, two time-points that showed global
224 differences in O-GlcNAcylation levels and are 12 hours apart, and quantified site-specific O-
225 GlcNAcylation using TMT-MS. In total, we identified 505 high-confidence O-GlcNAc sites on
226 346 proteins, with 338 sites (119 proteins) that were quantifiable (S5 File). Over 40% of O-
227 GlcNAcylated proteins (146 proteins) identified by TMT-MS were also identified by label-free
228 global O-GlcNAc proteomic analysis (Fig 2F). Multivariate PLS-DA analysis showed that O-
229 GlcNAcylation sites quantified by TMT-MS exhibits day-night differences (Fig 2G). 125 O-
230 GlcNAc sites on 101 proteins showed day-night O-GlcNAcylation differences (>20%-fold
231 changes) (Fig 2H). Consistent with O-GlcNAcylation determined by Western blot (Fig 1A-B) and
232 label-free global analysis (Fig 2D-E), over 60% of the 152 O-GlcNAc peptides quantified by TMT-
233 MS display higher O-GlcNAcylation at nighttime (Fig 2H and I). Notably, we also found sites that
234 exhibit higher O-GlcNAcylation at daytime. We reasoned these sites potentially belong to less
235 abundant nuclear proteins that are not well represented in Western blot (Fig 1A-B), highlighting
236 the importance of site-specific analysis.

237 We next performed functional enrichment analysis on the proteins harboring O-
238 GlcNAcylation sites with day-night differences in site-specific analysis (Fig S5). Consistent with
239 enrichment analysis of rhythmic O-GlcNAcylation identified in label-free global analysis (Fig S3),
240 we found proteins involved in transcriptional regulation (Fig 2I). These include general

241 transcriptional regulator (CCNT1, MED1, LIN54), proteins belonging to major chromatin
242 remodeler subfamilies (GATAD2A, GATAD2B, BICRAL, NFRKB), and RNA processing
243 enzymes involved in mRNA splicing and transport (THRAP3, SON, THOC2). Taken together, O-
244 GlcNAcylation likely mediates the metabolic regulation of daily hepatic transcriptome via other
245 mechanisms in addition to direct modulation of the molecular clock.
246
247 **TMT-MS profiles daily rhythm of nuclear phosphoproteome**
248 Since both O-GlcNAcylation and phosphorylation modify serine/threonine residues on
249 substrate proteins, many studies have been devoted to investigate G-P crosstalk
250 [23,27,47,53,54,65,66]. Within a 24-hour period, phosphoproteome has been shown to oscillate in
251 diverse tissue types, especially in mouse liver [55–57]. Therefore, we hypothesize that O-
252 GlcNAcylation contributes to rhythmic liver physiology via daily G-P crosstalk. To test this
253 hypothesis, we performed TMT-MS to analyze daily nuclear phosphoproteome using the same
254 tissues we used for label-free global O-GlcNAc proteomics analysis described above (Fig S2). We
255 identified 19593 phosphopeptides, belonging to 3272 phosphoproteins (S6 files). To identify
256 proteins with rhythmic phosphorylation independent of their protein expression, we performed a
257 separate TMT proteomic analysis for normalization (S3 and S6 Files). Multivariate PLS-DA
258 analysis showed that phosphoproteome exhibits time-of-day variability (Fig 3A), which is further
259 confirmed by pairwise multivariate analysis distinguishing each time point from the rest of the
260 dataset (Fig 3B). Rhythmicity analysis was performed using JTK and RAIN with different q-value
261 cutoffs ($q<0.1$, 0.2, 0.3 or 0.4) (Fig 3C). Phosphoproteins with RAIN $q<0.2$ were used for further
262 analysis. Compared with published circadian phosphoproteomics datasets [56, 57], we identified
263 1820 additional rhythmic phosphosites (Fig S6D, S7 File, S1 Table). Interestingly, we observed
264 that most of the phosphorylation events happen during the dark phase, coinciding with the timing
265 of O-GlcNAcylation (Fig 3D and E).
266 To find out the kinases that can potentially rhythmically phosphorylate the hepatic nuclear
267 proteome, PTMphinder [64] was used to enrich phospho-motifs of phosphopeptides peaking
268 during dark phase (Fig 3E), and kinases were predicted using group-based phosphorylation site
269 predicting and scoring (GPS) 5.0 [65]. To increase the confidence of our kinase prediction, we
270 also selected out the kinases that are either rhythmically expressed, rhythmically O-GlcNAcylated,
271 or rhythmically phosphorylated from our datasets (S8 File). We then classified these kinases by

272 their phases calculated by RAIN. The circadian kinases were identified by selecting the common
273 ones in the phase-matched rhythmic kinases in our proteomic datasets and the GPS 5.0-predicted
274 kinase list. We were able to find several circadian kinases that were identified in previous circadian
275 phosphoproteomic studies [56,57], such as CK1, AKT, and CDK. We also identified several
276 circadian kinases that although have not been found in previous circadian phosphoproteomics
277 analysis, were shown to regulate circadian rhythm via targeted analysis, such as S6K [66].
278 Functional enrichment analysis showed that rhythmic phosphoproteome are enriched in
279 proteins involved in transcriptional regulation, RNA processing, and chromatin organization (Fig
280 S6). We then performed protein complex analysis to further identify the molecular pathways that
281 are rhythmically phosphorylated (S9 File). Fig 3F illustrates protein complexes that are involved
282 in transcriptional regulation and were found to contain multiple subunits that are rhythmically
283 phosphorylated in our dataset. Consistent with previous findings, we identified a core clock protein
284 complex, PER2-SFPQ-SIN3A complexes (Fig 3F). Additionally, we identified several general
285 transcriptional complexes (Hdac1-Ino80-Kdm1a-Phb2-Rbp1-Taf5 and PU.1-associated
286 complexes), chromatin remodeling complexes (Ikaros and SWI/SNF complexes), and RNA
287 processing complexes (Cbll1-Virma-Wtap-Zc3h13 complexes) as rhythmically phosphorylated
288 (Fig 3F). Among phosphorylation sites we identified in this analysis, some of them have previously
289 been characterized with functions in gene expression regulation and beyond (S2 Table). For other
290 sites with unknown functions, we identified the phosphorylation events locating in or adjacent to
291 functional domains based on PhosphoSitePlus database [67] and these novel sites could have
292 potential functions regulating liver physiology (S3 Table). Taken together, our data suggest that
293 the daily rhythm of the phosphoproteome could regulate the rhythmic hepatic transcriptome.
294
295 **Crosstalk between O-GlcNAcylation and phosphorylation (G-P) regulates hepatic protein**
296 **function**
297 O-GlcNAcylation can occur at the same residues or adjacent residues targeted by
298 phosphorylation to regulate phosphorylation events [23,27,47,53,54,65,66]. Since both O-
299 GlcNAcylation and phosphorylation were found to oscillate over a day-night cycle, we sought to
300 identify rhythmic phosphorylation events that can be potentially regulated by daily O-
301 GlcNAcylation rhythm of substrate proteins. By comparing results of our label-free global O-
302 GlcNAc and TMT site-specific phosphoproteomic analysis, we found 14 proteins exhibiting both

303 rhythmic O-GlcNAcylation and phosphorylation (Fig 4A). Spearman correlation analysis between
304 overall O-GlcNAcylation of the proteins and each phosphorylation peptides of the same proteins
305 showed that most of the O-GlcNAcylation and phosphorylation on proteins are positively
306 correlated (Fig 4A), suggesting the two PTMs potentially facilitate each other. However, some O-
307 GlcNAcylation and phosphorylation sites on these proteins are negatively correlated, suggesting
308 these two PTMs can also inhibit each other in these cases (Fig 4A). Similarly, phase analysis
309 showed that most of the O-GlcNAcylation and phosphorylation occur within the same time
310 window over the 24-hour day-night cycle (Fig 4B). Analysis on individual phosphopeptide showed
311 that some phosphorylation happens in phase with O-GlcNAcylation (i.e. positive correlations),
312 such as pCLOCK(T461) (Fig 4C) and pARID1B(S1625/S1627) (Fig 4D), while other
313 phosphorylation events are out of phase with O-GlcNAcylation (i.e. negative correlations), as
314 exemplified by pPRR12(S911) (Fig 4F) and pLMNA(S573) (Fig 4G). pAHDC1(S1540), and
315 pAHDC1(S842) demonstrate the situation that depending on the specific sites on even a single
316 substrate protein, O-GlcNAcylation and phosphorylation can be in phase (Fig 4E) or out of phase
317 (Fig 4H). Additionally, protein complex analysis identified 3 protein complexes out of these 14
318 proteins with both rhythmic O-GlcNAcylation and phosphorylation, including transcription factor
319 complexes (e.g. Arntl-Clock-Cry1/2 complex) and chromatin remodeling complexs (e.g. 1-Fog1-
320 MeCP1 complex).

321 In addition to the 14 proteins with both oscillating O-GlcNAcylation and phosphorylation,
322 we expect that O-GlcNAc sites on more proteins could locate in G-P interplay motifs, given that
323 the overall O-GlcNAcylation status of proteins detected in our label-free global O-GlcNAcylation
324 analysis may underestimate potential rhythmicity of individual O-GlcNAc sites. To encourage
325 future studies on more daily G-P crosstalk, we took a subset of rhythmic phosphorylated proteins
326 that are also O-GlcNAcylated in our label-free global O-GlcNAc proteomic dataset, and searched
327 whether these rhythmic phosphosites belong to any G-P interplay motifs (S10 File). We found 167
328 phosphosites within G-P motifs on 134 proteins (S10 File). These 134 proteins include components
329 in general transcription machinery (MED7, PCF11, and TCEA3, etc.), gene-specific transcription
330 factors (NFIL3, SOX6 DBP, RBL2, etc.), histone modification (KAT5, KMT2D, and GATAD2A),
331 chromatin remodeling (SMARCC2), RNA processing (SRSF5, CWC25 and FIP1), and nucleo-
332 cytoplasmic transportation (POM121 and NUP98/153/214).

333 Finally, to further predict potential G-P crosstalk, we compared results of TMT site-
334 specific O-GlcNAc proteomics with phosphoproteomics. We found 109 pairs of O-GlcNAc sites
335 and phosphosites in close proximity (within 10 amino acids), indicating potential G-P crosstalks
336 (S10 File). Among them, 82 showed day-night differences of either O-GlcNAcylation or
337 phosphorylation. We found a number of potential G-P crosstalk regions harboring sites with day-
338 night differences in both O-GlcNAcylation and phosphorylation, such as in KRT8, NDC1, and
339 NUP35 (Fig 4I-L). Of these, phosphorylation levels at NDC1(S434) and NUP35(T258) exhibit
340 negative correlation with O-GlcNAcylation level at adjacent sites (Fig 4K-L). In conclusion, our
341 data suggest that G-P crosstalk has the potential to contribute to regulation of rhythmic protein
342 function in mouse liver.
343
344 **Daily G-P crosstalk on CLOCK**
345 To gain a deeper understanding of the potential crosstalk between O-GlcNAcylation and
346 phosphorylation over a 24-hr period, we asked whether proteins with rhythmic phosphorylation
347 and O-GlcNAcylation identified in our studies harbor previously identified G-P interplay motifs
348 [62,63]. We found 11 phosphorylation sites that harbor three different G-P interplay motifs (Fig
349 5A), where O-GlcNAcylation and phosphorylation either compete for the same modification site
350 or have inhibitory effects when in close proximity. Among these 11 phosphorylation sites, the
351 function of CLOCK(S431) has been characterized.
352 CLOCK(S431) is the priming phosphorylation site for glycogen synthase kinase-3 (GSK3)
353 [68]. Once CLOCK(S431) is phosphorylated, GSK3 phosphorylates S427, which promotes the
354 degradation of CLOCK. Given global O-GlcNAcylation of CLOCK has been shown to increase
355 its stability [32], we hypothesize that O-GlcNAcylation stabilizes CLOCK in a time-of-day manner
356 by competing with S431 phosphorylation to inhibit S427 phosphorylation (Fig 5B). To assess
357 whether CLOCK(S431) is a O-GlcNAc site, we performed O-GlcNAc chemoenzymatic labeling
358 followed by Western blotting in mouse HEK293T cells expressing either CLOCK(WT) or
359 CLOCK(S431A). A small fragment CLOCK aa260-460) was used in this experiment to better
360 observe O-GlcNAcylation within this region. We observed that CLOCK(S431A) variant exhibits
361 decreased O-GlcNAcylation as compared to CLOCK(WT), suggesting that CLOCK(S431) is
362 indeed O-GlcNAcylated (Fig 5C and D). To validate the daily CLOCK O-GlcNAcylation rhythm
363 detected in our label-free global O-GlcNAc proteomics analysis, we applied targeted

364 chemoenzymatic labeling following immunoprecipitation of CLOCK. Consistent with the results
365 from global O-GlcNAc analysis, CLOCK O-GlcNAcylation exhibits robust daily rhythmicity (Fig
366 5E and F, S7A). CLOCK was detected in immunocomplexes of α-CLOCK bound beads, but not
367 empty beads, demonstrating the specificity CLOCK immunoprecipitation (Fig S8A).

368 Although we detected S431 phosphorylation on multiple peptides in our dataset, the S431
369 phosphorylation always co-occurs with nearby phosphorylation events, making it difficult to
370 quantify the actual level of S431 phosphorylation. We instead used S427 phosphorylation as the
371 functional readout for the competition between O-GlcNAcylation and phosphorylation at S431.
372 When we overlaid CLOCK O-GlcNAcylation rhythm in mouse liver from targeted analysis with
373 the daily phosphorylation level at S427, we observed out of phase relationship (O-GlcNAcylation:
374 ZT20; pS427: ZT8, RAIN). Between ZT7 and ZT11, when CLOCK O-GlcNAcylation level is low,
375 S427 phosphorylation level remains high. The opposite is observed during the night period (ZT19)
376 (Fig 5F). These observations support that CLOCK O-GlcNAcylation and S427 phosphorylation
377 do not co-occur and CLOCK O-GlcNAcylation inhibits S427 phosphorylation.

378 Since CLOCK(S427/S431) belongs to a phospho-degron [68], we assayed CLOCK protein
379 level in mouse liver over a 24-hr cycle using Western blots (Fig 5E and G). The daily CLOCK
380 protein levels detected in our proteomic dataset and Western blots has similar trends with minor
381 difference at ZT4 (Fig S7B). We then compared levels of daily S427 phosphorylation and CLOCK
382 protein (Fig 5G). As S427 phospho-occupancy rises and maintains a relatively high level between
383 ZT3 and ZT11, CLOCK protein level decreases (Fig 5G). Between ZT15 and ZT23, CLOCK
384 phosphorylation level rises again, while CLOCK protein level stays low. All these observations
385 support the conclusion that daily rhythms of S427 phosphorylation contributes to the oscillation
386 of CLOCK protein abundance.

387 We then sought to investigate whether O-GlcNAcylation at S431 affects CLOCK
388 transcriptional activity since it has been established in the literature that CLOCK transcriptional
389 activity is tightly linked to its stability [68–71]. Specifically, less stable CLOCK has higher
390 transcriptional activity. This may seem counterintuitive but it has been established that qualitative
391 changes in highly unstable CLOCK promote its transcriptional activity (also seen in many other
392 transcription factors, reviewed in [72,73]). We assayed CLOCK transcriptional activity in
393 HEK293T cells using a *per2-luciferase* (*per2-luc*) reporter assay [74]. We compared *per2-luc*
394 expression in cells transfected with CLOCK(WT), S427A, S431A, or the double non-

395 phosphorylatable mutant S427/431A in the presence or absence of OGT (Fig 5H). To compensate
396 for the fact the CLOCK mutants affect CLOCK protein level, we adjusted the amount of CLOCK
397 plasmids for transfection to obtain an equal amount of CLOCK expression in each group of cells
398 (Fig S8B). As expected, we observed CLOCK(WT) increases *per2-luc* signal and this signal is
399 significantly reduced when CLOCK(WT) is coexpressed with OGT. This is consistent with
400 previous findings that CLOCK O-GlcNAcylation increases its stability [32]. We then tested the
401 single non-phosphorylatable mutants (S427A and S431A) and double mutant (S427/431A) and
402 observed that they all exhibited lower transcriptional activity when compared to CLOCK(WT),
403 and coexpression of OGT did not impact *per-luc* activity (Fig 5H). Taken together, these data
404 demonstrate the crosstalk between O-GlcNAcylation and phosphorylation at S431 modulates
405 CLOCK transcriptional activity through regulating S427 phosphorylation.
406
407 **Food intake at day time in mice disrupts protein O-GlcNAcylation rhythm**
408 We previously showed that O-GlcNAcylation is regulated by both feeding-fasting cycles
409 and the molecular clock in flies [30]. We hypothesize that timing of food intake could affect daily
410 O-GlcNAcylation rhythm in mouse liver. To test this hypothesis, we subjected mice to day-
411 restricted feeding (DRF) and compared their nuclear protein O-GlcNAcylation pattern with mice
412 subjected to NRF (Fig 6A). Mice treated with DRF lost their daily O-GlcNAcylation rhythm, and
413 the global O-GlcNAcylation level of hepatic nuclear proteins remained at a relatively high level
414 through the day-night cycle (Fig 6B and C). We recognize analysis of global O-GlcNAc level may
415 be more representative of the status of abundant nuclear proteins. To evaluate potential differential
416 responses of individual O-GlcNAcylation sites to changes in feeding time, we performed site-
417 specific O-GlcNAc TMT proteomic analysis of liver nuclear proteins extracted from mice
418 subjected to DRF (Fig 6D and E) in parallel to samples from NRF mice presented earlier (Fig 2F-
419 I). Consistent with global nuclear protein O-GlcNAcylation detected by Western blot (Fig 6B-C),
420 DRF leads to reduced number of sites with day-night differences in O-GlcNAcylation (from 128
421 down to 100 sites, or 101 to 74 proteins) (Fig 6D). Notably, O-GlcNAcylation levels in the
422 majority of detected peptides are inverted under DRF (Fig 6E), while a small fraction of peptides
423 showed unaltered day-night O-GlcNAcylation patterns or reduced day-night differences.
424 Functional enrichment analysis on the O-GlcNAc peptides with inverted day-night profiles in NRF
425 vs. DRF liver resulted in proteins involved in transcriptional regulation, chromatin remodeling,

426 and RNA processing (Fig 6F). These data suggest the dysregulation of nuclear protein O-
427 GlcNAcylation may contribute to the disruption in liver transcriptomic rhythm previously
428 observed in DRF condition.

429 To investigate whether the altered O-GlcNAcylation pattern in DRF mice (Fig 6A-F)
430 results from altered daily UDP-GlcNAc rhythm, we used targeted metabolomics to detect UDP-
431 GlcNAc levels in livers of mice subjected to either NRF or DRF. Our results showed that DRF
432 liver exhibited dampened daily UDP-GlcNAc rhythmicity and the level of UDP-GlcNAc remained
433 at a higher level overall when compared to that in NRF liver (Fig 6G). This suggests altered UDP-
434 GlcNAc level likely contributed to altered O-GlcNAcylation in DRF mice liver (Fig 6G), although
435 other yet established mechanisms are also involved given the various patterns of disruptions in O-
436 GlcNAcylation rhythms in mice subjected to DRF. To rule out the possibility that the altered UDP-
437 GlcNAc levels in DRF mouse liver is primarily due to increased food intake, we measured daily
438 total food consumption of NRF and DRF mice (Fig 6H). We did not observe a significant increase
439 in food consumption in the DRF group. DRF group instead fed slightly less than NRF group,
440 indicating that food consumption is not the major cause of increased UDP-GlcNAc level. In
441 conclusion, timing of food intake affects O-GlcNAcylation rhythm in mouse liver partially by
442 influencing the level of UDP-GlcNAc.

443

444 **Discussion**

445 We investigated the contribution of nutrient-sensitive O-GlcNAcylation as a post-
446 translational mechanism to regulate rhythmic hepatic gene expression. Despite a substantial body
447 of work showing that the rhythmic hepatic transcriptome is highly responsive to the timing of food
448 intake [11,14,15,19–22], our understanding of the mechanisms by which rhythmic feeding-fasting
449 activity regulates genome-wide gene expression is far from complete. Here, we showed that
450 nuclear proteins in mouse liver exhibit rhythmic O-GlcNAcylation over a 24-hour day-night cycle
451 when mice were fed at night (Fig 1). This is supported by both global and site-specific O-
452 GlcNAcylation analysis. Proteins involved in transcriptional regulation, histone modification,
453 chromatin remodeling and RNA processing are enriched among proteins with temporal changes
454 of O-GlcNAcylation (Fig 2, Fig S3, S5). Combining results from targeted metabolomics (Fig 1C,
455 6G), phosphoproteomics (Fig 3), biochemistry (Fig 1A-B, 5C-H, 6A-C) and G-P interplay analysis
456 (Fig 4, 5A-B), we formulated a model illustrating the role of O-GlcNAcylation in mediating the

457 effect of metabolic input on the daily hepatic transcriptomic rhythm (Fig 7). We propose that
458 environmental signaling via the molecular clock and the timing of metabolic input from food
459 intake converge to regulate daily rhythm in the O-GlcNAc proteome. O-GlcNAcylation targeting
460 the same site or proximal site has the potential to affect phosphorylation, as exemplified by
461 CLOCK. Therefore, O-GlcNAcylation can shape daily transcriptomic rhythm by either directly
462 modulating proteins involved in regulation of gene expression or in an indirect manner by
463 interacting with phosphorylation of these proteins.

464 To better understand the function of O-GlcNAcylation on hepatic gene expression, we
465 identified O-GlcNAcylated proteins using both label-free global analysis and TMT site-specific
466 analysis (Fig 2). There was substantial overlap between the O-GlcNAcylated proteins identified
467 using the two methods, and these proteins were enriched for transcriptional regulators. Previous
468 studies showed that O-GlcNAcylation modulates functional outcomes of several transcription
469 factors detected in our rhythmic O-GlcNAc proteome, including EWS, MEF2D, and GATA4 [75–
470 78]. O-GlcNAcylation increases the transcriptional activity and stability of GATA4 [77,78], while
471 O-GlcNAcylation of MEF2D reduces insulin secretion in pancreatic β-cells [76]. Therefore, it is
472 possible that the time-of-day specific functions of these proteins driven by rhythmic O-
473 GlcNAcylation contribute to daily transcriptomic rhythm. We anticipate that technologies in
474 quantitative O-GlcNAc proteomics will continue to advance and further reveal the prevalent nature
475 of O-GlcNAcylation in transcriptional regulators, similar to that of phosphorylation [79–81].
476 Future functional characterization studies are warranted to characterize the function of O-GlcNAc
477 sites with temporal differences identified in current study to understand how they regulate daily
478 rhythms in hepatic gene expression.

479 Since there exists crosstalk between O-GlcNAcylation and phosphorylation at the same or
480 adjacent site on its protein substrate, we investigated the possibility that rhythmic O-
481 GlcNAcylation can interact with the phosphoproteome to regulate the hepatic transcriptome (Fig
482 4-5). Given that many of the 14 proteins with rhythmic O-GlcNAcylation and phosphorylation are
483 known to play important roles in various cellular processes, such as transcriptional regulation
484 (AHDC1 and TIF1A), histone modification (KANSL1 and SETD1A), RNA processing (CDK13),
485 and chromatin modification (ARID1B, BRD8 and P66B), it is important to understand how daily
486 G-P crosstalk could modulate the activities of these proteins to regulate daily hepatic physiology.
487 Additionally, a broader motif search on O-GlcNAcylated proteins with rhythmic phosphorylation

488 predicted that 167 rhythmic phosphosites could potentially be regulated by G-P interplay motifs
489 (S10 File). Fast evolving MS-based quantitative O-GlcNAc profiling [82–86] will continue to
490 provide more insights into G-P interplay. Indeed, in addition to G-P interplay at CLOCK phospho-
491 degron (Fig 5), our TMT site-specific O-GlcNAc proteomic revealed O-GlcNAcylation at
492 CLOCK(S450), proximal to S441 and S446 phosphorylation sites. How individual O-
493 GlcNAcylation sites collectively regulate CLOCK remains to be investigated. Recently, CLOCK
494 has been shown to be phosphorylated in response to osmotic stress [87] and is modified by another
495 nutrient-sensitive PTM, S-palmitoylation [88]. How O-GlcNAcylation interact with other PTMs
496 in response to complex inputs to regulate daily physiology also remains an open question.

497 Our results showed that O-GlcNAcylation is rhythmic in mouse liver with a peak phase
498 that aligns with the window of food intake (Fig 1). Given the nutrient-sensitive nature of O-
499 GlcNAcylation, it is perhaps not surprising to observe similar phenomenon in mouse heart [29]
500 and fly body [30]. Therefore, O-GlcNAcylation may represent a conserved mechanism by which
501 nutrient input regulates daily protein functions under natural feeding conditions. We observed that
502 DRF dampens the global O-GlcNAcylation rhythm of hepatic nuclear proteins, instead of shifting
503 the phase of O-GlcNAcylation to align with the altered feeding period (Fig 6). However, it is clear
504 from site-specific analysis of O-GlcNAcylated proteins extracted from DRF vs NRF mice that the
505 situation is more complex and different O-GlcNAcylation sites respond differently when timing
506 of food intake is altered. Whereas some O-GlcNAcylation sites similarly show reduced day-night
507 differences, similar to what we observed in the global O-GlcNAcylation analysis, some O-
508 GlcNAcylation sites exhibited inverted day-night patterns between DRF and NRF. O-
509 GlcNAcylation of these proteins may therefore contribute to the DRF-induced phase shift of many
510 transcripts observed in previous studies [11,14,15,89–91]. Future site-specific and functional
511 investigations will be essential to reveal how O-GlcNAcylation of these proteins regulate their
512 target genes in response to food intake.

513 It is important to note that there are other mechanisms involved in regulating the rhythms
514 of daily hepatic transcriptome in addition to O-GlcNAcylation of nuclear proteins. These
515 additional mechanisms could include O-GlcNAcylation of proteins in other subcellular
516 compartments. O-GlcNAcylation of cytoplasmic proteins are also likely to oscillate. O-
517 GlcNAcylation of cytoplasmic proteins can regulate biological processes such as translation and
518 immune response [23,26], nuclear shuttling of proteins [92–94], and relay signals into nucleus via

519 signaling pathways [20,21,95,96]. How compartmentalization of UDP-GlcNAc [78] regulates
520 daily O-GlcNAcylation of nuclear and cytoplasmic proteins remains unknown. Despite our
521 understanding of O-GlcNAcylation regulation of nutrient-sensitive signaling pathways, such as
522 those involving mTOR [97], AMPK [98,99], and insulin[100], whether and how O-
523 GnglcNAcylation interacts with these nutrient-sensitive signaling pathways and other nutrient-
524 sensitive PTMs in a time-of-day manner remains to be investigated. Moreover, we observed that
525 DRF can alter daily rhythms of bile acids and S-adenosylmethionine (SAM) and likely
526 downstream signaling pathways (Fig S9). Bile acid can regulate gene expression through a nuclear
527 receptor, farnesoid X receptor (FXR) [16,101], whereas SAM is the substrate for methylation of
528 DNA, RNA and proteins [102–105]. Therefore, a comprehensive understanding of hepatic
529 transcriptome in response to feeding time will require an integration of nuclear and cytoplasmic
530 protein O-GlcNAcylation, and other nutrient-sensitive mechanisms.

531 In summary, we showed that O-GlcNAcylation exhibits daily oscillation in hepatic nuclear
532 proteins in mice and subjected mice to DRF disrupts daily O-GlcNAcylation rhythm. Using
533 proteomic approaches, we identified nuclear proteins exhibiting rhythmic O-GlcNAcylation and
534 phosphorylation and evaluated G-P crosstalk at the proteomic level over a day-night cycle. Finally,
535 our findings on CLOCK, a protein in the core molecular clock loop, highlight the daily crosstalk
536 between O-GlcNAcylation and phosphorylation and its functional outcomes. Our results provide
537 new insights into metabolic regulation of daily biological rhythms at the PTM level and shed light
538 on the deleterious effects of improper mealtimes.

539

540 **Materials and Methods**

541 **Animal treatments and collection of liver samples**

542 All experiments including animal feeding, treatment, and tissue collection were carried out
543 in accordance with the guidelines of Institutional Animal Care and Use Committees (IACUC) of
544 the University of California, Davis. C57BL/6 male mice were ordered from JAX laboratory at the
545 age of 6 weeks. Mice were first entrained for 2 weeks *ad libitum* in 12h light:12h dark cycle. Mice
546 were then randomized into two time-restricted feeding (TRF) groups: night-restricted feeding
547 (NRF) between ZT12-24 (ZT, zeitgeber time; ZT0 indicates light on, while ZT12 indicates light
548 off) and day-restricted feeding (DRF) between ZT0-12. Normal chow food was provided in the
549 above time-restricted feeding treatments and food intake was measured by comparing the food

550 weight before and after each feeding window. The mice were TRF-treated for three weeks. Three
551 weeks is enough time for DRF group to adapt to the new feeding window and fed comparable
552 amount as NRF group [106]. It also allows the entrainment of the hepatic clock to be complete
553 [14,15] and the rhythmic transcriptome would be altered [11]. After TRF treatment, mice were
554 sacrificed every 4 hours over a 24-hour period and liver samples were collected. Samples were
555 then flash frozen in liquid nitrogen, ground into powders and stored at -80 °C until sample
556 processing.
557
558 **Extraction of mouse liver nuclei proteins**
559 Mouse liver nuclei were extracted according to Nagata et al. [107] with the following
560 modifications. Liver samples were dounced in Buffer A (250mM sucrose, 10mM Tris HCl pH7.5,
561 5mM $MgCl_2$,100µM PUGNAc, and Roche EDTA-free protease inhibitor cocktail) with a loose
562 pestle. The suspension was passed through a cell strainer (70µm pore size, Fisher Scientific,
563 Hampton, NH) by centrifuging at 300g for 1 min at 4°C. The crude nuclei were pelleted by
564 centrifugation at 600g for 15 mins at 4°C. To further purify the crude nuclei, the pellets were
565 resuspended in 9 volumes of ice-cold Buffer B (2M sucrose, 1mM $MgCl_2$, and 10mM Tris HCl
566 pH7.5) and were then centrifuged at 16000g for 15 mins. The supernatant was discarded and the
567 pure nuclear pellets were resuspended in boiling buffer (100mM Tris pH8.0, 2% SDS, 100µM
568 PUGNAc, and Roche EDTA-free protease inhibitor cocktail) [59]. Nuclear proteins were extracted
569 by heating at 95°C for 5 min. After centrifuging at 16000g for 5 mins to separate the soluble and
570 non-soluble nuclear fractions, the nuclear protein lysate was transferred to a new tube.
571
572 **Expression and purification of bovine β-1,4-galactosyltransferase 1 (GalT1 Y289L)**
573 GalT1 (Y289L), the chemoenzymatic labeling enzyme for detecting O-GlcNAcylated
574 proteins, was expressed and purified according to Thompson et al. [59] The bovine GalT1 was
575 obtained from Genomics-online (Cat#: ABIN3462403) and GalT1 tyrosine 289 is mutated into
576 leucine to increase its activity for the chemoenzymatic labeling reaction [108,109]. GalT1(Y289L)
577 was subcloned into pET22-6xHis vector and transformed into BL21(DE3) competent cells for
578 expression of the GalT1(Y289L) protein. The harvested cells were lysed in PBS containing 1mM
579 EDTA by sonication. After centrifuging at 14000g for 30 min, the pellet was collected given
580 GalT1(Y289L) is insoluble in PBS. The pellet was suspended in wash buffer (1xPBS, 25% sucrose,

581 1mM EDTA, and 0.1% Triton X-100) and spun down; this was repeated 5 times. The pellet was
582 then resuspended in PBS containing 1mM EDTA and this was repeated twice to remove detergent.
583 After the last centrifuge step, the pellet was resuspended in denaturing buffer (5M guanidine
584 hydrochloride, 0.3M sodium sulfite) and treated with S-sulfonating agent, 2-Nitro-5-
585 thiosulfobenzoate (NTSB). Ice-cold water was added to precipitate the GalT1(Y289L) protein and
586 the mixture was centrifuged at 10,000g for 10 min. This step was repeated 3 times to remove
587 residual NTSB. The final pellet was resuspended in 5M guanidine hydrochloride and diluted 10
588 times in refolding buffer (0.5M L-arginine, 50mM Tris pH8.0, 5mM EDTA, 4mM cysteamine,
589 and 2mM cystaminea). The resulting GalT1(Y289L) solution was dialyzed in dialysis buffer
590 (50mM Tris pH8.0, 5mM EDTA, 4mM cysteamine, and 2mM cystamine) and concentrated to
591 2mg/ml.
592
593 **Chemoenzymatic labeling of O-GlcNAcylated proteins**
594 Chemoenzymatic labeling of O-GlcNAcylated nuclear proteins was performed according
595 to Thompson et al. [59] with the following modifications. The nuclear protein lysate was quantified
596 and 100μg protein was used for labeling. Protein lysate was treated with 25mM DTT at 95°C for
597 5 mins and 50mM iodoacetamide at room temperature for 1 hour in the dark. Proteins were
598 precipitated using chloroform-methanol method and dissolved in 40μl 1% SDS with 20mM
599 HEPES pH7.9 by heating up at 95°C for 5 mins. The O-GlcNAc group was first labeled with azide
600 in the labeling buffer (20mM HEPES pH7.9, 50mM NaCl, 2% IGEPAL-CA630, 25μM PUGNAc,
601 25mM NaF, 0.5mM PMSF, 5.5 mM $MnCl_2$, 25μM UDP-GalNAz, 50μg/ml GalT1(Y289L), and
602 Roche EDTA-free protease inhibitor cocktail). To remove the labeling reagents, proteins were
603 precipitated using chloroform-methanol method and dissolved in 37.5μl 1% SDS with 20mM
604 HEPES pH7.9. Biotin was attached to the azide group in the biotinylation buffer (1xPBS, 100μM
605 biotin alkyne, 2mM sodium ascorbate, 100μM Tris (benzyltriazolylmethyl) amine, and 1mM
606 $CuSO_4$). To prepare for Western blot after O-GlcNAc labeling, samples were precipitated and
607 dissolved in 50μl 1% SDS with 20mM HEPES pH7.9. O-GlcNAc proteins were detected using α-
608 streptavidin-HRP (Cell Signaling Technologies, Danvers, MA) (1:10000). For background
609 deduction, unlabeled samples were processed in parallel with GalT1(Y289L) excluded in the
610 labeling buffer.
611

612 **Targeted gas chromatography coupled to time-of-flight (GC-TOF) mass spectrometry (MS)**
613 **analysis and HILIC-TripleTOF MS/MS analysis**
614 10mg liver samples were analyzed using GC-TOF MS and HILIC-TripleTOF MS/MS
615 approaches as previously described [30,110]. Samples were extracted with
616 acetonitrile/isopropanol/water 3:3:2 (v/v/v). For GC-TOF MS analysis, 0.5µl samples were
617 injected into an Agilent 6890 gas chromatograph (Agilent, Santa Clara, CA) and analyzed using a
618 Leco Pegasus IV time of flight mass (TOF) spectrometer. Result files were processed using the
619 metabolomics BinBase database. For HILIC-TripleTOF MS/MS, 5µl samples were injected onto
620 a Waters Acquity UPLC BEH Amide column (Waters, Milford, MA) and analyzed using a 1x
621 6600 TripleTOF high resolution mass spectrometer (SCIEX, Framingham, MA). Mass spectra
622 were analyzed and interpreted using MS-DIAL v3.90 [111]. Peak heights from both analyses were
623 reported as quantification. Standard compounds from the hexosamine biosynthesis pathway (HBP)
624 were diluted into multiple concentrations and analyzed in parallel to generate standard curves. The
625 concentration of each detectable HBP metabolites in liver samples was then calculated based on
626 the peak height and standard curves.
627
628 **Sample preparation for label-free global O-GlcNAc proteomics**
629 Nuclear proteins were chemoenzymatically labeled as described above with 1mg protein
630 per samples. After the final precipitation, samples were dissolved in 400µl 1% SDS with 50mM
631 Tris pH7.5. 600µl supplementary buffer (50mM Tris pH7.5, 375mM NaCl, and 2.5% IGEPAL-
632 CA630) was added to dilute protein into immunoprecipitation (IP) buffer (50mM Tris pH7.5,
633 150mM NaCl, 0.4% SDS, and 1% IGEPAL-CA630). The protein sample is quantified using Qubit
634 before IP. O-GlcNAc proteins were immunoprecipitated using Dynabeads™ MyOne™
635 Streptavidin T1 (Fisher Scientific) and the IP reactions were incubated at room temperature for 2
636 hours. The beads were washed with wash buffer (50 mM Tris pH7.5, 400 mM NaCl, 1% IGEPAL-
637 CA630, and 0.4% SDS) for 5 times and 50mM NH_4HCO_3 for 8 times. After removing all the
638 solutions through magnetic separation, beads were stored at -80°C prior to mass spectrometry
639 analysis. To identify non-specific binding, unlabeled samples were processed in parallel with
640 GalT1(Y289L) excluded in the labeling buffer.
641
642 **Label-free MS to identify O-GlcNAc proteins**

643 The bead-bound proteins were digested on beads according to Mohammed et al. [112].
644 Briefly, samples were digested using 10µl (10ng/µl) of trypsin in 100 mM NH_4HCO_3 overnight at
645 37 °C. Another 10µl (10ng/µl) of trypsin in 100 mM NH_4HCO_3 was added the next day to further
646 digest for 4 hours. The digested peptides were extracted twice with 5% formic acid and 60%
647 acetonitrile.

648 Samples were analyzed by liquid chromatography–mass spectrometry (LC–MS) according
649 to Sharma et al. [113]. The Nano-LC-MSMS was performed using a Dionex rapid-separation
650 liquid chromatography system interfaced with an Eclipse (Fisher Scientific). Samples were loaded
651 onto a fused silica trap column (Acclaim PepMap 100, 75 µm × 2 cm, Fisher Scientific) and
652 washed for 5 min at 5 µl/min with 0.1% TFA. An analytical column (Nanoease MZ peptide BEH
653 C18, 130A, 1.7 µm, 75 µm× 250 mm, Waters, Milfored, MA) for LC-MS/MS was brought in-line
654 with the trap column. A segmented linear gradient was used to fractionate peptides at 300nl/min:
655 4–15% solution B in 30 min (solution A: 0.2% formic acid, and solution B: 0.16% formic acid,
656 80% acetonitrile), 15–25% solution B in 40 min, 25–50% solution B in 44 min, and 50-90%
657 solution B in 11 min. Before the next run started, solution B should return to 4% for 5 min. Data-
658 dependent acquisition procedure was applied to acquire the spectrometry data. A cyclic series of a
659 full scan were performed with a resolution of 120,000. The 20 most intense ions were analyzed by
660 MS/MS (higher-energy collisional dissociation (HCD), relative collision energy 27%) with a
661 dynamic exclusion duration of 20s.

662 LC-MS/MS data were analyzed with Thermo Proteome Discoverer 2.4 (Fisher Scientific)
663 into MASCOT Generic Format (MGF). The resulting peak list was searched against Uniprot
664 mouse database and a database consisted of common lab contaminants (CRAP) using in house
665 version of X!Tandem (GPM Fury [114]). During searching, fragment mass error was set at 20 ppm
666 and parent mass error was set at ±7 ppm. Carbamidomethylation on cysteine was set as fixed
667 modification. In primary search, methionine monooxidation was set as variable modifications,
668 while in refinement search, asparagine deamination, tryptophan oxidation and dioxidation,
669 methionine dioxidation, and glutamine to pyro-glutamine were included. Protease was set as
670 trypsin C-terminal of R/K unless followed by P with 1 miscut allowed during the preliminary
671 search and 5 miscuts allowed during refinement. For minimum acceptable peptide and protein
672 expectation scores, 10−2 and 10−4 were respectively applied. The overall peptide false-positive
673 rate was set to 0.07% [115].

674

675 **Tandem mass tag (TMT) site-specific O-GlcNAc proteomics**

676 Sample preparation for quantitative O-GlcNAc proteomics was performed according to a
677 procedure described previously [86], with some modifications. In brief, proteins (1.25 mg for each
678 condition) extracted from liver nuclear lysates were reduced with DTT and alkylated with IAA,
679 followed by chloroform-methanol precipitation. Proteins were then dissolved in 400 µl 1% SDS
680 with 20 mM HEPES pH7.9 by heating up at 95°C for 5 mins. Chemoenzymatic labeling was
681 initiated by adding 490 µl of H_2O, 800 µl of labeling buffer (50 mM HEPES pH7.9, 125mM NaCl,
682 5% NP-40), 105 µl of 100 mM $MnCl_2$, 100 µl of 0.5 mM UDP-GalNAz, 5 µg GalT1(Y289L), 0.5
683 µl of PNGase F, and 1 µl of FastAP Thermosensitive Alkaline Phosphatase (Fisher Scientific), and
684 incubating at 4°C overnight. Proteins were chloroform-methanol precipitated and dissolved in 1
685 mL of 0.5% SDS with 20mM HEPES pH 7.9 for click chemistry by adding 11 µl of 10 mM PC
686 Biotin Alkyne (Vector Laboratories, Newark, CA), 33 µl of 10 mM $CuSO_4$-BTTAA (1:2,
687 measured as $CuSO_4$, Vector Laboratories), and 5 µL of 50 mM sodium ascorbate, and incubating
688 at room temperature for 2 h. After precipitation, proteins were resuspended and digested by 50 µg
689 of trypsin in 1.6 M urea with 50 mM HEPES pH 7.9. Peptides were desalted and resuspended in
690 1.25 mL of 100 mM triethylammonium bicarbonate (TEAB) buffer pH 8.5 for TMTpro16 labeling
691 (Fisher Scientific), with two kits used by following the manufacturer's protocol. Labeled samples
692 were pooled at 1:1 ratio and incubated with 1.2 mL of high-capacity NeutrAvidin™ agarose slurry
693 (Fisher Scientific) for 3 h. The conjugated peptides were released in 0.1% formic acid (FA) by
694 irradiation at 365 nm for 1 h. Subsequently, the released peptides were fractionated by High pH
695 Reversed-Phase Peptide Fractionation Kit (Fisher Scientific) following the manufacturer's
696 protocol. Ten fractions were collected, dried down, and dissolved in 0.1% FA for nanoUPLC-
697 MS/MS analysis.

698 The nanoUPLC-MS/MS analysis was performed on a nanoAcquity UPLC system (Waters,
699 Milford, MA) coupled with an Orbitrap Fusion Lumos mass spectrometer (Fisher Scientific),
700 similar as described previously [86,116]. In brief, samples were loaded onto a C18 Trap column
701 (Waters Acquity UPLC M-Class Trap, Symmetry C18, 100 Å, 5 µm, 180 µm x 20 mm) at 10
702 µL/min for 4 min. Separation was carried out on an analytical column (Waters Acquity UPLC M-
703 Class, Peptide BEH C18, 300 Å, 1.7 µm, 75 µm × 150 mm) at a column temperature of 45 °C and
704 a flow rate of 400 nL/min. A 300-minute gradient was used with buffer A (2% ACN, 0.1% formic

705 acid) and buffer B (0.1% formic acid in ACN) as follows: 1% buffer B at 0 min, 5% buffer B at 1
706 min, 30% buffer B at 210 min, 45% buffer B at 260 min, 90% buffer B at 270 min, 90% buffer B
707 at 290 min, 1% buffer B at 290.1 min, and 1% buffer B at 300 min. The MS data were acquired in
708 data dependent acquisition (DDA) mode by Orbitrap Fusion Lumos mass spectrometer with an ion
709 spray voltage of 2.4 kV and an ion transfer temperature of 275 °C. The mass spectra were recorded
710 with Xcalibur 4.7. The MS parameters were set as below: Detector Type: Orbitrap; Orbitrap
711 Resolution: 120,000; Scan Range: 350-1800 m/z; RF Lens: 30%; AGC Target: Standard;
712 Maximum Injection Time Mode: Auto; Microscans: 1. Charge state: 2-8; Cycle Time: 3 s. HCD
713 product-dependent EThcD (HCD-pd-EThcD) with a dynamic exclusion duration of 40 s was
714 applied for MS/MS acquisition. EThcD was triggered by the oxonium ions of HexNAc (m/z
715 126.055, 138.055, 144.066, 168.065, 186.076, and 204.086), as well as the major fragments
716 resulting from the PC-biotin alkyne (m/z 300.130 and 503.210) observed in HCD scans. MS/MS
717 parameters were set as below: Isolation Mode: Quadrupole; Isolation Window: 0.7 m/z; HCD
718 collision energy: 30%. Detector Type: Orbitrap; Resolution: 50,000; AGC Target: Standard.
719 Supplemental activation (SA) collision energy of EThcD was set as 30%.

720 Raw data were analyzed with Proteome Discoverer 2.4 (Fisher Scientific) with the Sequest
721 search engine against Uniprot mouse database (TaxID: 10090, downloaded on February 2, 2023;
722 17137 sequences). The MS mass tolerance was set at ± 10 ppm, MS/MS mass tolerance were set
723 at ± 0.02 Da. TMTpro on K and N-terminus of peptides and carbamiodomethyl on cysteine was
724 set as static modification. Mass addition of 502.202 Da (AMTzHexNAc2) on Ser/Thr/Tyr/Asn
725 were set as dynamic modification, as well as asparagine deamidation, methionine oxidation,
726 protein N-terminal acetylation, N-terminal methionine loss or N-terminal methionine loss plus
727 acetylation. Protease was set as trypsin digest with 2 mis-cleavages allowed. Percolator was used
728 for results validation. Concatenated reverse database was used for target-Decoy strategy. High
729 confidence for protein and peptides were defined as FDR < 0.01, medium confidence was defined
730 as FDR <0.05.

731 For reporter ion quantification, HCD was selected as the activation type. S/N was used for
732 reporter quantification peaks if all spectrum files have S/N values. Otherwise, intensities were used.
733 Quantification value was corrected for isotopic impurity of reporter ions. Protein abundance of
734 each channel was calculated using summed S/N of all unique+razor peptides with AMTzHexNAc2

735 on Ser/Thr/Tyr. Co-isolation threshold was set at 50%. Average reporter S/N threshold was set at
736 10. SPS mass matches percentage threshold was set at 65%.
737
738 **Tandem mass tag (TMT) site-specific phosphoproteomics**
739 For parallel phosphoproteomic analysis using the same mouse livers used for label-free
740 global O-GlcNAc proteomics analysis, mouse liver nuclei were extracted as described above. The
741 nuclear pellets were resuspended in 2x laemmili buffer with 50 mM DTT. Nuclei were sonicated,
742 followed by incubating at 95 °C for 10 min. After centrifugation at 25000g for10 min at 4 °C, the
743 soluble fraction was saved in a new tube, while the insoluble fraction was further extracted using
744 8 M Urea. The insoluble fraction was centrifuged again, and the supernatant was combined with
745 the soluble fraction. Protein concentration was determined by Pierce™ 660nm Protein Assay Kit
746 (Fisher Scientific). 300µg of lysate were run into SDS-PAGE for TMT-MS analysis. We chose to
747 use TMT labeling method to increase the comparability of samples [117]. However, as the
748 currently available TMT labeling method can maximumly label 18 samples (TMTpro-18plex) in
749 one run, we were only able to process 3 biological replicates of mouse livers [117].
750 The gel slices were incubated with 10 mM DTT at 60°C for 30 min, and then with 20 mM
751 iodoacetamide at room temperature for 1 hour in dark. The samples were digested by trypsin at
752 1:50 (w: w, trypsin: sample) and incubated at 37°C overnight. The digested peptides were extracted
753 and dried under vacuum and washed with 50% acetonitrile to pH neutral. The digested peptides
754 were labeled with Thermo TMT18plex (Lot# for TMTpro16: XA341491; Lot# for last two
755 channels: XA338617) followed by the manufacture's protocol. Labeled samples were pooled at
756 1:1 ratio for a small volume and analyzed with LC-MS/MS to get normalization factor. The
757 labeling efficiency is 97.9%. Based on the normalization factor, the samples were pooled together
758 and desalted with SepPack tC18 columns (Varian, WAT054960).
759 The desalted samples were fractionated by high-pH RPLC chromatography using Agilent
760 1100 series. The samples were solubilized in 200 µl of 20 mM ammonium (pH10), and injected
761 onto an Xbridge column (Waters, C18 3.5 µm 2.1X150 mm) using a linear gradient of 1%B/min
762 from 2-45% of B (buffer A: 20 mM ammonium, pH10, B: 20 mM ammonium in 90% acetonitrile,
763 pH10). UV 214 was monitored. 1 min fractions were collected. 5% of fractions 29 to 46 was saved
764 for proteome analysis and the rest of all fractions were dried until there is around 50µl left for each

765 fraction. Then the fractions were combined and dry completely under speed vacuum for
766 phosphopeptide enrichment.

767 IMAC enrichment of phosphopeptides was adapted from Mertins et al. [118] with
768 modifications. Ion-chelated IMAC beads were prepared from Ni-NTA Superflow agarose beads
769 (Qiagen, MA). Nickel ion was stripped with 50mM EDTA and iron was chelated by passing the
770 beads through aqueous solution of 200mM $FeCl_3$ followed by three times of water wash and one
771 time wash with binding buffer (40% acetonitrile, 1% formic acid). The combined basic RP
772 fractions were solubilized in binding buffer and incubated with IMAC beads for 1 hour. After three
773 times of wash with binding buffer, phosphopeptides were eluted with 2x beads volume of 500mM
774 potassium hydrogen phosphate, pH7.0 and the eluate was neutralized with 10% formic acid. The
775 enriched phosphopeptides were further desalted by Empore 3M C18 (2215) StageTip[2] prior to
776 nanoLC-MS/MS analysis.

777 Nano-LC-MSMS was performed using a Dionex rapid-separation liquid chromatography
778 system interfaced with an Eclipse (Fisher Scientific). The enriched phosphopeptides and selected
779 desalted fractions 29-46 were loaded onto an Acclaim PepMap 100 trap column (75µm x 2cm,
780 Fisher Scientific) and washed with Buffer A (0.1% trifluoroacetic acid) for 5 min with a flow rate
781 of 5µl/min. The trap was brought in-line with the nano analytical column (nanoEase, MZ peptide
782 BEH C18, 130A, 1.7um, 75umx20cm, Waters) with flow rate of 300nL/min with a multistep
783 gradient (4% to 15% buffer B [0.16% formic acid and 80% acetonitrile] in 20 min, then 15%–25%
784 B in 40 min, followed by 25%–50% B in 30 min). The scan sequence began with an MS1 spectrum
785 (Orbitrap analysis, resolution 120000, scan range from 350–1600 Th, automatic gain control (AGC)
786 target 1E6, maximum injection time 100 ms). The top S (3 sec) duty cycle scheme were used for
787 determining number of MSMS performed for each cycle.

788 For proteomic samples, SPS method was used. Peptide ions were first collected for MS/MS
789 by collision-induced dissociation (CID) and analyzed in quadrupole ion trap analysis (automatic
790 gain control (AGC) 2E4, normalized collision energy (NCE) 35, maximum injection time 120 ms,
791 and isolation window at 0.7). Following acquisition of each MS2 spectrum, 10 MS2 fragment ions
792 were captured in the MS3 precursor population using isolation waveforms with multiple frequency
793 notches. MS3 precursors were fragmented by HCD and analyzed using the Orbitrap (NCE 55,
794 AGC 1.5E5, maximum injection time 150 ms, resolution was 50,000 at 400 Th).

795 For phosphopeptide, MS/MS method was used. Parent masses were isolated in the
796 quadrupole with an isolation window of 0.7m/z, AGC 1E5, and fragmented with HCD with a
797 normalized collision energy of 34%. The fragments were scanned in Orbitrap with resolution of
798 50000. The MS/MS scan ranges were determined by the charge state of the parent ion but lower
799 limit was set at 110 amu.

800 LC-MS/MS data were analyzed with Proteome Discoverer 2.4 (Fisher Scientific) with
801 sequent search engine against Uniprot mouse database and a database consisted of common lab
802 contaminants. For proteome data, The MS mass tolerance was set at ±10ppm, MS/MS mass
803 tolerance were set at ±0.4Da. TMTpro on K and N-terminus of peptides and carbamiodomethyl on
804 cysteine was set as static modification. Methionine oxidation, protein N-terminal acetylation, N-
805 terminal methionine loss or N-terminal methionine loss plus acetylation were set as dynamic
806 modifications. Protease was set as trypsin digest with 2 miscuts allowed. For phosphopeptide
807 enriched sample runs, The MS mass tolerance was set at ±10ppm, the MS/MS mass tolerance were
808 set at ±0.02Da. TMTpro on K and N-terminus of peptides and carbamiodomethyl on cysteine was
809 set as static modification. Serine, threonine, and tyrosine phosphorylation, methionine oxidation,
810 protein N-terminal acetylation, N-terminal methionine loss or N-terminal methionine loss plus
811 acetylation were set as dynamic modifications. Protease was set as trypsin digest with 2 miscuts
812 allowed. Percolator was used for results validation. Concatenated reverse database was used for
813 target-Decoy strategy. High confidence for protein and peptides were defined as FDR<0.01,
814 medium confidence was defined as FDR <0.05.

815 For reporter ion quantification, reporter abundance was set to use signal/noise ratio (S/N)
816 if all spectrum files have S/N values. Otherwise, intensities were used. Quan value was corrected
817 for isotopic impurity of reporter ions. Co-isolation threshold was set at 75%. Average reporter S/N
818 threshold was set at 10. SPS mass matches percentage threshold was set at 65%. Protein abundance
819 of each channel was calculated using summed S/N of all unique+razor peptide. For proteome data,
820 the abundance was further normalized to summed abundance value for each channel over all
821 peptides identified within a file. The same normalization factors were also used to normalize
822 phosphopeptide abundance. Following the analytic method of TMT phosphoproteomics dataset in
823 Li et al. [119], each phosphopeptide was further normalized to corresponding master protein
824 abundance value if the protein group also reported abundance value in proteome data. If the protein

825 abundance value was missing, then the original abundance was used. Whether a specific
826 phosphopetide is normalized or not is indicated in S6 File under the "Normalized" column.
827
828 **CLOCK O-GlcNAcylation detection**
829 Around 300-400mg liver tissue was used for CLOCK O-GlcNAcylation detection. The
830 protocol was adapted from Yoshitane et al. [120] and Cao et al.[121] with the following
831 modifications. Crude nuclei were extracted as described above with modified Buffer A (10mM
832 HEPES pH7.9, 10mM KCl, 0.1mM EDTA, 1mM DTT, 1mM PMSF, 50mM NaF, 100μM
833 PUGNAc, and Roche EDTA-free protease inhibitor cocktail). Nuclear proteins were extracted
834 using nuclear extraction buffer (NEB) (20mM HEPES pH7.9, 10% Glycerol, 400mM NaCl, 1%
835 Triton X-100, 0.1% sodium deoxycholate, 1mM EDTA, 5mM $MgCl_2$, 1mM DTT, 0.5mM PMSF,
836 10mM NaF, Roche PhoSTOP, 100μM PUGNAc, and Roche EDTA-free protease inhibitor
837 cocktail) by rotating at 4°C for 30 mins. The soluble and non-soluble nuclear fractions were
838 separated by centrifuging at 16000g for 15 mins. Prior to immunoprecipitation, samples were
839 diluted using buffer D (20mM HEPES, pH7.9, 10% Glycerol, 1mM EDTA, 1mM DTT, 0.5mM
840 PMSF, 10mM NaF, Roche PhosSTOP, 100μM PUGNAc, and Roche EDTA-free protease
841 inhibitor cocktail) at 3:5 (V_{NEB}: V_D). Immunoprecipitation was performed using 4μl α-CLOCK
842 (Cat# ab3517, Abcam, Boston, MA) in combination with 20 μl gammabind Sepharose beads (GE
843 HealthCare, Chicago, IL). 5μl of beads was collected for detection of CLOCK protein, and
844 Western blot was performed with α-CLOCK (1:3000).
845 For O-GlcNAcylation detection, the rest of the beads was washed twice with wash buffer
846 (20mM HEPES, pH7.9, 10% Glycerol, 150mM NaCl, 1mM EDTA, 1mM DTT, 2mM $MgCl_2$,
847 0.5mM PMSF, 10mM NaF, 100μM PUGNAc, and Roche EDTA-free protease inhibitor cocktail)
848 and twice with reaction buffer (20mM HEPES pH7.9, 50mM NaCl, 25mM NaF, 0.5mM PMSF,
849 5mM $MnCl_2$, 1μM PUGNAc, and Roche EDTA-free protease inhibitor cocktail). After washing,
850 16μl of reaction buffer, 2μl of GalT1(Y289L) and 2μl of 0.5mM UDP-GalNAz were added and
851 the mixture incubated at 4°C overnight. On the second day, the beads were washed twice with the
852 reaction buffer to remove excess UDP-GalNAz, and 37.5μl 1% SDS with 20mM HEPES pH7.9
853 was added to the resin. Finally, biotinylation was performed using a biotinylation buffer (1xPBS,
854 100μM biotin alkyne, 2mM sodium ascorbate, 100μM Tris (benzyltriazolylmethyl) amine, and
855 1mM $CuSO_4$). To prepare for Western blot, samples were precipitated using the chloroform-

856 methanol method and dissolved in 50µl 1% SDS with 20mM HEPES pH7.9. O-GlcNAcylated
857 proteins were detected using α-streptavidin-HRP (Cell Signaling Technologies) (1:5000). For
858 detecting the O-GlcNAcylation of CLOCK(aa260-460) overexpressed in HEK293T cells, similar
859 method was used except that cells were extracted using RIPA buffer supplemented with Roche
860 PhoSTOP and 100µM PUGNAc,
861
862 **Luciferase reporter assay to test CLOCK transcriptional activity**
863 For luciferase assay, HEK293T cells were transfected with 100ng *per2-luc*, 100ng *Renilla-*
864 *luc*, 50ng pcDNA3.1-*Bmal1*-Flag, 50ng pcDNA3.1-Myc-*Ogt* or 50ng pcDNA3.1-Myc, 400ng
865 pcDNA3.1-*Clock*(WT)-Flag or 1000ng pcDNA3.1-*Clock*(X)-Flag, where X is either S427A,
866 S431A or S427A/S431A. pcDNA3.1-*Clock*(WT)-Flag was a kind gift from Dr. Erquan Zhang and
867 *Clock* mutants were generated by mutagenesis. Measurements were performed 24 hours after
868 transfection and Dual luciferase reporter assay kit (Vazyme, Nanjing, China) was used according
869 to manufacturer's instructions.
870
871 **Bioinformatic and statistical analysis**
872 For label-free MS O-GlcNAc proteomics, peptide count was first normalized to the input
873 protein amount for IP with streptavidin beads. Similar to the TMT phosphoproteomics analysis,
874 the O-GlcNAcylated protein peptide counts were further normalized to their protein level obtained
875 from the TMT-MS analysis performed in parallel using the same samples, if the protein was
876 detected [119]. If the protein expression level was not sufficiently resolved, the original peptide
877 count was maintained [119]. Whether a specific O-GlcNAc protein is normalized or not is
878 indicated in S2 File under the "Normalized" column. To identify O-GlcNAcylated proteins,
879 labeled samples and unlabeled samples were compared using Student's t test with p value cutoff
880 of 0.05, and the unlabeled samples were used for background deduction (n = 3).
881 PLS-DA and MANOVA analysis were performed using mixOmics [122]. Rhythmicity,
882 phase and period length of O-GlcNAc proteins and phosphopeptides were determined using
883 Rhythmic Analysis Incorporating Nonparametric (RAIN) [60] and MetaCycle [123]. For kinase
884 analysis, the kinase motifs on phosphopeptides were enriched using PTMphinder [64] and the
885 enriched motifs were then fed into group-based phosphorylation site predicting and scoring (GPS)
886 5.0 to predict the kinases [65]. We utilized the CORUM database [61] to identify protein

887 complexes with rhythmic O-GlcNAcylation and/or phosphorylation on complex subunit(s).
888 Spearman correlation was used to determine the correlation between rhythmic O-GlcNAc
889 proteome versus rhythmic phosphoproteome on the same protein. RAIN, PTMphinder, protein
890 complex analysis, Spearman correlation analysis were performed in R v4.2.2. The O-
891 GlcNAcylation levels of CLOCK(aa260-460), and the median levels of O-GlcNAcylation and
892 UDP-GlcNAc in DRF and NRF groups were compared using Student's t test in GraphPad Prism
893 10.0 (GraphPad Software, La Jolla California USA), while the feeding amount between DRF and
894 NRF was compared using Mann-Whitney test. For comparing the protein levels and transcriptional
895 activity of CLOCK(S427/S431) mutants, one-way ANOVA with post-hoc Dunnett's test were
896 performed in Prism 10.0.
897

898 **Reference**

899 1. Bass JT. The circadian clock system's influence in health and disease. Genome Med. 2017;9: 94.
900 doi:10.1186/s13073-017-0485-2

901 2. Patke A, Young MW, Axelrod S. Molecular mechanisms and physiological importance of circadian
902 rhythms. Nat Rev Mol Cell Biol. 2020;21: 67–84. doi:10.1038/s41580-019-0179-2

903 3. Davis S, Mirick DK, Stevens RG. Night shift work, light at night, and risk of breast cancer. J Natl
904 Cancer Inst. 2001;93: 1557–1562. doi:10.1093/jnci/93.20.1557

905 4. Fujino Y, Iso H, Tamakoshi A, Inaba Y, Koizumi A, Kubo T, et al. A prospective cohort study of shift
906 work and risk of ischemic heart disease in Japanese male workers. Am J Epidemiol. 2006;164:
907 128–135. doi:10.1093/aje/kwj185

908 5. Gao Y, Gan T, Jiang L, Yu L, Tang D, Wang Y, et al. Association between shift work and risk of type
909 2 diabetes mellitus: a systematic review and dose-response meta-analysis of observational studies.
910 Chronobiol Int. 2020;37: 29–46. doi:10.1080/07420528.2019.1683570

911 6. Roenneberg T, Merrow M. The Circadian Clock and Human Health. Curr Biol. 2016;26: R432-443.
912 doi:10.1016/j.cub.2016.04.011

913 7. Takahashi JS. Transcriptional architecture of the mammalian circadian clock. Nat Rev Genet. 2017;18:
914 164–179. doi:10.1038/nrg.2016.150

915 8. Moore RY, Eichler VB. Loss of a circadian adrenal corticosterone rhythm following suprachiasmatic
916 lesions in the rat. Brain Res. 1972;42: 201–206. doi:10.1016/0006-8993(72)90054-6

917 9. Stephan FK, Zucker I. Circadian rhythms in drinking behavior and locomotor activity of rats are
918 eliminated by hypothalamic lesions. Proc Natl Acad Sci U S A. 1972;69: 1583–1586.
919 doi:10.1073/pnas.69.6.1583

920 10. Schibler U, Gotic I, Saini C, Gos P, Curie T, Emmenegger Y, et al. Clock-Talk: Interactions
921 between Central and Peripheral Circadian Oscillators in Mammals. Cold Spring Harb Symp Quant
922 Biol. 2015;80: 223–232. doi:10.1101/sqb.2015.80.027490

923 11. Xin H, Deng F, Zhou M, Huang R, Ma X, Tian H, et al. A multi-tissue multi-omics analysis reveals
924 distinct kineztics in entrainment of diurnal transcriptomes by inverted feeding. iScience. 2021;24:
925 102335. doi:10.1016/j.isci.2021.102335

926 12. Koronowski KB, Kinouchi K, Welz P-S, Smith JG, Zinna VM, Shi J, et al. Defining the
927 Independence of the Liver Circadian Clock. Cell. 2019;177: 1448-1462.e14.
928 doi:10.1016/j.cell.2019.04.025

929 13. Reinke H, Asher G. Crosstalk between metabolism and circadian clocks. Nat Rev Mol Cell Biol.
930 2019;20: 227–241. doi:10.1038/s41580-018-0096-9

931 14. Stokkan KA, Yamazaki S, Tei H, Sakaki Y, Menaker M. Entrainment of the circadian clock in the
932 liver by feeding. Science. 2001;291: 490–493. doi:10.1126/science.291.5503.490

933 15. Damiola F, Le Minh N, Preitner N, Kornmann B, Fleury-Olela F, Schibler U. Restricted feeding
934 uncouples circadian oscillators in peripheral tissues from the central pacemaker in the
935 suprachiasmatic nucleus. Genes Dev. 2000;14: 2950–2961. doi:10.1101/gad.183500

936 16. Panda S. Circadian physiology of metabolism. Science. 2016;354: 1008–1015.
937 doi:10.1126/science.aah4967

938 17. Lamia KA, Sachdeva UM, DiTacchio L, Williams EC, Alvarez JG, Egan DF, et al. AMPK regulates
939 the circadian clock by cryptochrome phosphorylation and degradation. Science. 2009;326: 437–
940 440. doi:10.1126/science.1172156

941 18. Asher G, Reinke H, Altmeyer M, Gutierrez-Arcelus M, Hottiger MO, Schibler U. Poly(ADP-ribose)
942 polymerase 1 participates in the phase entrainment of circadian clocks to feeding. Cell. 2010;142:
943 943–953. doi:10.1016/j.cell.2010.08.016

944 19. Weger BD, Gobet C, David FPA, Atger F, Martin E, Phillips NE, et al. Systematic analysis of
945 differential rhythmic liver gene expression mediated by the circadian clock and feeding rhythms.
946 Proc Natl Acad Sci USA. 2021;118: e2015803118. doi:10.1073/pnas.2015803118

947 20. Vollmers C, Gill S, DiTacchio L, Pulivarthy SR, Le HD, Panda S. Time of feeding and the intrinsic
948 circadian clock drive rhythms in hepatic gene expression. Proc Natl Acad Sci U S A. 2009;106:
949 21453–21458. doi:10.1073/pnas.0909591106

950 21. Greenwell BJ, Trott AJ, Beytebiere JR, Pao S, Bosley A, Beach E, et al. Rhythmic Food Intake
951 Drives Rhythmic Gene Expression More Potently than the Hepatic Circadian Clock in Mice. Cell
952 Reports. 2019;27: 649-657.e5. doi:10.1016/j.celrep.2019.03.064

953 22. Atger F, Gobet C, Marquis J, Martin E, Wang J, Weger B, et al. Circadian and feeding rhythms
954 differentially affect rhythmic mRNA transcription and translation in mouse liver. Proc Natl Acad
955 Sci U S A. 2015;112: E6579-6588. doi:10.1073/pnas.1515308112

956 23. Chatham JC, Zhang J, Wende AR. Role of *O* -linked *N* -acetylglucosamine protein modification in
957 cellular (patho)physiology. Physiological Reviews. 2021;101: 427–493.
958 doi:10.1152/physrev.00043.2019

959 24. Wulff-Fuentes E, Berendt RR, Massman L, Danner L, Malard F, Vora J, et al. The human O-
960 GlcNAcome database and meta-analysis. Sci Data. 2021;8: 25. doi:10.1038/s41597-021-00810-4

961 25. Ma J, Hou C, Wu C. Demystifying the O-GlcNAc Code: A Systems View. Chem Rev. 2022;
962 acs.chemrev.1c01006. doi:10.1021/acs.chemrev.1c01006

963 26. Wang Y, Fang X, Wang S, Wang B, Chu F, Tian Z, et al. The role of O-GlcNAcylation in innate
964 immunity and inflammation. J Mol Cell Biol. 2023;14: mjac065. doi:10.1093/jmcb/mjac065

965 27. Liu X, Chiu JC. Nutrient-sensitive protein O-GlcNAcylation shapes daily biological rhythms. Open
966 Biology. 2022;12: 220215. doi:10.1098/rsob.220215

967 28. Liu X, Cai YD, Chiu JC. Regulation of protein O-GlcNAcylation by circadian, metabolic, and
968 cellular signals. J Biol Chem. 2023;300: 105616. doi:10.1016/j.jbc.2023.105616

969 29. Durgan DJ, Pat BM, Laczy B, Bradley JA, Tsai J-Y, Grenett MH, et al. O-GlcNAcylation, Novel
970 Post-Translational Modification Linking Myocardial Metabolism and Cardiomyocyte Circadian
971 Clock*. Journal of Biological Chemistry. 2011;286: 44606–44619. doi:10.1074/jbc.M111.278903

972 30. Liu X, Blaženović I, Contreras AJ, Pham TM, Tabuloc CA, Li YH, et al. Hexosamine biosynthetic
973 pathway and O-GlcNAc-processing enzymes regulate daily rhythms in protein O-GlcNAcylation.
974 Nat Commun. 2021;12: 4173. doi:10.1038/s41467-021-24301-7

975 31. Hart GW. Nutrient regulation of signaling and transcription. Journal of Biological Chemistry.
976 2019;294: 2211–2231. doi:10.1074/jbc.AW119.003226

977 32. Li M-D, Ruan H-B, Hughes ME, Lee J-S, Singh JP, Jones SP, et al. O-GlcNAc Signaling Entrains
978 the Circadian Clock by Inhibiting BMAL1/CLOCK Ubiquitination. Cell Metabolism. 2013;17:
979 303–310. doi:10.1016/j.cmet.2012.12.015

980 33. Han I, Kudlow JE. Reduced O glycosylation of Sp1 is associated with increased proteasome
981 susceptibility. Mol Cell Biol. 1997;17: 2550–2558. doi:10.1128/MCB.17.5.2550

982 34. Zhang F, Su K, Yang X, Bowe DB, Paterson AJ, Kudlow JE. O-GlcNAc modification is an
983 endogenous inhibitor of the proteasome. Cell. 2003;115: 715–725. doi:10.1016/s0092-
984 8674(03)00974-7

985 35. Yang A-Q, Li D, Chi L, Ye X-S. Validation, Identification, and Biological Consequences of the
986 Site-specific O-GlcNAcylation Dynamics of Carbohydrate-responsive Element-binding Protein
987 (ChREBP). Mol Cell Proteomics. 2017;16: 1233–1243. doi:10.1074/mcp.M116.061416

988 36. Issad T, Kuo M. O-GlcNAc modification of transcription factors, glucose sensing and glucotoxicity.
989 Trends Endocrinol Metab. 2008;19: 380–389. doi:10.1016/j.tem.2008.09.001

990 37. Hardivillé S, Banerjee PS, Selen Alpergin ES, Smith DM, Han G, Ma J, et al. TATA-Box Binding
991 Protein O-GlcNAcylation at T114 Regulates Formation of the B-TFIID Complex and Is Critical

992 for Metabolic Gene Regulation. Mol Cell. 2020;77: 1143-1152.e7.
993 doi:10.1016/j.molcel.2019.11.022

994 38. Noach N, Segev Y, Levi I, Segal S, Priel E. Modification of topoisomerase I activity by glucose and
995 by O-GlcNAcylation of the enzyme protein. Glycobiology. 2007;17: 1357–1364.
996 doi:10.1093/glycob/cwm105

997 39. Ranuncolo SM, Ghosh S, Hanover JA, Hart GW, Lewis BA. Evidence of the Involvement of O-
998 GlcNAc-modified Human RNA Polymerase II CTD in Transcription in Vitro and in Vivo. Journal
999 of Biological Chemistry. 2012;287: 23549–23561. doi:10.1074/jbc.M111.330910

1000 40. Lewis BA, Burlingame AL, Myers SA. Human RNA Polymerase II Promoter Recruitment in Vitro
1001 Is Regulated by O-Linked N-Acetylglucosaminyltransferase (OGT). J Biol Chem. 2016;291:
1002 14056–14061. doi:10.1074/jbc.M115.684365

1003 41. Shi F-T, Kim H, Lu W, He Q, Liu D, Goodell MA, et al. Ten-eleven translocation 1 (Tet1) is
1004 regulated by O-linked N-acetylglucosamine transferase (Ogt) for target gene repression in mouse
1005 embryonic stem cells. J Biol Chem. 2013;288: 20776–20784. doi:10.1074/jbc.M113.460386

1006 42. Li H-J, Wang Y, Li B-X, Yang Y, Guan F, Pang X-C, et al. Roles of ten-eleven translocation family
1007 proteins and their O-linked β-N-acetylglucosaminylated forms in cancer development. Oncol Lett.
1008 2021;21: 1. doi:10.3892/ol.2020.12262

1009 43. Vella P, Scelfo A, Jammula S, Chiacchiera F, Williams K, Cuomo A, et al. Tet Proteins Connect the
1010 O-Linked N-acetylglucosamine Transferase Ogt to Chromatin in Embryonic Stem Cells.
1011 Molecular Cell. 2013;49: 645–656. doi:10.1016/j.molcel.2012.12.019

1012 44. Zhang Q, Liu X, Gao W, Li P, Hou J, Li J, et al. Differential regulation of the ten-eleven
1013 translocation (TET) family of dioxygenases by O-linked β-N-acetylglucosamine transferase
1014 (OGT). J Biol Chem. 2014;289: 5986–5996. doi:10.1074/jbc.M113.524140

1015 45. Leturcq M, Lefebvre T, Vercoutter-Edouart A-S. O-GlcNAcylation and chromatin remodeling in
1016 mammals: an up-to-date overview. Biochem Soc Trans. 2017;45: 323–338.
1017 doi:10.1042/BST20160388

1018 46. Zhang S, Roche K, Nasheuer H-P, Lowndes NF. Modification of histones by sugar β-N-
1019 acetylglucosamine (GlcNAc) occurs on multiple residues, including histone H3 serine 10, and is
1020 cell cycle-regulated. J Biol Chem. 2011;286: 37483–37495. doi:10.1074/jbc.M111.284885

1021 47. Fong JJ, Nguyen BL, Bridger R, Medrano EE, Wells L, Pan S, et al. β-N-Acetylglucosamine (O-
1022 GlcNAc) Is a Novel Regulator of Mitosis-specific Phosphorylations on Histone H3. Journal of
1023 Biological Chemistry. 2012;287: 12195–12203. doi:10.1074/jbc.M111.315804

1024 48. Wang P, Peng C, Liu X, Liu H, Chen Y, Zheng L, et al. OGT mediated histone H2B S112
1025 GlcNAcylation regulates DNA damage response. J Genet Genomics. 2015;42: 467–475.
1026 doi:10.1016/j.jgg.2015.07.002

1027 49. Dehennaut V, Leprince D, Lefebvre T. O-GlcNAcylation, an Epigenetic Mark. Focus on the
1028 Histone Code, TET Family Proteins, and Polycomb Group Proteins. Front Endocrinol (Lausanne).
1029 2014;5: 155. doi:10.3389/fendo.2014.00155

1030 50. Zhao M-J, Yao X, Wei P, Zhao C, Cheng M, Zhang D, et al. O-GlcNAcylation of TDP-43
1031 suppresses proteinopathies and promotes TDP-43's mRNA splicing activity. EMBO Rep. 2021;22:
1032 e51649. doi:10.15252/embr.202051649

1033 51. Tan W, Jiang P, Zhang W, Hu Z, Lin S, Chen L, et al. Posttranscriptional regulation of de novo
1034 lipogenesis by glucose-induced O-GlcNAcylation. Molecular Cell. 2021;81: 1890-1904.e7.
1035 doi:10.1016/j.molcel.2021.02.009

1036 52. Tan Z-W, Fei G, Paulo JA, Bellaousov S, Martin SES, Duveau DY, et al. O-GlcNAc regulates gene
1037 expression by controlling detained intron splicing. Nucleic Acids Res. 2020;48: 5656–5669.
1038 doi:10.1093/nar/gkaa263

1039 53. Laarse SAM, Leney AC, Heck AJR. Crosstalk between phosphorylation and O‐Glc NA cylation:
1040 friend or foe. FEBS J. 2018;285: 3152–3167. doi:10.1111/febs.14491

1041 54. Kaasik K, Kivimäe S, Allen JJ, Chalkley RJ, Huang Y, Baer K, et al. Glucose Sensor O-
1042 GlcNAcylation Coordinates with Phosphorylation to Regulate Circadian Clock. Cell Metabolism.
1043 2013;17: 291–302. doi:10.1016/j.cmet.2012.12.017

1044 55. Wang Y, Song L, Liu M, Ge R, Zhou Q, Liu W, et al. A proteomics landscape of circadian clock in
1045 mouse liver. Nat Commun. 2018;9: 1553. doi:10.1038/s41467-018-03898-2

1046 56. Wang J, Mauvoisin D, Martin E, Atger F, Galindo AN, Dayon L, et al. Nuclear Proteomics
1047 Uncovers Diurnal Regulatory Landscapes in Mouse Liver. Cell Metabolism. 2017;25: 102–117.
1048 doi:10.1016/j.cmet.2016.10.003

1049 57. Robles MS, Humphrey SJ, Mann M. Phosphorylation Is a Central Mechanism for Circadian Control
1050 of Metabolism and Physiology. Cell Metabolism. 2017;25: 118–127.
1051 doi:10.1016/j.cmet.2016.10.004

1052 58. Huang R, Chen J, Zhou M, Xin H, Lam SM, Jiang X, et al. Multi-omics profiling reveals rhythmic
1053 liver function shaped by meal timing. Nat Commun. 2023;14: 6086. doi:10.1038/s41467-023-
1054 41759-9

1055 59. Thompson JW, Griffin ME, Hsieh-Wilson LC. Methods for the Detection, Study, and Dynamic
1056 Profiling of O-GlcNAc Glycosylation. Methods Enzymol. 2018;598: 101–135.
1057 doi:10.1016/bs.mie.2017.06.009

1058 60. Thaben PF, Westermark PO. Detecting Rhythms in Time Series with RAIN. J Biol Rhythms.
1059 2014;29: 391–400. doi:10.1177/0748730414553029

1060 61. Tsitsiridis G, Steinkamp R, Giurgiu M, Brauner B, Fobo, Frishman G, et al. CORUM: the
1061 comprehensive resource of mammalian protein complexes-2022. Nucleic acids research. 2023;51.
1062 doi:10.1093/nar/gkac1015

1063 62. Yao H, Li A, Wang M. Systematic Analysis and Prediction of *In Situ* Cross Talk of O-
1064 GlcNAcylation and Phosphorylation. BioMed Research International. 2015;2015: 1–12.
1065 doi:10.1155/2015/279823

1066 63. Leney AC, El Atmioui D, Wu W, Ovaa H, Heck AJR. Elucidating crosstalk mechanisms between
1067 phosphorylation and O-GlcNAcylation. Proc Natl Acad Sci USA. 2017;114.
1068 doi:10.1073/pnas.1620529114

1069 64. Wozniak JM, Gonzalez DJ. PTMphinder: an R package for PTM site localization and motif
1070 extraction from proteomic datasets. PeerJ. 2019;7: e7046. doi:10.7717/peerj.7046

1071 65. Wang C, Xu H, Lin S, Deng W, Zhou J, Zhang Y, et al. GPS 5.0: An Update on the Prediction of
1072 Kinase-specific Phosphorylation Sites in Proteins. Genomics Proteomics Bioinformatics. 2020;18:
1073 72–80. doi:10.1016/j.gpb.2020.01.001

1074 66. Butcher GQ, Lee B, Hsieh F, Obrietan K. Light- and clock-dependent regulation of ribosomal S6
1075 kinase activity in the suprachiasmatic nucleus. Eur J Neurosci. 2004;19: 907–915.
1076 doi:10.1111/j.0953-816x.2004.03155.x

1077 67. Hornbeck PV, Zhang B, Murray B, Kornhauser JM, Latham V, Skrzypek E. PhosphoSitePlus, 2014:
1078 mutations, PTMs and recalibrations. Nucleic Acids Res. 2015;43: D512-520.
1079 doi:10.1093/nar/gku1267

1080 68. Spengler ML, Kuropatwinski KK, Schumer M, Antoch MP. A serine cluster mediates BMAL1-
1081 dependent CLOCK phosphorylation and degradation. Cell Cycle. 2009;8: 4138–4146.
1082 doi:10.4161/cc.8.24.10273

1083 69. Stratmann M, Suter DM, Molina N, Naef F, Schibler U. Circadian Dbp transcription relies on highly
1084 dynamic BMAL1-CLOCK interaction with E boxes and requires the proteasome. Mol Cell.
1085 2012;48: 277–287. doi:10.1016/j.molcel.2012.08.012

1086 70. Kwon I, Lee J, Chang SH, Jung NC, Lee BJ, Son GH, et al. BMAL1 shuttling controls
1087 transactivation and degradation of the CLOCK/BMAL1 heterodimer. Mol Cell Biol. 2006;26:
1088 7318–7330. doi:10.1128/MCB.00337-06

1089 71. Lee J, Lee Y, Lee MJ, Park E, Kang SH, Chung CH, et al. Dual modification of BMAL1 by
1090 SUMO2/3 and ubiquitin promotes circadian activation of the CLOCK/BMAL1 complex. Mol Cell
1091 Biol. 2008;28: 6056–6065. doi:10.1128/MCB.00583-08

1092 72. Thomas D, Tyers M. Transcriptional regulation: Kamikaze activators. Curr Biol. 2000;10: R341-
1093 343. doi:10.1016/s0960-9822(00)00462-0

1094 73. Tansey WP. Transcriptional activation: risky business. Genes Dev. 2001;15: 1045–1050.
1095 doi:10.1101/gad.896501

1096 74. Liu AC, Tran HG, Zhang EE, Priest AA, Welsh DK, Kay SA. Redundant function of REV-
1097 ERBalpha and beta and non-essential role for Bmal1 cycling in transcriptional regulation of
1098 intracellular circadian rhythms. PLoS Genet. 2008;4: e1000023.
1099 doi:10.1371/journal.pgen.1000023

1100 75. Nosella ML, Tereshchenko M, Pritišanac I, Chong PA, Toretsky JA, Lee HO, et al. O-Linked-N-
1101 Acetylglucosaminylation of the RNA-Binding Protein EWS N-Terminal Low Complexity Region
1102 Reduces Phase Separation and Enhances Condensate Dynamics. J Am Chem Soc. 2021;143:
1103 11520–11534. doi:10.1021/jacs.1c04194

1104 76. Yoshida M, Yokoi N, Takahashi H, Hatano N, Hayami T, Ogawa W, et al. O-GlcNAcylation of
1105 myocyte-specific enhancer factor 2D negatively regulates insulin secretion from pancreatic β-cells.
1106 Biochem Biophys Res Commun. 2022;605: 90–96. doi:10.1016/j.bbrc.2022.03.036

1107 77. Cannon MV, Silljé HHW, Sijbesma JWA, Vreeswijk-Baudoin I, Ciapaite J, van der Sluis B, et al.
1108 Cardiac LXRα protects against pathological cardiac hypertrophy and dysfunction by enhancing
1109 glucose uptake and utilization. EMBO Mol Med. 2015;7: 1229–1243.
1110 doi:10.15252/emmm.201404669

1111 78. Kang D, Lee J, Yook G, Jeong S, Shin J, Kim M-S, et al. Regulation of senescence-associated
1112 secretory phenotypes in osteoarthritis by cytosolic UDP-GlcNAc retention and O-GlcNAcylation.
1113 Nat Commun. 2025;16: 1094. doi:10.1038/s41467-024-55085-1

1114 79. Khidekel N, Ficarro SB, Peters EC, Hsieh-Wilson LC. Exploring the *O* -GlcNAc proteome: Direct
1115 identification of *O* -GlcNAc-modified proteins from the brain. Proc Natl Acad Sci USA. 2004;101:
1116 13132–13137. doi:10.1073/pnas.0403471101

1117 80. Wang S, Yang F, Petyuk VA, Shukla AK, Monroe ME, Gritsenko MA, et al. Quantitative
1118 proteomics identifies altered O-GlcNAcylation of structural, synaptic and memory-associated
1119 proteins in Alzheimer's disease. J Pathol. 2017;243: 78–88. doi:10.1002/path.4929

1120 81. Song H, Ma J, Bian Z, Chen S, Zhu J, Wang J, et al. Global profiling of O-GlcNAcylated and/or
1121 phosphorylated proteins in hepatoblastoma. Sig Transduct Target Ther. 2019;4: 40.
1122 doi:10.1038/s41392-019-0067-4

1123 82. Liu J, Hao Y, Wang C, Jin Y, Yang Y, Gu J, et al. An Optimized Isotopic Photocleavable Tagging
1124 Strategy for Site-Specific and Quantitative Profiling of Protein O-GlcNAcylation in Colorectal
1125 Cancer Metastasis. ACS Chem Biol. 2022;17: 513–520. doi:10.1021/acschembio.1c00981

1126 83. Xu S, Yin K, Xu X, Fu L, Wu R. O-GlcNAcylation reduces proteome solubility and regulates the
1127 formation of biomolecular condensates in human cells. Nat Commun. 2025;16: 4068.
1128 doi:10.1038/s41467-025-59371-4

1129 84. Hao Y, Li Z, Du X, Xie Q, Li D, Lei S, et al. Characterization and chemoproteomic profiling of
1130 protein O-GlcNAcylation in SOD1-G93A mouse model. Mol Med. 2025;31: 82.
1131 doi:10.1186/s10020-025-01134-4

1132 85. Lei C, Chen Z, Hao Y, Huang W, Chu T, Xiao K, et al. Quantitative and site-specific
1133 chemoproteomic profiling of O-GlcNAcylation in Drosophila. Bioorg Med Chem. 2025;124:
1134 118191. doi:10.1016/j.bmc.2025.118191

1135 86. Hou C, Deng J, Wu C, Zhang J, Byers S, Moremen KW, et al. Ultradeep O-GlcNAc proteomics
1136 reveals widespread O-GlcNAcylation on tyrosine residues of proteins. Proc Natl Acad Sci U S A.
1137 2024;121: e2409501121. doi:10.1073/pnas.2409501121

1138 87. Yoshitane H, Imamura K, Okubo T, Otobe Y, Kawakami S, Ito S, et al. mTOR-AKT Signaling in
1139 Cellular Clock Resetting Triggered by Osmotic Stress. Antioxid Redox Signal. 2022.
1140 doi:10.1089/ars.2021.0059

1141 88. Peng F, Lu J, Su K, Liu X, Luo H, He B, et al. Oncogenic fatty acid oxidation senses circadian
1142 disruption in sleep-deficiency-enhanced tumorigenesis. Cell Metab. 2024;36: 1598-1618.e11.
1143 doi:10.1016/j.cmet.2024.04.018

1144 89. Longo VD, Panda S. Fasting, Circadian Rhythms, and Time-Restricted Feeding in Healthy
1145 Lifespan. Cell Metabolism. 2016;23: 1048–1059. doi:10.1016/j.cmet.2016.06.001

1146 90. Asher G, Sassone-Corsi P. Time for food: the intimate interplay between nutrition, metabolism, and
1147 the circadian clock. Cell. 2015;161: 84–92. doi:10.1016/j.cell.2015.03.015

1148 91. Manella G, Sabath E, Aviram R, Dandavate V, Ezagouri S, Golik M, et al. The liver-clock
1149 coordinates rhythmicity of peripheral tissues in response to feeding. Nat Metab. 2021;3: 829–842.
1150 doi:10.1038/s42255-021-00395-7

1151 92. Andrali SS, Qian Q, Ozcan S. Glucose mediates the translocation of NeuroD1 by O-linked
1152 glycosylation. J Biol Chem. 2007;282: 15589–15596. doi:10.1074/jbc.M701762200

1153 93. Al-Hakim AK, Göransson O, Deak M, Toth R, Campbell DG, Morrice NA, et al. 14-3-3 cooperates
1154 with LKB1 to regulate the activity and localization of QSK and SIK. J Cell Sci. 2005;118: 5661–
1155 5673. doi:10.1242/jcs.02670

1156 94. James LR, Tang D, Ingram A, Ly H, Thai K, Cai L, et al. Flux through the hexosamine pathway is a
1157 determinant of nuclear factor kappaB- dependent promoter activation. Diabetes. 2002;51: 1146–
1158 1156. doi:10.2337/diabetes.51.4.1146

1159 95. Li Z, Fu B, Wei A, Wu Y, Huang M, Zhang E, et al. d-Glucosamine induces circadian phase delay
1160 by promoting BMAL1 degradation through AMPK/mTOR pathway. Life Sci. 2023;325: 121765.
1161 doi:10.1016/j.lfs.2023.121765

1162 96. Crosby P, Hamnett R, Putker M, Hoyle NP, Reed M, Karam CJ, et al. Insulin/IGF-1 Drives
1163 PERIOD Synthesis to Entrain Circadian Rhythms with Feeding Time. Cell. 2019;177: 896-
1164 909.e20. doi:10.1016/j.cell.2019.02.017

1165 97. Xu C, Pan X, Wang D, Guan Y, Yang W, Chen X, et al. O-GlcNAcylation of Raptor transduces
1166 glucose signals to mTORC1. Mol Cell. 2023;83: 3027-3040.e11.
1167 doi:10.1016/j.molcel.2023.07.011

1168 98. Luo B, Parker GJ, Cooksey RC, Soesanto Y, Evans M, Jones D, et al. Chronic hexosamine flux
1169 stimulates fatty acid oxidation by activating AMP-activated protein kinase in adipocytes. J Biol
1170 Chem. 2007;282: 7172–7180. doi:10.1074/jbc.M607362200

1171 99. Bullen JW, Balsbaugh JL, Chanda D, Shabanowitz J, Hunt DF, Neumann D, et al. Cross-talk
1172 between Two Essential Nutrient-sensitive Enzymes. Journal of Biological Chemistry. 2014;289:
1173 10592–10606. doi:10.1074/jbc.M113.523068

1174 100. Vosseller K, Wells L, Lane MD, Hart GW. Elevated nucleocytoplasmic glycosylation by O-GlcNAc
1175 results in insulin resistance associated with defects in Akt activation in 3T3-L1 adipocytes. Proc
1176 Natl Acad Sci U S A. 2002;99: 5313–5318. doi:10.1073/pnas.072072399

1177 101. Makishima M, Okamoto AY, Repa JJ, Tu H, Learned RM, Luk A, et al. Identification of a nuclear
1178 receptor for bile acids. Science. 1999;284: 1362–1365. doi:10.1126/science.284.5418.1362

1179 102. Ouyang Y, Wu Q, Li J, Sun S, Sun S. S-adenosylmethionine: A metabolite critical to the regulation
1180 of autophagy. Cell Prolif. 2020;53: e12891. doi:10.1111/cpr.12891

1181 103. Wei B, Xu L, Guo W, Wang Y, Wu J, Li X, et al. SHP2-Mediated Inhibition of DNA Repair
1182 Contributes to cGAS-STING Activation and Chemotherapeutic Sensitivity in Colon Cancer.
1183 Cancer Res. 2021;81: 3215–3228. doi:10.1158/0008-5472.CAN-20-3738

1184 104. Katada S, Sassone-Corsi P. The histone methyltransferase MLL1 permits the oscillation of circadian
1185 gene expression. Nat Struct Mol Biol. 2010;17: 1414–1421. doi:10.1038/nsmb.1961

1186 105. Aguilar-Arnal L, Katada S, Orozco-Solis R, Sassone-Corsi P. NAD+-SIRT1 control of H3K4
1187 trimethylation through circadian deacetylation of MLL1. Nat Struct Mol Biol. 2015;22: 312–318.
1188 doi:10.1038/nsmb.2990

1189 106. Oyama Y, Iwasaka H, Koga H, Shingu C, Matsumoto S, Noguchi T. Uncoupling of peripheral and
1190 master clock gene rhythms by reversed feeding leads to an exacerbated inflammatory response
1191 after polymicrobial sepsis in mice. Shock. 2014;41: 214–221.
1192 doi:10.1097/SHK.0000000000000094

1193 107. Nagata T, Redman RS, Lakshman R. Isolation of intact nuclei of high purity from mouse liver. Anal
1194 Biochem. 2010;398: 178–184. doi:10.1016/j.ab.2009.11.017

1195 108. Khidekel N, Arndt S, Lamarre-Vincent N, Lippert A, Poulin-Kerstien KG, Ramakrishnan B, et al. A
1196 chemoenzymatic approach toward the rapid and sensitive detection of O-GlcNAc posttranslational
1197 modifications. J Am Chem Soc. 2003;125: 16162–16163. doi:10.1021/ja038545r

1198 109. Ramakrishnan B, Qasba PK. Structure-based design of beta 1,4-galactosyltransferase I (beta 4Gal-
1199 T1) with equally efficient N-acetylgalactosaminyltransferase activity: point mutation broadens
1200 beta 4Gal-T1 donor specificity. J Biol Chem. 2002;277: 20833–20839.
1201 doi:10.1074/jbc.M111183200

1202 110. Fiehn O. Metabolomics by Gas Chromatography-Mass Spectrometry: Combined Targeted and
1203 Untargeted Profiling. Curr Protoc Mol Biol. 2016;114: 30.4.1-30.4.32.
1204 doi:10.1002/0471142727.mb3004s114

1205 111. Tsugawa H, Cajka T, Kind T, Ma Y, Higgins B, Ikeda K, et al. MS-DIAL: data-independent
1206 MS/MS deconvolution for comprehensive metabolome analysis. Nat Methods. 2015;12: 523–526.
1207 doi:10.1038/nmeth.3393

1208 112. Mohammed H, Taylor C, Brown GD, Papachristou EK, Carroll JS, D'Santos CS. Rapid
1209 immunoprecipitation mass spectrometry of endogenous proteins (RIME) for analysis of chromatin
1210 complexes. Nat Protoc. 2016;11: 316–326. doi:10.1038/nprot.2016.020

1211 113. Sharma S, Yang J, Grudzien-Nogalska E, Shivas J, Kwan KY, Kiledjian M. Xrn1 is a deNADding
1212 enzyme modulating mitochondrial NAD-capped RNA. Nat Commun. 2022;13: 889.
1213 doi:10.1038/s41467-022-28555-7

1214 114. Craig R, Beavis RC. TANDEM: matching proteins with tandem mass spectra. Bioinformatics.
1215 2004;20: 1466–1467. doi:10.1093/bioinformatics/bth092

115. Gupta N, Bandeira N, Keich U, Pevzner PA. Target-decoy approach and false discovery rate: when things may go wrong. J Am Soc Mass Spectrom. 2011;22: 1111–1120. doi:10.1007/s13361-011-0139-3

116. Hou C, Wu C, Wu Z, Cheng Y, Li W, Sun H, et al. Systematic Evaluation of Affinity Enrichment Methods for O-GlcNAc Proteomics. J Proteome Res. 2024;23: 4422–4432. doi:10.1021/acs.jproteome.4c00388

117. Li J, Cai Z, Bomgarden RD, Pike I, Kuhn K, Rogers JC, et al. TMTpro-18plex: The Expanded and Complete Set of TMTpro Reagents for Sample Multiplexing. J Proteome Res. 2021;20: 2964–2972. doi:10.1021/acs.jproteome.1c00168

118. Mertins P, Qiao JW, Patel J, Udeshi ND, Clauser KR, Mani DR, et al. Integrated proteomic analysis of post-translational modifications by serial enrichment. Nat Methods. 2013;10: 634–637. doi:10.1038/nmeth.2518

119. Li J, Paulo JA, Nusinow DP, Huttlin EL, Gygi SP. Investigation of Proteomic and Phosphoproteomic Responses to Signaling Network Perturbations Reveals Functional Pathway Organizations in Yeast. Cell Rep. 2019;29: 2092-2104.e4. doi:10.1016/j.celrep.2019.10.034

120. Yoshitane H, Takao T, Satomi Y, Du N-H, Okano T, Fukada Y. Roles of CLOCK phosphorylation in suppression of E-box-dependent transcription. Mol Cell Biol. 2009;29: 3675–3686. doi:10.1128/MCB.01864-08

121. Cao X, Yang Y, Selby C, Liu Z, Sancar A. Molecular mechanism of the repressive phase of the mammalian circadian clock. Proceedings of the National Academy of Sciences of the United States of America. 2021;118. doi:10.1073/pnas.2021174118

122. Rohart F, Gautier B, Singh A, Lê Cao K-A. mixOmics: An R package for ’omics feature selection and multiple data integration. PLoS Comput Biol. 2017;13: e1005752. doi:10.1371/journal.pcbi.1005752

123. Wu G, Anafi RC, Hughes ME, Kornacker K, Hogenesch JB. MetaCycle: an integrated R package to evaluate periodicity in large scale data. Bioinformatics. 2016;32: 3351–3353. doi:10.1093/bioinformatics/btw405

Acknowledgments: We would like to thank the West Coast Metabolomics Center at UC Davis for their technical support. This work is supported by National Institutes of Health grants R01DK124068, R56DK124068, and R21AG082480 to J.C.C. and STI2030-Major Projects 2021ZD0203400 to Y.Z.

Author contributions: J.C.C., Y.K.X. and X.L. conceptualized and designed the study. J.C.C. and Y.Z. acquired the funding. J.C.C., X.L., Y.D.C., and Y.Z. coordinated and supervised the investigation. X.L., Y.D.C., C.H., X.L., Y.L., A.J.P.M., X.X., Y.L., H.Z., C.Z., C.C., and J.M. performed research and analyzed data. X.L., Y.D.C. and J.C.C. contributed to critical interpretation of the data. X.L., Y.D.C. and J.C.C. drafted the manuscript.

Competing Interests: The authors declare no competing interests.

Data Availability Statement: All data needed to evaluate the conclusions in the paper are present in the paper and/or the Supplementary Materials. The raw metabolomics dataset has been deposited in the open metabolomics database, Metabolomics Workbench (https://www.metabolomicsworkbench.org/), under accession no. [ST002952] and [ST002950]. The raw label-free global and TMT site-specific O-GlcNAc proteomics, TMT-phosphoproteomics and proteomics datasets have been deposited into MassIVE repository (MSV000094417) (MassIVE: ftp://massive.ucsd.edu/v07/MSV000094417/). Data will be made public upon publication.

1267

1268 **Figure Legends**

1269

1270 **Fig 1. Protein O-GlcNAcylation exhibits daily rhythmicity in mouse liver nuclei. (A)**
1271 Representative western blot showing the daily rhythm of nuclear protein O-GlcNAcylation in liver
1272 samples from mice subjected to night-restricted feeding (NRF). Total nuclear proteins were stained
1273 with Coomassie blue (bottom panel) and used for normalization. ZT, zeitgeber time (hr). ZT0
1274 denotes lights-on time and ZT12 denotes lights-off time. **(B)** Quantification of protein O-
1275 GlcNAcylation signals in panel **(A)** (n = 3). α-streptavidin signal of the whole lane was quantified.
1276 **(C)** Daily rhythm of UDP-GlcNAc quantified using targeted metabolomics (n = 3). The grey
1277 shading in **(B)** and **(C)** illustrates the dark phase of the 24-hr day-night cycle. The red bars indicate
1278 when food was available. ZT: zeitgeber time (hr). Data are presented as mean ±SEM, and the blue
1279 shaded area represents SEM. P values indicate rhythmicity (RAIN).

1280

1281 **Fig 2. Label-free global and TMT site-specific O-GlcNAc proteomics identify daily changes**
1282 **of nuclear protein O-GlcNAcylation. (A)** Score plot for PLS-DA model of label-free O-GlcNAc
1283 proteomics. **(B)** Negative log MANOVA p values for overall time and each time point tested in
1284 pairwise PLS-DA models. The red dash line represents MANOVA p value cutoff for significance.
1285 **(C)** The number of proteins with rhythmic O-GlcNAcylation detected by RAIN and JTK using
1286 different cut-offs (n = 3). **(D)** Heat map showing the oscillation pattern of rhythmically O-
1287 GlcNAcylated proteins (n = 3). **(E)** Circular histogram showing the number of O-GlcNAcylated
1288 proteins peaking at each phase. The peak phase of O-GlcNAcylated proteins was calculated using
1289 RAIN. The gray shading illustrates the dark phase of a day-night cycle. (**F**) Venn diagram
1290 showing >40% O-GlcNAcylated proteins were identified in both global protemics and site-specific
1291 O-GlcNAc proteomics. (**G**) Score plot for PLS-DA model of TMT site-specific O-GlcNAc
1292 proteomics. (**H**) Volcano plot displaying relative abundance of O-GlcNAcylation peptides
1293 between day and night. Horizontal dash line represents $p<0.05$ cutoff (Student's t-test). Vertical
1294 dash lines represent fold change >20% (n = 4). **(I)** Heatmaps showing the relative O-
1295 GlcNAcylation level at indicated sites at ZT11 (day) and ZT23 (night) (n = 4).

1296

1297 **Fig 3. Daily nuclear phosphoproteome of mouse liver from NRF mice. (A)** Score plot for PLS-
1298 DA model. **(B)** Negative log MANOVA p values for overall time and each time point tested in
1299 pairwise PLS-DA models. The red dash line is showing the MANOVA p value cutoff for
1300 significance. **(C)** The number of proteins with rhythmic O-GlcNAcylation detected by RAIN and
1301 JTK using different cut-offs (n = 3). **(D)** Heat map showing daily rhythmicity of phosphopeptides
1302 (n = 3). **(E)** Circular histogram showing the number of phosphopeptides peaking at each phase as
1303 determined by RAIN. The kinases that rhythmically phosphorylate the daily phosphoproteome
1304 were predicted based on the enriched peptide motifs in each peaking phase. The enriched peptide
1305 motifs and corresponding kinases were illustrated in the boxes. The color of boxes and shading
1306 corresponds to the phosphorylation motifs enriched from phosphopeptides peaking in the indicated
1307 phases. The gray shading illustrates the dark phase of a day-night cycle. **(F)** Rhythmically
1308 phosphorylated proteins were classified into protein complexes based on known association and
1309 function, and the subunits with daily rhythmicity in phosphorylation were plotted in graphs. The
1310 protein complexes were further classified and grouped according to their biological functions as
1311 indicated on the left boxes. The gray lines indicate the oscillation of each phosphopeptide, while
1312 the orange lines indicate the average phosphorylation pattern of each protein subunit. Each gray
1313 line represents the average of three biological replicates. When only one peptide of individual
1314 protein was rhythmically phosphorylated (Per2-Sfpq-Sin3A complex panel), we used orange lines
1315 to represent phosphorylation status of individual peptides, hence there are no gray lines in that
1316 specific panel. The gray shading on each graph illustrates the dark phase of a day-night cycle.
1317
1318 **Fig 4. Interaction between the O-GlcNAc proteome and phosphoproteome over a day-night**
1319 **cycle. (A)** Spearman correlation analysis showing the correlation between rhythmic O-
1320 GlcNAcylation identified by label-free global O-GlcNAc proteomics and phosphorylation on each
1321 protein that exhibits daily rhythmicity of two PTMs. The color of the bars represents coefficient
1322 values as shown in the color scale on the right. The asterisks indicate the sites with potential O-
1323 GlcNAcylation and phosphorylation interplay motif. The color scale also includes a histogram
1324 showing the frequency of coefficient values between O-GlcNAcylation and phosphorylation in
1325 proteins. **(B)** Circular density graphs showing the peak phase of O-GlcNAcylation and
1326 phosphorylation events on proteins that exhibit rhythmicity in both modifications. The gray
1327 shading illustrates the dark phase of a day-night cycle. **(C-H)** Examples of global O-

1328 GlcNAcylation compared to the temporal phosphorylation profiles on the same proteins. CLOCK
1329 and ARID1B represent proteins with in-phase rhythmic O-GlcNAcylation and phosphorylation **(C**
1330 **and D)**, while PRR12 and LMNA represent proteins with out-of-phase rhythmic O-GlcNAcylation
1331 and phosphorylation **(F and G)**. AHDC1 represent proteins with both in-phase **(E)** and out-of-
1332 phase **(H)** rhythmic O-GlcNAcylation and phosphorylation. Data are presented as mean ± SEM (n
1333 = 3), and the shaded area around the curve represents SEM. (**I-L**) Examples of site-specific O-
1334 GlcNAcylation (at ZT11 and ZT23) identified by TMT site-specific O-GlcNAc proteomics (n=4)
1335 compared to the temporal phosphorylation profiles (n=3) on the indicated sites at 6 time-points.
1336 The gray shading illustrates the dark phase of a day-night cycle. Data are presented as mean ±
1337 SEM, and the shaded area around the curve represents SEM.
1338
1339 **Fig 5. O-GlcNAcylation interacts with phosphorylation to regulate rhythmic function of**
1340 **CLOCK. (A)** Schematics showing different types of O-GlcNAcylation and phosphorylation
1341 interplay motifs. Phosphorylation sites located within these motifs are indicated in the bubbles
1342 around each motif. O-GlcNAcylation either targets the same sites or approximal sites as indicated
1343 in each motif. **(B)** Model showing competition between O-GlcNAcylation and phosphorylation at
1344 CLOCK(S431) to inhibit CLOCK(S427) phosphorylation. Since S431 and S427 belong to a
1345 phospho-degron, O-GlcNAcylation at S431 could stabilize CLOCK by reducing phosphorylation
1346 at both sites and affect the transcriptional activity of CLOCK. **(C)** Representative plot showing
1347 that CLOCK S431A mutant reduce the O-GlcNAcylation level of CLOCK(aa260-460). **(D)**
1348 Quantification of protein O-GlcNAcylation signals in panel **(C)** (n = 5). Student's t test p value is
1349 indicated. **(E)** Representative blot showing the daily rhythms of CLOCK O-GlcNAcylation (Top
1350 panel) and protein level (Middle panel). Total nuclear proteins were stained with Coomassie blue
1351 (Bottom panel) and used for normalization. Mice were subjected to NRF. **(F)** Graph comparing
1352 the daily patterns of CLOCK global O-GlcNAcylation vs CLK(S427) phosphorylation levels. **(G)**
1353 Graph comparing the daily patterns of CLOCK(S427) phosphorylation vs CLOCK protein levels.
1354 The gray shading illustrates the dark phase of a day-night cycle. Data are presented as mean ±
1355 SEM (n = 3), and the shading area around the curves represents SEM. *$p < 0.05$, **$p < 0.0021$,
1356 ***$p < 0.0002$, two-way ANOVA with post-hoc Fisher's LSD tests. **(H)** Luciferase reporter assay
1357 performed in HEK293T cells showing that OGT and CLOCK mutations affect the transcriptional

1358 activity of CLOCK. **p < 0.0021, ****p < 0.0001, one-way ANOVA with post-hoc Dunnett's
1359 test.
1360
1361 **Fig 6. Time of feeding affects daily protein O-GlcNAcylation rhythm in mouse liver. (A)**
1362 Schematics showing the study design. 8-week-old C57BL/6 male mice were subjected to either
1363 NRF or DRF. The NRF group was only fed during the dark phase (ZT12-24), while the DRF group
1364 was only fed during the light phase (ZT0-12). After 3 weeks of treatment, mouse livers were
1365 collected at 4h intervals over one day, and global O-GlcNAcylation of liver nuclear proteins were
1366 detected. **(B)** Representative blot showing the daily rhythm of nuclear protein O-GlcNAcylation
1367 in liver samples from the NRF vs DRF mice (Top panel). Total nuclear proteins were stained with
1368 Coomassie blue (Bottom panel) and used for normalization. **(C)** Quantification of protein O-
1369 GlcNAcylation signals in **(B)** (n = 3). The α-streptavidin signal of the entire lane was quantified.
1370 The NRF data is replotted from Fig. 1B. **(D)** Venn diagram to compare the O-GlcNAc sites with
1371 day vs night difference in NRF and DRF liver. (**E**-**F**) Heatmaps showing the relative abundance
1372 of site-specific O-GlcNAcylation between ZT11 (day) and ZT23 (night). Heatmap is generated
1373 using detected O-GlcNAcylated peptides in **(E)** and O-GlcNAc sites in **(F)**. **(G)** Daily rhythm of
1374 UDP-GlcNAc were quantified using targeted metabolomics (n = 3). The NRF data is replotted
1375 from Fig. 1C. The dashed lines represent the median levels of O-GlcNAcylation **(C)** or UDP-
1376 GlcNAc **(G)** in NRF and DRF groups, and Student's t test was used to assess significant difference.
1377 The gray shading illustrates the dark phase of a day-night cycle. Data are presented as mean ±
1378 SEM, and the shading area around the curves represents SEM. **(H)** Food consumption of NRF and
1379 DRF mice over a 24-hr period (n=5). P=0.0952, Mann-Whitney test.
1380
1381 **Fig 7. Model describing how daily rhythmic O-GlcNAc proteome integrates environmental**
1382 **and metabolic signals to regulate transcriptomic and physiological rhythms.** Environmental
1383 cues signaling through the molecular clock and metabolic cues from feeding-fasting cycles
1384 regulate daily rhythms in the O-GlcNAc proteome. Rhythmic O-GlcNAcylation can directly shape
1385 daily rhythmicity in transcriptome and physiology. In addition, rhythmic O-GlcNAcylation can
1386 also interact with rhythmic phosphorylation. Different forms of crosstalk between O-GlcNAc
1387 proteome and phosphoproteome are shown in the middle box. The red solid arrows indicate the

1388 regulations described in this study, while the dashed arrow indicates regulations discovered by
1389 previous studies [30,57,58]. Figure created using BioRender.com, licensed to the lab of J.C.C.
1390

Supporting Information Captions

S1 Fig. Validation of chemoenzymatic labeling method for O-GlcNAcylation detection in mouse liver tissues. Two samples for the NRF group were chosen to show time-specific difference of liver nuclear O-GlcNAcylation (Lanes 3-4). Lanes 1-2 show the unlabeled samples processed in parallel with the labeled samples in Lanes 3-4. GalT1 enzyme was excluded during the processing of unlabeled samples.

S2 Fig. Study design for O-GlcNAc proteomics and TMT phosphoproteomics analysis. Flow chart illustrating the design of the proteomics experiments using mice subjected to NRF. Liver samples were collected at 6 time-points over a 24h day-night cycle. Nuclear extracts were used for site-specific TMT phosphoproteomics and global O-GlcNAc proteomics. During the process of TMT phosphoproteomics, samples were first labeled with TMT tags, and the majority of the samples were used for enrichment of phospho-peptide followed by MS analysis. A small portion of TMT-labled samples were used for proteomic analysis, where samples were directly subjected to MS analysis without enrichment. The protein levels obtained from proteomic analysis were used for normalizing phosphoproteomic and O-GlcNAc proteomic datasets. During the process of O-GlcNAc proteomics, the O-GlcNAcylation groups on proteins were biontinylated using the chemoenzymatic labeling. The O-GlcNAcylated proteins were purified using streptavidin beads followed by MS analysis. Unlabeled samples were processed in parallel, where the biotin was not attached to the O-GlcNAcylated proteins. Unlabeled samples were used for identifying the *bona fide* O-GlcNAcylated proteins during bioinformatic analysis. G in the hexagons represent the O-GlcNAc groups on proteins. Figure created using BioRender.com, licensed to the lab of J.C.C.

S3 Fig. Functional enrichment analysis of rhythmic O-GlcNAc proteome identified by label-free MS. (A-C) Rhythmically O-GlcNAcylated proteins were entered into the Database for Annotation, Visualization and Integrated Discovery (DAVID) for enrichment of GO terms. The enriched biological processes **(A)**, molecular functions **(B)** and cellular compartments **(C)** were illustrated using bubble plots. The color of the bubbles indicates the -log10 false discovery rate (FDR), while the size of the bubbles indicates the number of genes in each enriched term.

S4 Fig. Examples of rhythmic O-GlcNAc proteins that regulates gene expression. Rhythmically O-GlcNAcylated proteins were classified based on their known association in protein complexes, and the daily rhythmicity of the oscillating subunits were plotted. Multiple protein complexes were further classified and grouped according to their biological function as indicated on the left boxes. The gray shading illustrates the dark phase of a day-night cycle. Data are presented as mean ± SEM (n = 3), and the blue shading area around the curve represents ±SEM. q values indicate rhythmicity (RAIN).

S5 Fig. Functional enrichment analysis of O-GlcNAc proteome with day-night difference identified by TMT MS. (A-C) Rhythmically O-GlcNAcylated proteins were entered into the DAVID for enrichment of GO terms. The enriched biological processes **(A)**, molecular functions **(B)** and cellular compartments **(C)** were illustrated using bubble plots. The color of the bubbles indicates the -log10 false discovery rate (FDR), while the size of the bubbles indicates the number of genes in each enriched term.

S6 Fig. Functional enrichment and comparison analysis of rhythmic phosphoproteome in mouse liver nuclei. (A-C) Rhythmically phosphorylated proteins were entered into the DAVID database for enrichment of GO terms. The enriched biological processes **(A)**, molecular functions **(B)** and cellular compartments **(C)** were illustrated using bubble plots. The color of the bubbles indicates the -log10 false discovery rate (FDR), while the size of the bubbles indicates the number of genes in each enriched term. **(D)** Venn diagram to compare the rhythmic phosphosites newly discovered in our study vs sites previously published in two studies [1,2]. The number of rhythmic phoshosites is larger than that of rhythmic phosphopeptides, as one phosphopeptides could contain multiple phosphosites.

S7 Fig. Comparison of CLOCK detection using mass spectrometry and western blotting. (A-B) Comparison of CLOCK O-GlcNAcylation **(A)** and protein level **(B)** detected by mass spectrometry and western blotting. The gray shading illustrates the dark phase of a day-night cycle. Data are presented as mean ± SEM, and the shading area around the curves represents SEM (n= 2 or 3). **$p < 0.0021$, two-way ANOVA with post-hoc Fisher's LSD tests.

S8 Fig. Validation of CLOCK immunoprecipitation (IP) and expression. (A) Representative blots showing that CLOCK antibody can specifically IP CLOCK protein in mouse liver. NRF ZT3 liver were used for IP with or without CLOCK antibody. **(B)** Representative blot showing that CLOCK variants expressed in HEK293T cells were at similar levels after adjusting the plasmid amount for transfection. Optimized plasmid amount was then used in experiments for Fig 5H.

S9 Fig. Metabolic pathways other than hexosamine biosynthetic pathway (HBP) that can be involved in the regulation of gene expression. Since many metabolites were shown to regulate the function of clock proteins and other cellular proteins (Reviewed in Panda[3]), we searched for metabolites that are rhythmic under NRF condition in our metabolomic dataset, and evaluated the impact of timing of food consumption on these rhythms by comparing their rhythmicity to that under DRF. The gray shading illustrates the dark phase of a day-night cycle. Data are presented as mean ± SEM, and the shading area around the curves represents SEM (n= 3). p values from RAIN analysis for NRF (blue) and DRF (orange) are presented under each graph. *$p < 0.05$, **$p < 0.0021$, ***$p < 0.0002$, ****$p < 0.0001$, two-way ANOVA with post-hoc Fisher's LSD tests.

S1 Table. Comparison between our study and published liver phosphoproteome datasets.

S2 Table. Known functions of rhythmic phosphorylation sites that are identified in protein complexes.

S3 Table. The domains within or nearby of the rhythmic phosphosites with unknown function, and only phosphosites identified in protein complexes are included.

S1 File. Targeted metabolomics of NRF and DRF mouse liver for hexosamine biosynthetic pathway (HBP). Peak intensities of metabolites detected using GC-MS and calculated concentration of HBP metabolites.

S2 File. Nuclear label-free O-GlcNAc proteome of NRF mouse liver. Rhythmicity test of O-GlcNAc proteome.

S3 File. Nuclear proteome of NRF mouse liver. Peptide counts and rhythmicity analysis of nuclear proteome.

S4 File. Protein complex analysis for rhythmic label-free global O-GlcNAc proteome. List of protein complexes that contain rhythmically O-GlcNAcylated proteins, with the rhythmic subunits and the function of protein complexes indicated.

S5 File. Nuclear TMT site-specific O-GlcNAc proteome. Normalize peptide counts and t test of nuclear O-GlcNAc proteome in NRF and DRF mouse liver.

S6 File. Nuclear phosphoproteome of NRF mouse liver. (Tab 1) Normalized peptide counts and rhythmicity analysis of nuclear phosphoproteome. (Tab 2) Peptide-Spectrum Match (PSM) of TMT phosphoproteome for evaluating the quality of data.

S7 File. Comparison between our phosphoproteomics dataset and published rhythmic phosphoproteome. (Tab 1) Newly identified rhythmic phosphosites in our study. (Tab 2) Common rhythmic phosphosites in our and published studies.

S8 File. Rhythmic kinases detected in proteomic, phosphoproteomic and O-GlcNAc proteomic datasets. (Tab 1-3) Lists of kinases and their rhythmicity analysis from our proteomic, phosphoproteomics and O-GlcNAc proteomic datasets, respectively.

S9 File. Protein complex analysis for rhythmic phosphoproteome. List of protein complexes that contain rhythmically phosphorylated proteins, with the rhythmic subunits and the function of protein complexes indicated.

S10 File. Analysis for G-P interaction. (Tab 1) List of proteins with potential G-P interplay predicted by G-P interplay motif analysis using the rhythmic phosphosites as reference. (Tab 2) Predicted G-P interplay sites in close proximity (<10 amino acid) by comparing site-specific O-GlcNAc proteomics and phosphoproteomics.

1514 **Supporting information references**

1515

1516 1. Robles MS, Humphrey SJ, Mann M. Phosphorylation Is a Central Mechanism for Circadian Control of
1517 Metabolism and Physiology. Cell Metabolism. 2017;25: 118–127. doi:10.1016/j.cmet.2016.10.004

1518 2. Wang J, Mauvoisin D, Martin E, Atger F, Galindo AN, Dayon L, et al. Nuclear Proteomics Uncovers
1519 Diurnal Regulatory Landscapes in Mouse Liver. Cell Metabolism. 2017;25: 102–117.
1520 doi:10.1016/j.cmet.2016.10.003

1521 3. Panda S. Circadian physiology of metabolism. Science. 2016;354: 1008–1015.
1522 doi:10.1126/science.aah4967

1523 4. Huang R, Chen J, Zhou M, Xin H, Lam SM, Jiang X, et al. Multi-omics profiling reveals rhythmic
1524 liver function shaped by meal timing. Nat Commun. 2023;14: 6086. doi:10.1038/s41467-023-
1525 41759-9

1526 5. Wang Y, Song L, Liu M, Ge R, Zhou Q, Liu W, et al. A proteomics landscape of circadian clock in
1527 mouse liver. Nat Commun. 2018;9: 1553. doi:10.1038/s41467-018-03898-2

1528 6. Pflum MK, Tong JK, Lane WS, Schreiber SL. Histone deacetylase 1 phosphorylation promotes
1529 enzymatic activity and complex formation. J Biol Chem. 2001;276: 47733–47741.
1530 doi:10.1074/jbc.M105590200

1531 7. Kwak Y, Jeong J, Lee S, Park Y-U, Lee S-A, Han D-H, et al. Cyclin-dependent kinase 5 (Cdk5)
1532 regulates the function of CLOCK protein by direct phosphorylation. J Biol Chem. 2013;288:
1533 36878–36889. doi:10.1074/jbc.M113.494856

1534 8. Spengler ML, Kuropatwinski KK, Schumer M, Antoch MP. A serine cluster mediates BMAL1-
1535 dependent CLOCK phosphorylation and degradation. Cell Cycle. 2009;8: 4138–4146.
1536 doi:10.4161/cc.8.24.10273

1537 9. Luciano AK, Zhou W, Santana JM, Kyriakides C, Velazquez H, Sessa WC. CLOCK phosphorylation
1538 by AKT regulates its nuclear accumulation and circadian gene expression in peripheral tissues. J
1539 Biol Chem. 2018;293: 9126–9136. doi:10.1074/jbc.RA117.000773

1540 10. Farkas T, Hansen K, Holm K, Lukas J, Bartek J. Distinct phosphorylation events regulate p130- and
1541 p107-mediated repression of E2F-4. J Biol Chem. 2002;277: 26741–26752.
1542 doi:10.1074/jbc.M200381200

1543 11. Heyd F, Lynch KW. Phosphorylation-dependent regulation of PSF by GSK3 controls CD45
1544 alternative splicing. Mol Cell. 2010;40: 126–137. doi:10.1016/j.molcel.2010.09.013

1545

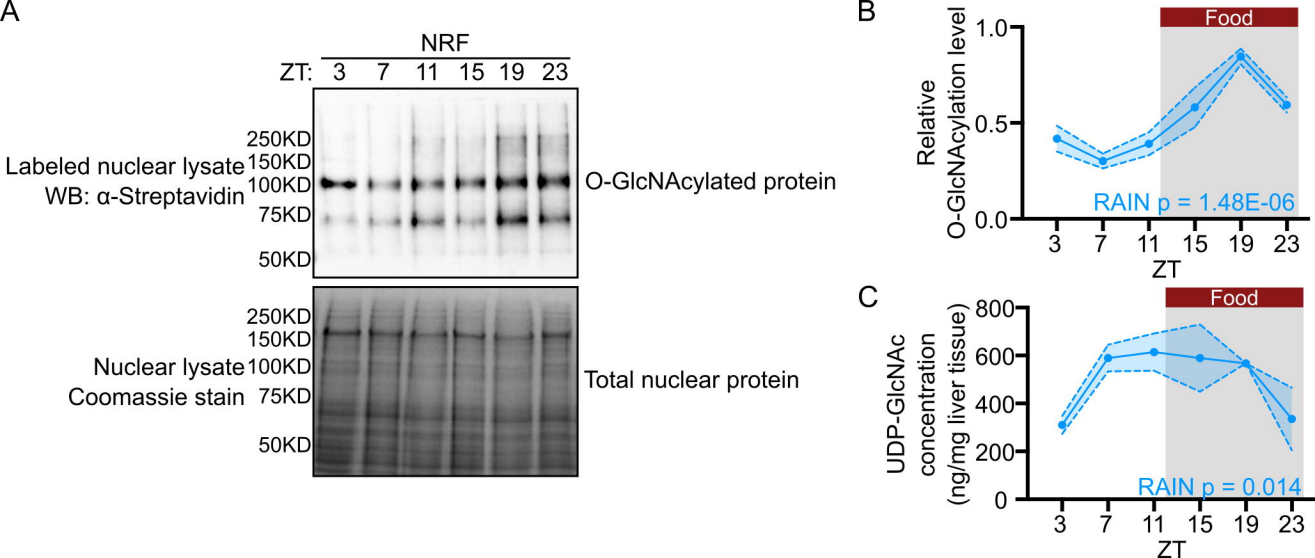
A
NRF
ZT: 3 7 11 15 19 23
250KD
150KD
100KD
75KD
50KD
Labeled nuclear lysate
WB: α-Streptavidin
O-GlcNAcylated protein
Nuclear lysate
Coomassie stain
Total nuclear protein
B
Food
Relative O-GlcNAcylation level
1.0
0.5
0.0
RAIN p = 1.48E-06
3 7 11 15 19 23
ZT
C
Food
UDP-GlcNAc concentration (ng/mg liver tissue)
800
600
400
200
0
RAIN p = 0.014
3 7 11 15 19 23
ZT

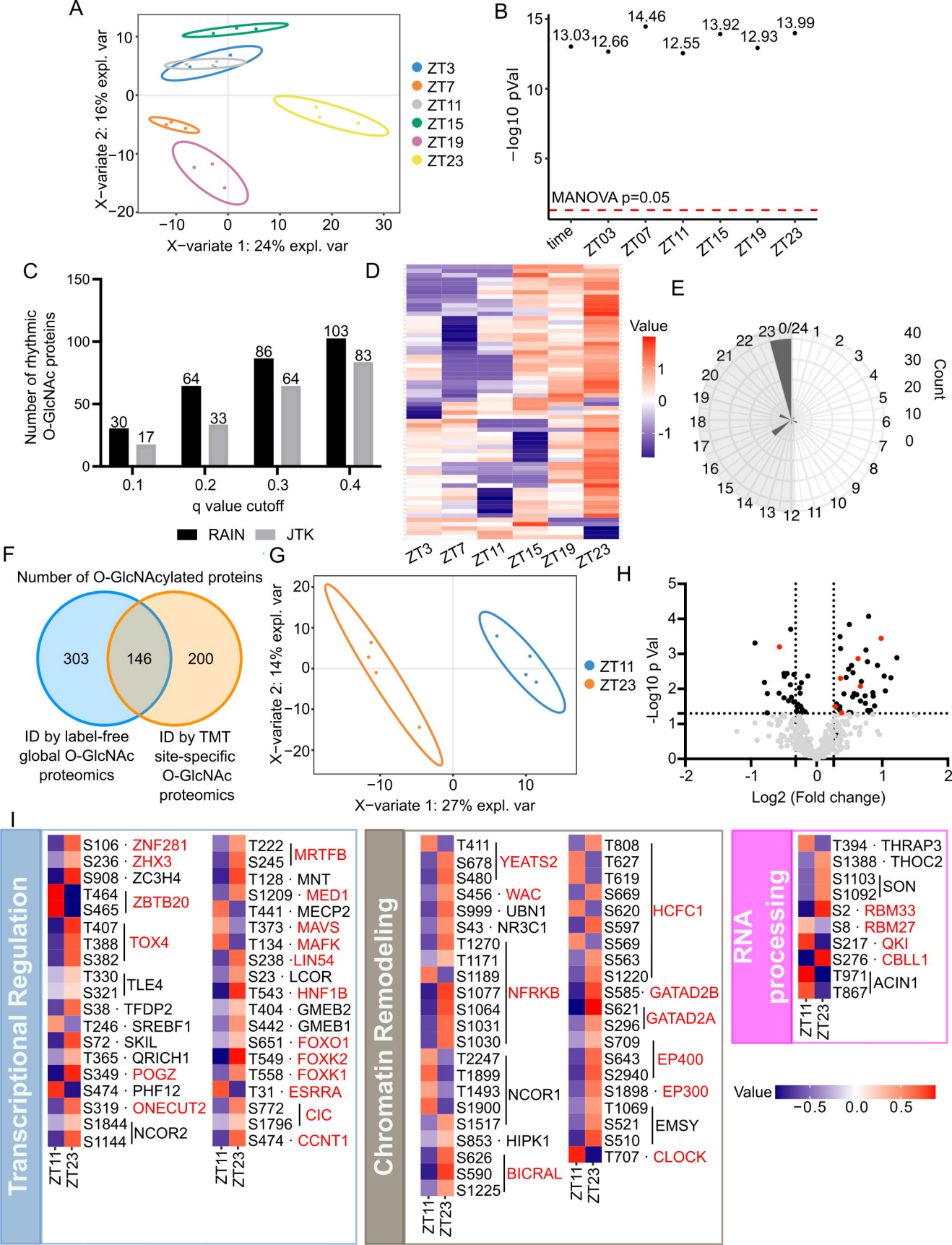
A
X−variate 2: 16% expl. var
X−variate 1: 24% expl. var
ZT3
ZT7
ZT11
ZT15
ZT19
ZT23
B
−log10 pVal
MANOVA p=0.05
13.03
12.66
14.46
12.55
13.92
12.93
13.99
time
ZT03
ZT07
ZT11
ZT15
ZT19
ZT23
C
Number of rhythmic O-GlcNAc proteins
q value cutoff
RAIN
JTK
30
17
64
33
86
64
103
83
D
Value
ZT3
ZT7
ZT11
ZT15
ZT19
ZT23
E
Count
F
Number of O-GlcNAcylated proteins
303
146
200
ID by label-free global O-GlcNAc proteomics
ID by TMT site-specific O-GlcNAc proteomics
G
X−variate 2: 14% expl. var
X−variate 1: 27% expl. var
ZT11
ZT23
H
-Log10 p Val
Log2 (Fold change)
I
Transcriptional Regulation
S106 · ZNF281
S236 · ZHX3
S908 · ZC3H4
T464
S465
ZBTB20
T407
T388
S382
TOX4
T330
S321
TLE4
S38 · TFDP2
T246 · SREBF1
S72 · SKIL
T365 · QRICH1
S349 · POGZ
S474 · PHF12
S319 · ONECUT2
S1844
S1144
NCOR2
T222
S245
MRTFB
T128 · MNT
S1209 · MED1
T441 · MECP2
T373 · MAVS
T134 · MAFK
S238 · LIN54
S23 · LCOR
T543 · HNF1B
T404 · GMEB2
S442 · GMEB1
S651 · FOXO1
T549 · FOXK2
T558 · FOXK1
T31 · ESRRA
S772
S1796
CIC
S474 · CCNT1
ZT11
ZT23
Chromatin Remodeling
T411
S678
S480
YEATS2
S456 · WAC
S999 · UBN1
S43 · NR3C1
T1270
T1171
S1189
S1077
S1064
S1031
S1030
NFRKB
T2247
T1899
T1493
S1900
S1517
NCOR1
S853 · HIPK1
S626
S590
S1225
BICRAL
T808
T627
T619
S669
S620
S597
S569
S563
S1220
HCFC1
S585 · GATAD2B
S621
S296
GATAD2A
S709
S643
S2940
EP400
S1898 · EP300
T1069
S521
S510
EMSY
T707 · CLOCK
RNA processing
T394 · THRAP3
S1388 · THOC2
S1103
S1092
SON
S2 · RBM33
S8 · RBM27
S217 · QKI
S276 · CBLL1
T971
T867
ACIN1
Value
−0.5
0.0
0.5

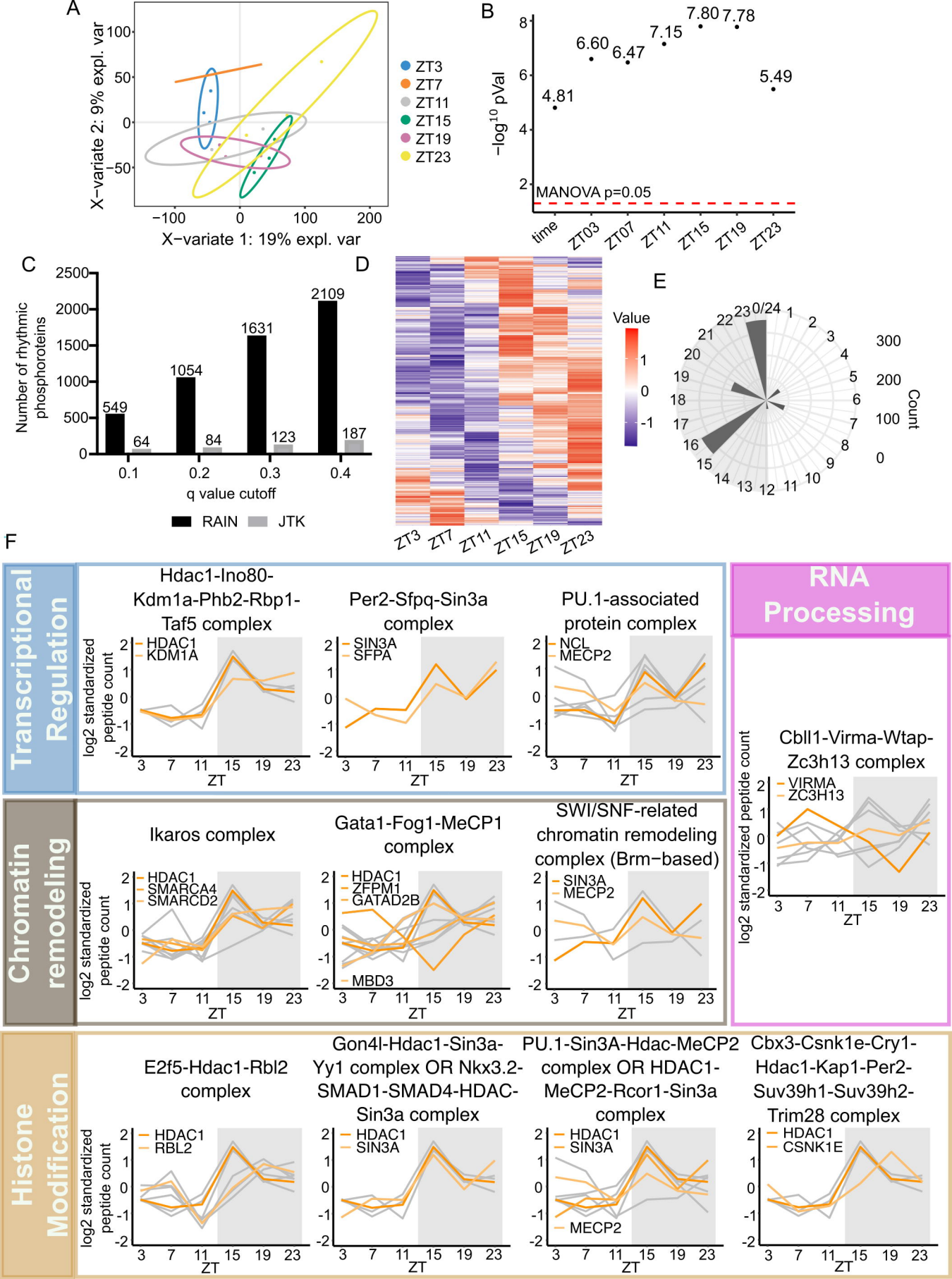
A
X−variate 2: 9% expl. var
X−variate 1: 19% expl. var
ZT3
ZT7
ZT11
ZT15
ZT19
ZT23
B
−log10 pVal
MANOVA p=0.05
4.81
6.60
6.47
7.15
7.80
7.78
5.49
time
ZT03
ZT07
ZT11
ZT15
ZT19
ZT23
C
Number of rhythmic phosphoroteins
549
64
1054
84
1631
123
2109
187
q value cutoff
RAIN
JTK
D
Value
ZT3
ZT7
ZT11
ZT15
ZT19
ZT23
E
Count
F
Transcriptional Regulation
Hdac1-Ino80-Kdm1a-Phb2-Rbp1-Taf5 complex
HDAC1
KDM1A
Per2-Sfpq-Sin3a complex
SIN3A
SFPA
PU.1-associated protein complex
NCL
MECP2
log2 standardized peptide count
ZT
Chromatin remodeling
Ikaros complex
HDAC1
SMARCA4
SMARCD2
Gata1-Fog1-MeCP1 complex
HDAC1
ZFPM1
GATAD2B
MBD3
SWI/SNF-related chromatin remodeling complex (Brm−based)
SIN3A
MECP2
RNA Processing
Cbll1-Virma-Wtap-Zc3h13 complex
VIRMA
ZC3H13
Histone Modification
E2f5-Hdac1-Rbl2 complex
HDAC1
RBL2
Gon4l-Hdac1-Sin3a-Yy1 complex OR Nkx3.2-SMAD1-SMAD4-HDAC-Sin3a complex
HDAC1
SIN3A
PU.1-Sin3A-Hdac-MeCP2 complex OR HDAC1-MeCP2-Rcor1-Sin3a complex
HDAC1
SIN3A
MECP2
Cbx3-Csnk1e-Cry1-Hdac1-Kap1-Per2-Suv39h1-Suv39h2-Trim28 complex
HDAC1
CSNK1E

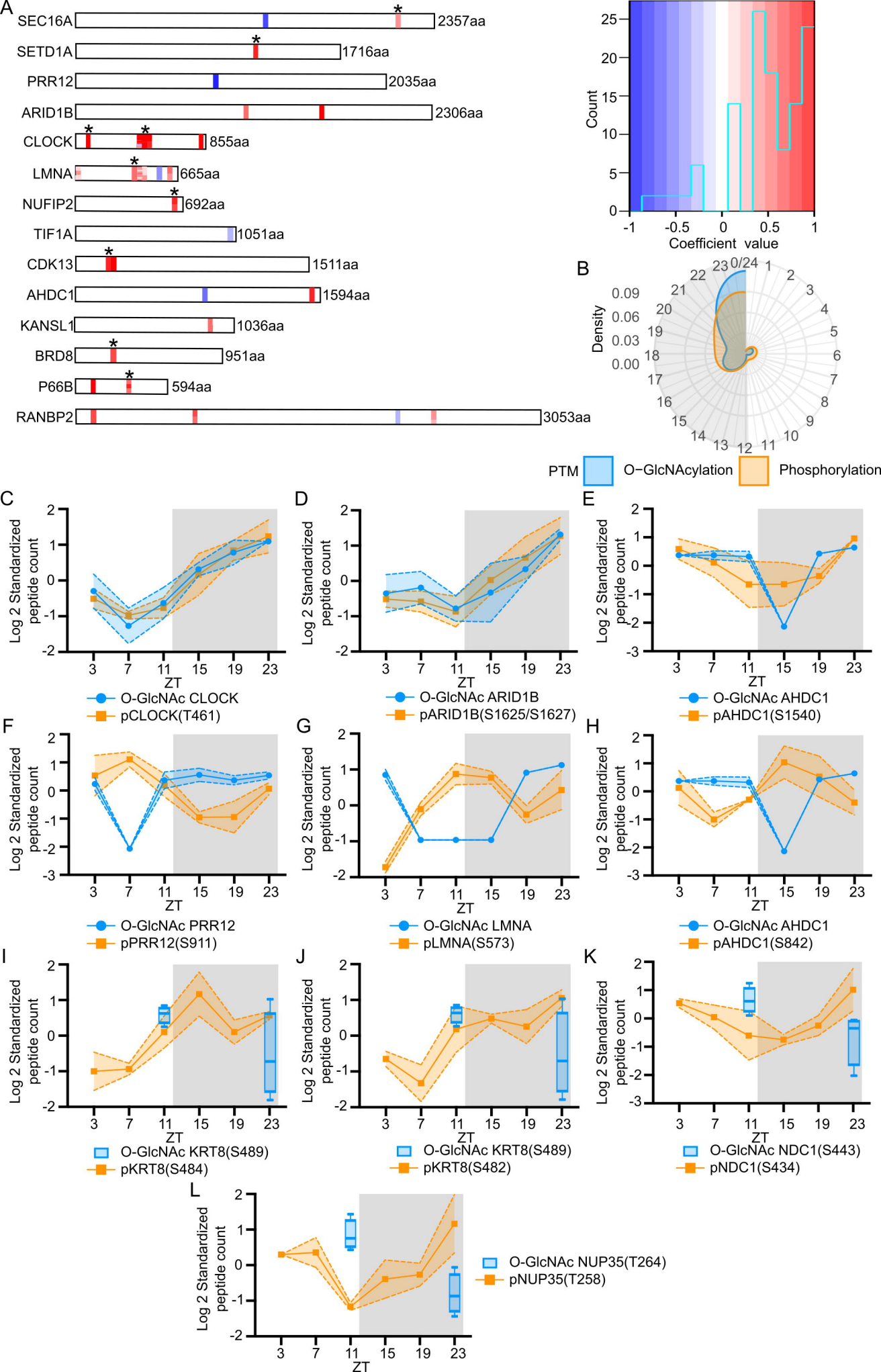
A
SEC16A
2357aa
SETD1A
1716aa
PRR12
2035aa
ARID1B
2306aa
CLOCK
855aa
LMNA
665aa
NUFIP2
692aa
TIF1A
1051aa
CDK13
1511aa
AHDC1
1594aa
KANSL1
1036aa
BRD8
951aa
P66B
594aa
RANBP2
3053aa
Count
Coefficient value
B
Density
PTM
O−GlcNAcylation
Phosphorylation
C
O-GlcNAc CLOCK
pCLOCK(T461)
D
O-GlcNAc ARID1B
pARID1B(S1625/S1627)
E
O-GlcNAc AHDC1
pAHDC1(S1540)
F
O-GlcNAc PRR12
pPRR12(S911)
G
O-GlcNAc LMNA
pLMNA(S573)
H
O-GlcNAc AHDC1
pAHDC1(S842)
I
O-GlcNAc KRT8(S489)
pKRT8(S484)
J
O-GlcNAc KRT8(S489)
pKRT8(S482)
K
O-GlcNAc NDC1(S443)
pNDC1(S434)
L
O-GlcNAc NUP35(T264)
pNUP35(T258)
Log 2 Standardized peptide count
ZT

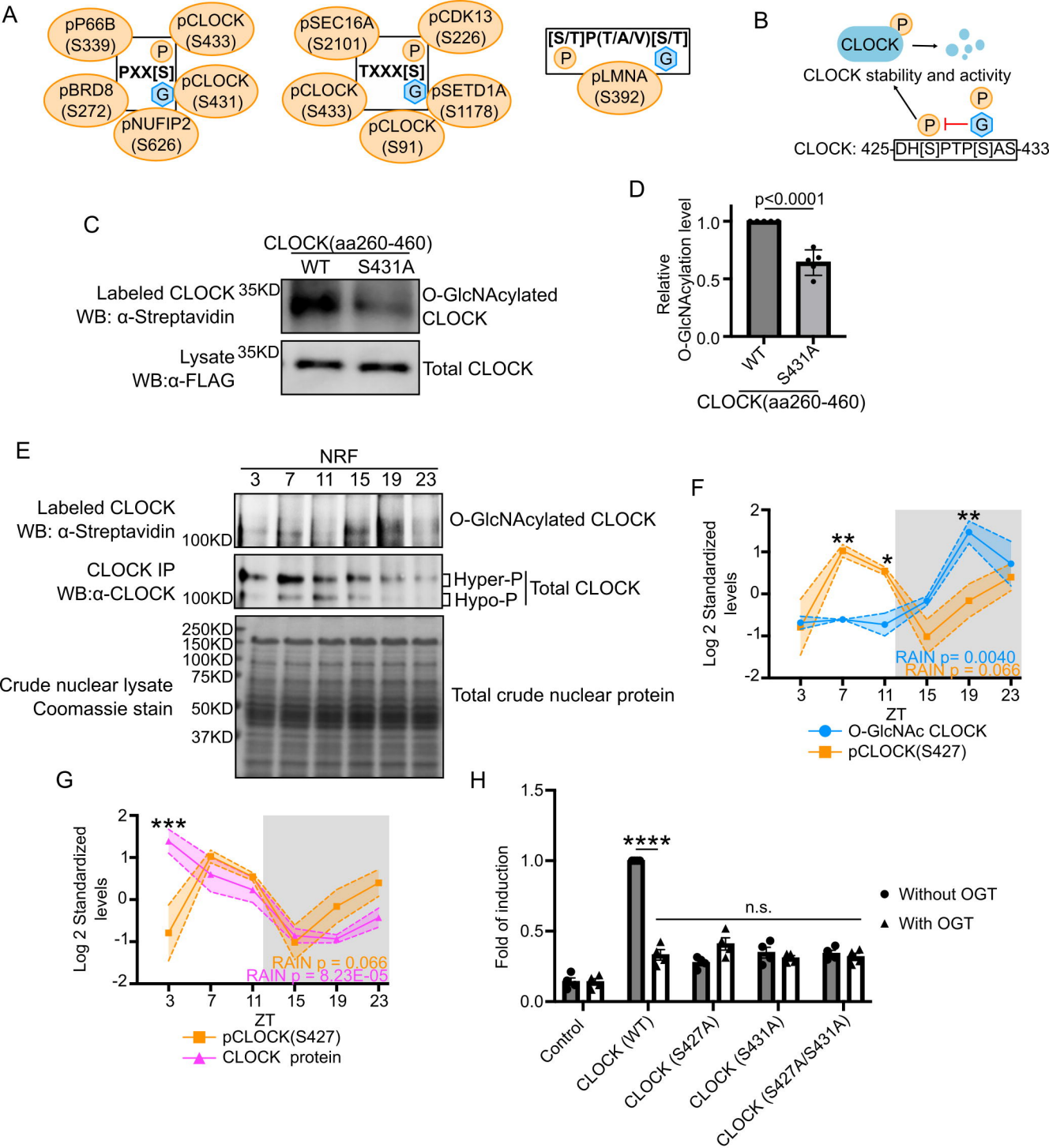
A
pP66B (S339)
pCLOCK (S433)
P
PXX[S]
G
pBRD8 (S272)
pCLOCK (S431)
pNUFIP2 (S626)
pSEC16A (S2101)
pCDK13 (S226)
P
TXXX[S]
G
pCLOCK (S433)
pSETD1A (S1178)
pCLOCK (S91)
[S/T]P(T/A/V)[S/T]
P
G
pLMNA (S392)
B
CLOCK
P
CLOCK stability and activity
P
P
G
CLOCK: 425-DH[S]PTP[S]AS-433
C
CLOCK(aa260-460)
WT
S431A
Labeled CLOCK
WB: α-Streptavidin
35KD
O-GlcNAcylated CLOCK
Lysate
WB:α-FLAG
35KD
Total CLOCK
D
p<0.0001
Relative O-GlcNAcylation level
1.0
0.5
0.0
WT
S431A
CLOCK(aa260-460)
E
NRF
3
7
11
15
19
23
Labeled CLOCK
WB: α-Streptavidin
100KD
O-GlcNAcylated CLOCK
CLOCK IP
WB:α-CLOCK
100KD
Hyper-P
Hypo-P
Total CLOCK
250KD
150KD
100KD
75KD
50KD
37KD
Crude nuclear lysate
Coomassie stain
Total crude nuclear protein
F
Log 2 Standardized levels
2
1
0
-1
-2
**
*
**
RAIN p= 0.0040
RAIN p = 0.066
3
7
11
15
19
23
ZT
O-GlcNAc CLOCK
pCLOCK(S427)
G
Log 2 Standardized levels
2
1
0
-1
-2
***
RAIN p = 0.066
RAIN p = 8.23E-05
3
7
11
15
19
23
ZT
pCLOCK(S427)
CLOCK protein
H
Fold of induction
1.5
1.0
0.5
0.0
****
n.s.
Without OGT
With OGT
Control
CLOCK (WT)
CLOCK (S427A)
CLOCK (S431A)
CLOCK (S427A/S431A)

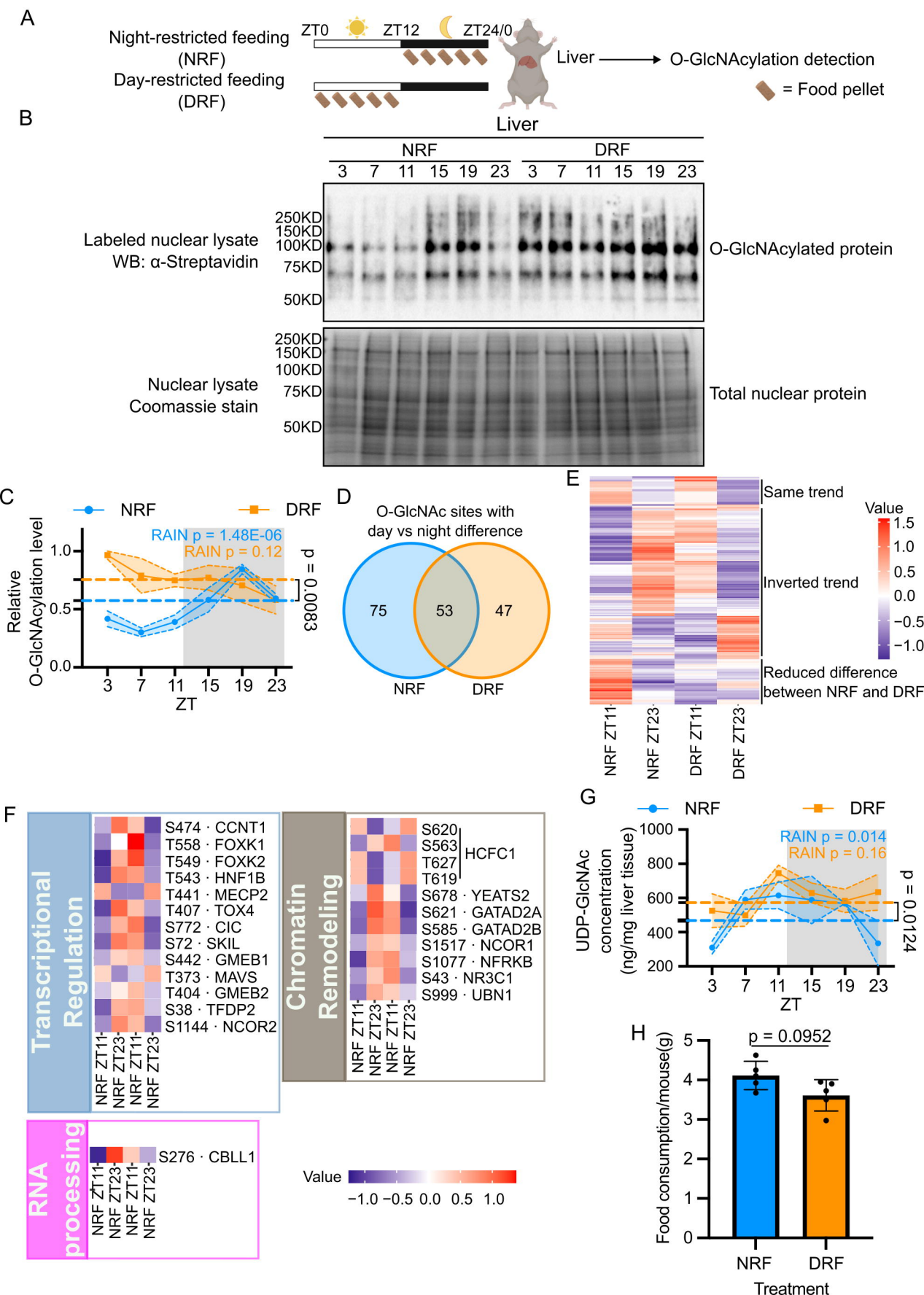
A
Night-restricted feeding (NRF)
Day-restricted feeding (DRF)
ZT0
ZT12
ZT24/0
Liver
O-GlcNAcylation detection
= Food pellet
B
Liver
NRF
DRF
3 7 11 15 19 23 3 7 11 15 19 23
Labeled nuclear lysate
WB: α-Streptavidin
250KD
150KD
100KD
75KD
50KD
O-GlcNAcylated protein
Nuclear lysate
Coomassie stain
Total nuclear protein
C
NRF
DRF
RAIN p = 1.48E-06
RAIN p = 0.12
p = 0.0083
Relative O-GlcNAcylation level
ZT
D
O-GlcNAc sites with day vs night difference
75
53
47
NRF
DRF
E
Same trend
Inverted trend
Reduced difference between NRF and DRF
Value
NRF ZT11
NRF ZT23
DRF ZT11
DRF ZT23
F
Transcriptional Regulation
S474 · CCNT1
T558 · FOXK1
T549 · FOXK2
T543 · HNF1B
T441 · MECP2
T407 · TOX4
S772 · CIC
S72 · SKIL
S442 · GMEB1
T373 · MAVS
T404 · GMEB2
S38 · TFDP2
S1144 · NCOR2
Chromatin Remodeling
S620
S563
T627
T619
HCFC1
S678 · YEATS2
S621 · GATAD2A
S585 · GATAD2B
S1517 · NCOR1
S1077 · NFRKB
S43 · NR3C1
S999 · UBN1
RNA processing
S276 · CBLL1
Value
G
NRF
DRF
RAIN p = 0.014
RAIN p = 0.16
p = 0.0124
UDP-GlcNAc concentration (ng/mg liver tissue)
ZT
H
p = 0.0952
Food consumption/mouse(g)
NRF
DRF
Treatment

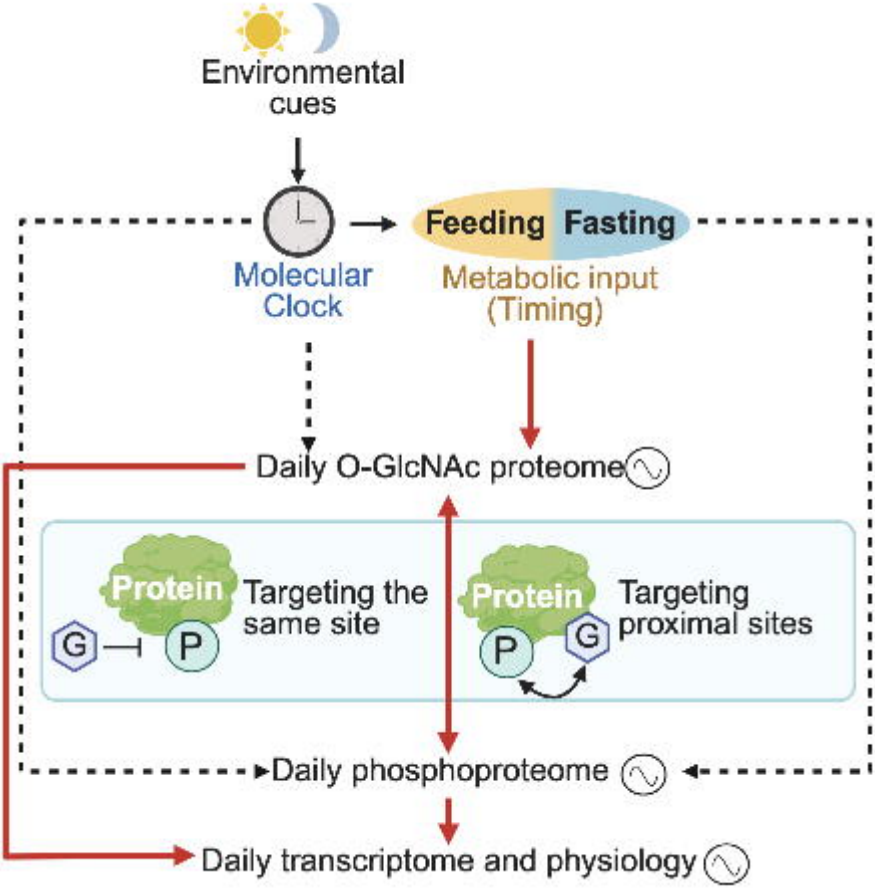
Environmental cues
Molecular Clock
Feeding
Fasting
Metabolic input (Timing)
Daily O-GlcNAc proteome
Protein
G
P
Targeting the same site
Protein
P
G
Targeting proximal sites
Daily phosphoproteome
Daily transcriptome and physiology

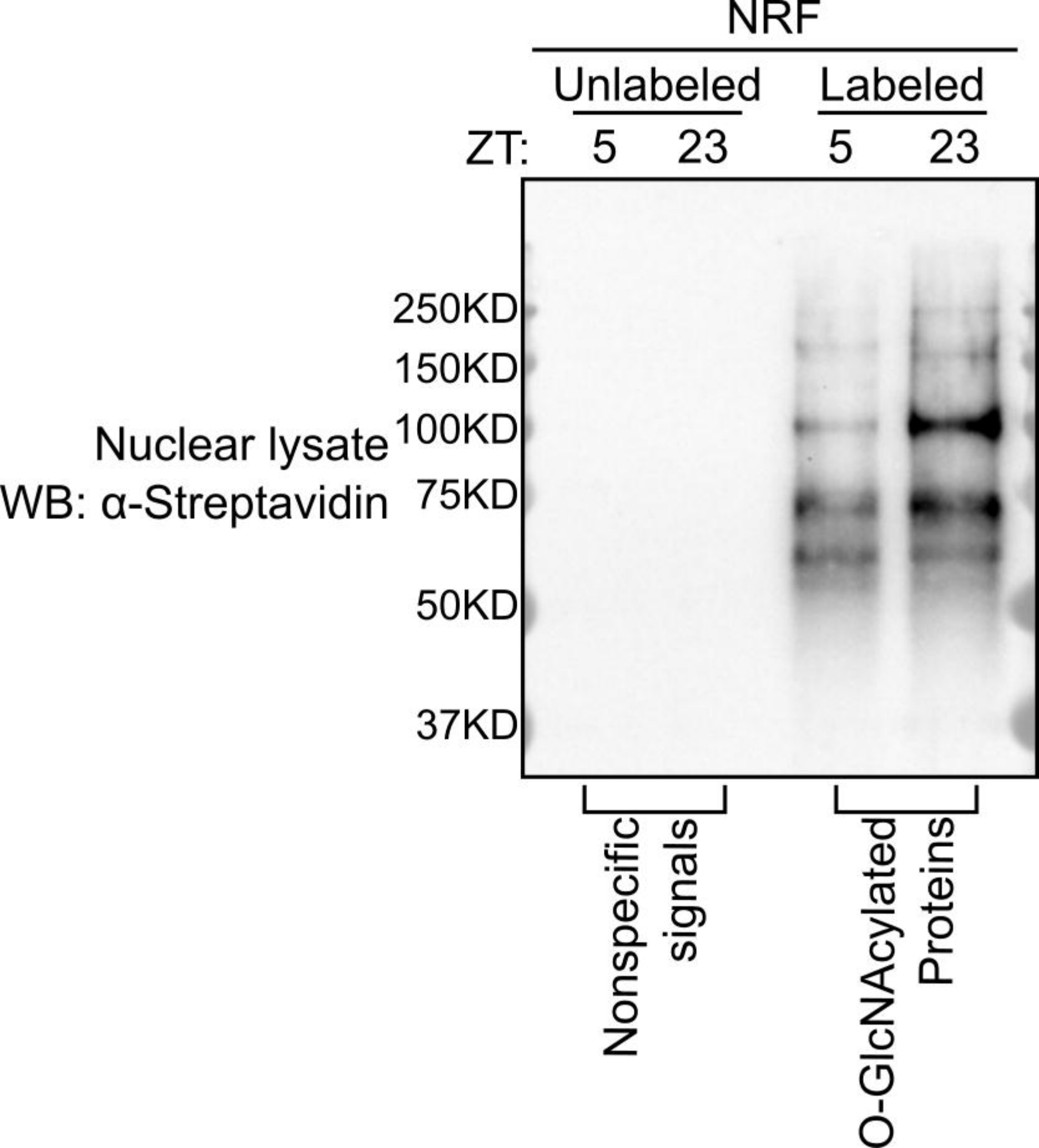
NRF
Unlabeled
Labeled
ZT:
5
23
5
23
250KD
150KD
100KD
75KD
50KD
37KD
Nuclear lysate
WB: α-Streptavidin
Nonspecific signals
O-GlcNAcylated Proteins

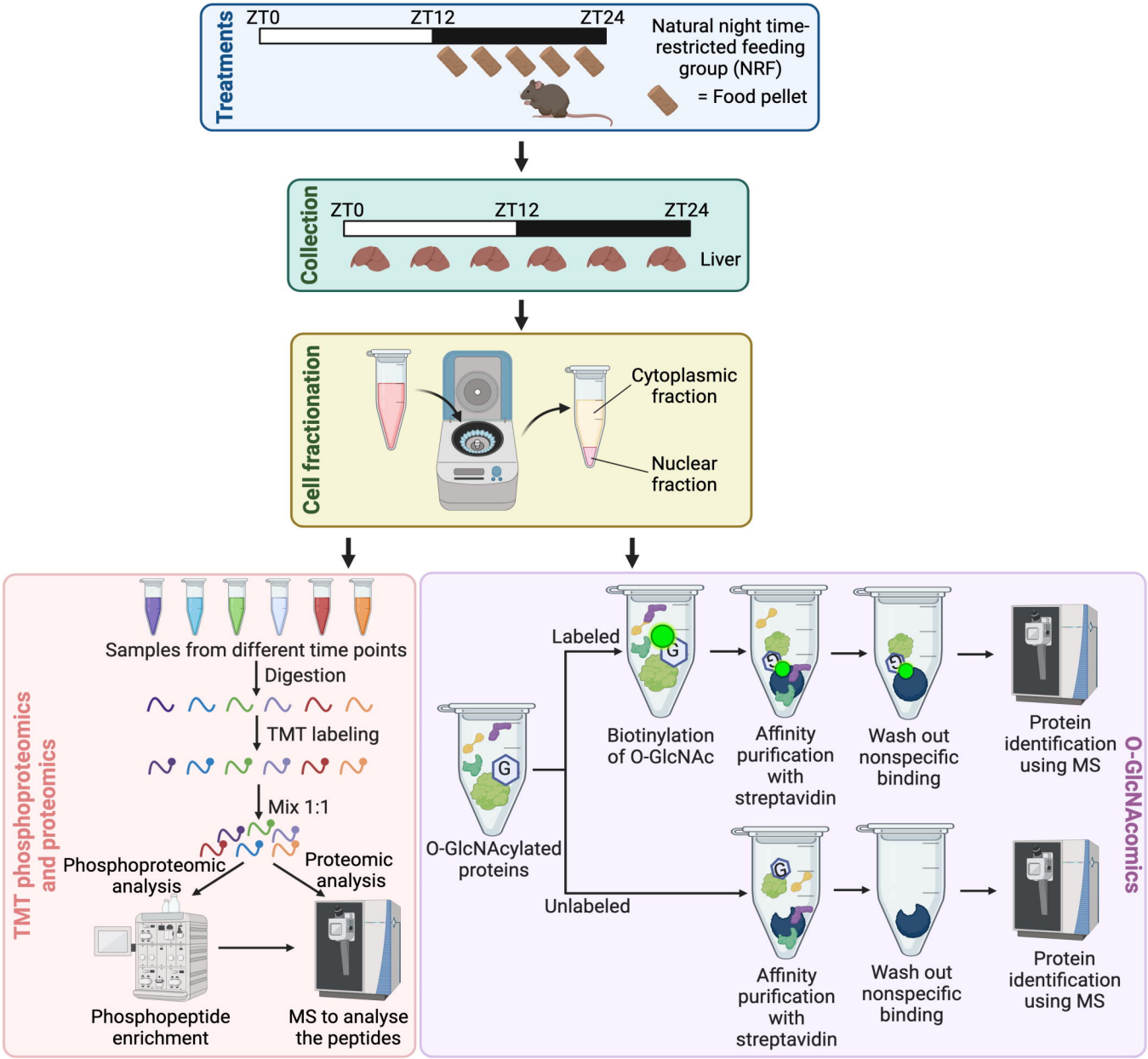
Treatments
ZT0
ZT12
ZT24
Natural night time-restricted feeding group (NRF)
= Food pellet
Collection
ZT0
ZT12
ZT24
Liver
Cell fractionation
Cytoplasmic fraction
Nuclear fraction
TMT phosphoproteomics and proteomics
Samples from different time points
Digestion
TMT labeling
Mix 1:1
Phosphoproteomic analysis
Proteomic analysis
Phosphopeptide enrichment
MS to analyse the peptides
O-GlcNAcomics
O-GlcNAcylated proteins
Labeled
Biotinylation of O-GlcNAc
Affinity purification with streptavidin
Wash out nonspecific binding
Protein identification using MS
Unlabeled
Affinity purification with streptavidin
Wash out nonspecific binding
Protein identification using MS

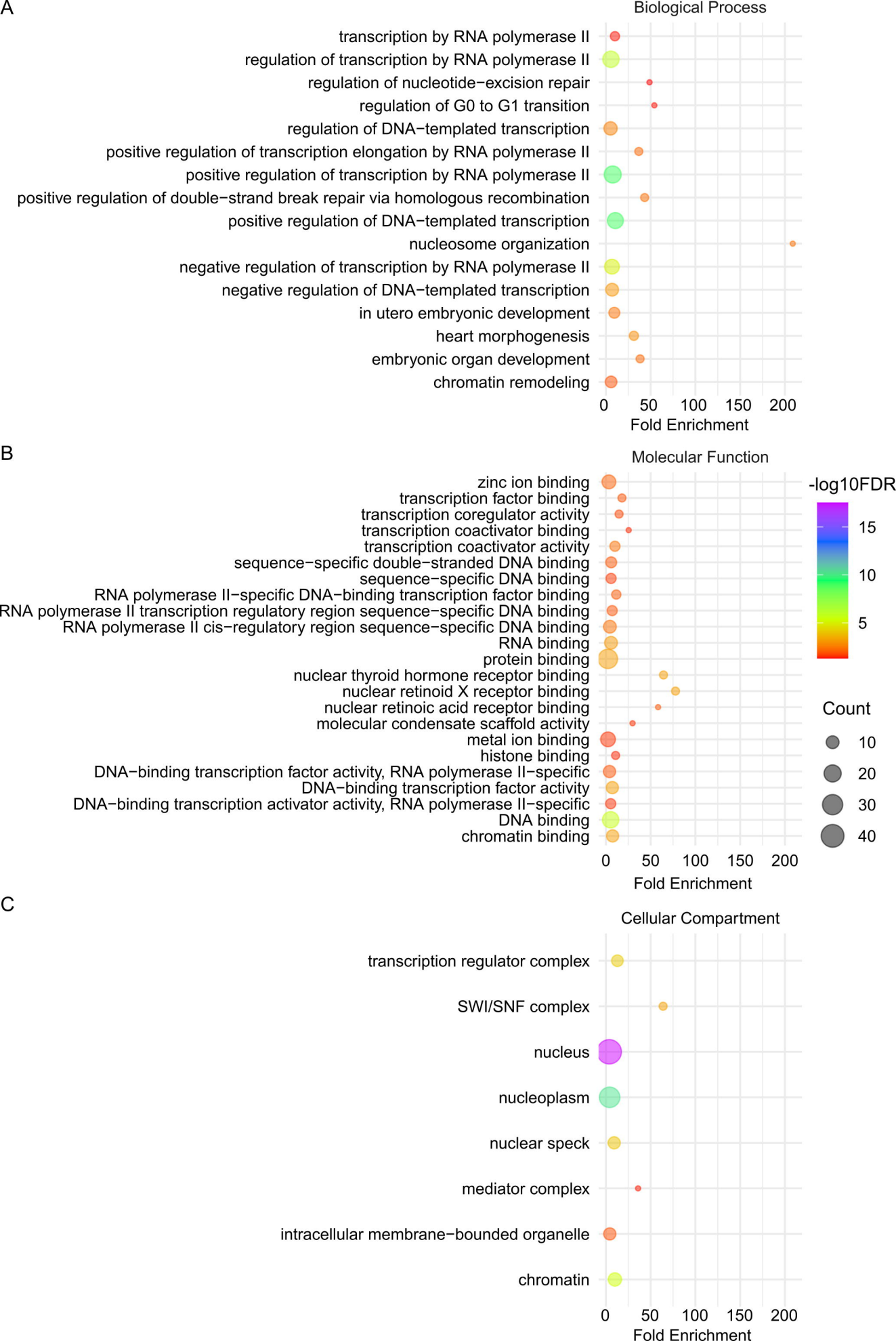
A
Biological Process
transcription by RNA polymerase II
regulation of transcription by RNA polymerase II
regulation of nucleotide−excision repair
regulation of G0 to G1 transition
regulation of DNA−templated transcription
positive regulation of transcription elongation by RNA polymerase II
positive regulation of transcription by RNA polymerase II
positive regulation of double−strand break repair via homologous recombination
positive regulation of DNA−templated transcription
nucleosome organization
negative regulation of transcription by RNA polymerase II
negative regulation of DNA−templated transcription
in utero embryonic development
heart morphogenesis
embryonic organ development
chromatin remodeling
0
50
100
150
200
Fold Enrichment
B
Molecular Function
zinc ion binding
transcription factor binding
transcription coregulator activity
transcription coactivator binding
transcription coactivator activity
sequence−specific double−stranded DNA binding
sequence−specific DNA binding
RNA polymerase II−specific DNA−binding transcription factor binding
RNA polymerase II transcription regulatory region sequence−specific DNA binding
RNA polymerase II cis−regulatory region sequence−specific DNA binding
RNA binding
protein binding
nuclear thyroid hormone receptor binding
nuclear retinoid X receptor binding
nuclear retinoic acid receptor binding
molecular condensate scaffold activity
metal ion binding
histone binding
DNA−binding transcription factor activity, RNA polymerase II−specific
DNA−binding transcription factor activity
DNA−binding transcription activator activity, RNA polymerase II−specific
DNA binding
chromatin binding
0
50
100
150
200
Fold Enrichment
-log10FDR
15
10
5
Count
10
20
30
40
C
Cellular Compartment
transcription regulator complex
SWI/SNF complex
nucleus
nucleoplasm
nuclear speck
mediator complex
intracellular membrane−bounded organelle
chromatin
0
50
100
150
200
Fold Enrichment

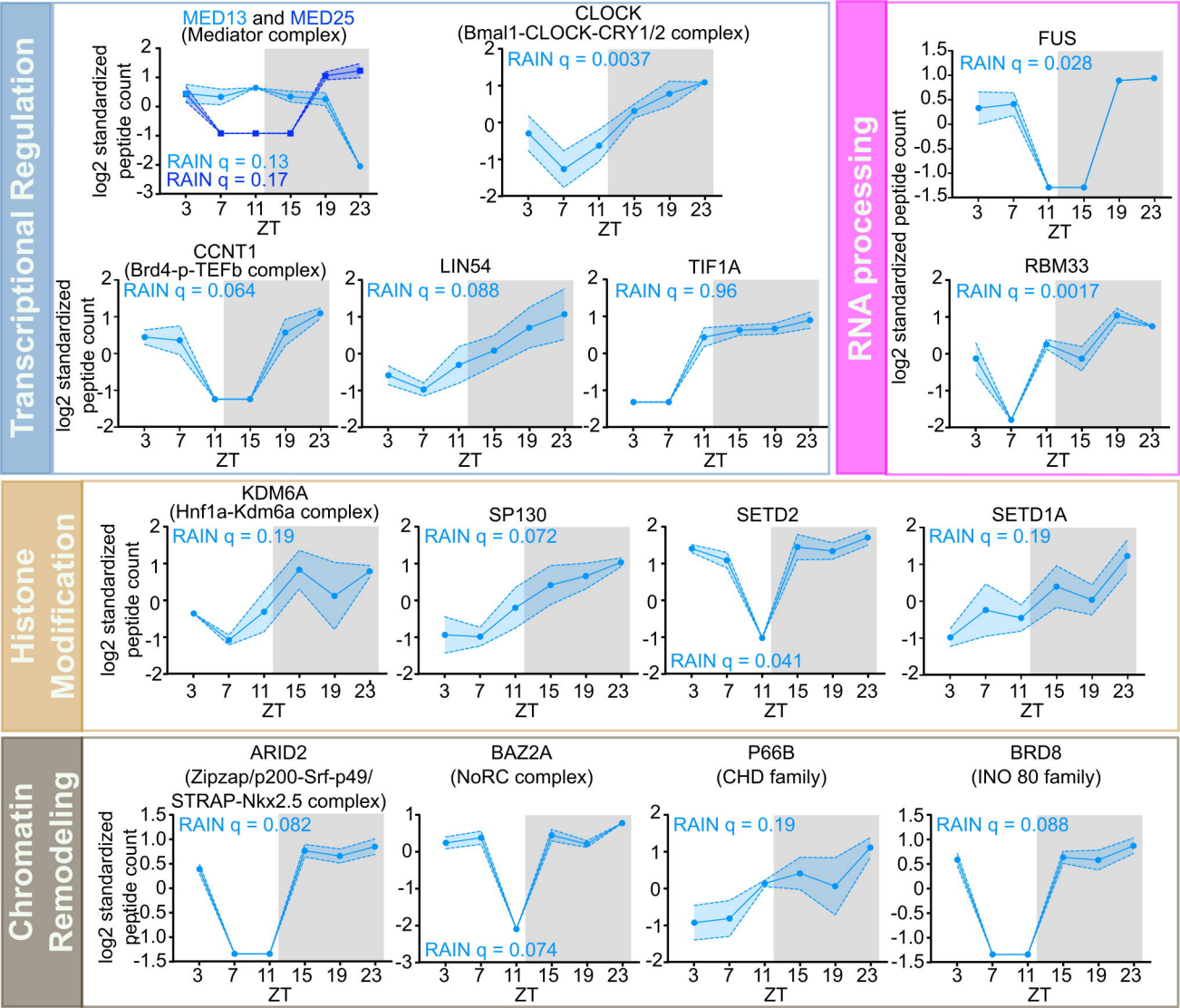
Transcriptional Regulation
MED13 and MED25
(Mediator complex)
RAIN q = 0.13
RAIN q = 0.17
CLOCK
(Bmal1-CLOCK-CRY1/2 complex)
RAIN q = 0.0037
CCNT1
(Brd4-p-TEFb complex)
RAIN q = 0.064
LIN54
RAIN q = 0.088
TIF1A
RAIN q = 0.96
RNA processing
FUS
RAIN q = 0.028
RBM33
RAIN q = 0.0017
Histone Modification
KDM6A
(Hnf1a-Kdm6a complex)
RAIN q = 0.19
SP130
RAIN q = 0.072
SETD2
RAIN q = 0.041
SETD1A
RAIN q = 0.19
Chromatin Remodeling
ARID2
(Zipzap/p200-Srf-p49/
STRAP-Nkx2.5 complex)
RAIN q = 0.082
BAZ2A
(NoRC complex)
RAIN q = 0.074
P66B
(CHD family)
RAIN q = 0.19
BRD8
(INO 80 family)
RAIN q = 0.088
log2 standardized peptide count
ZT

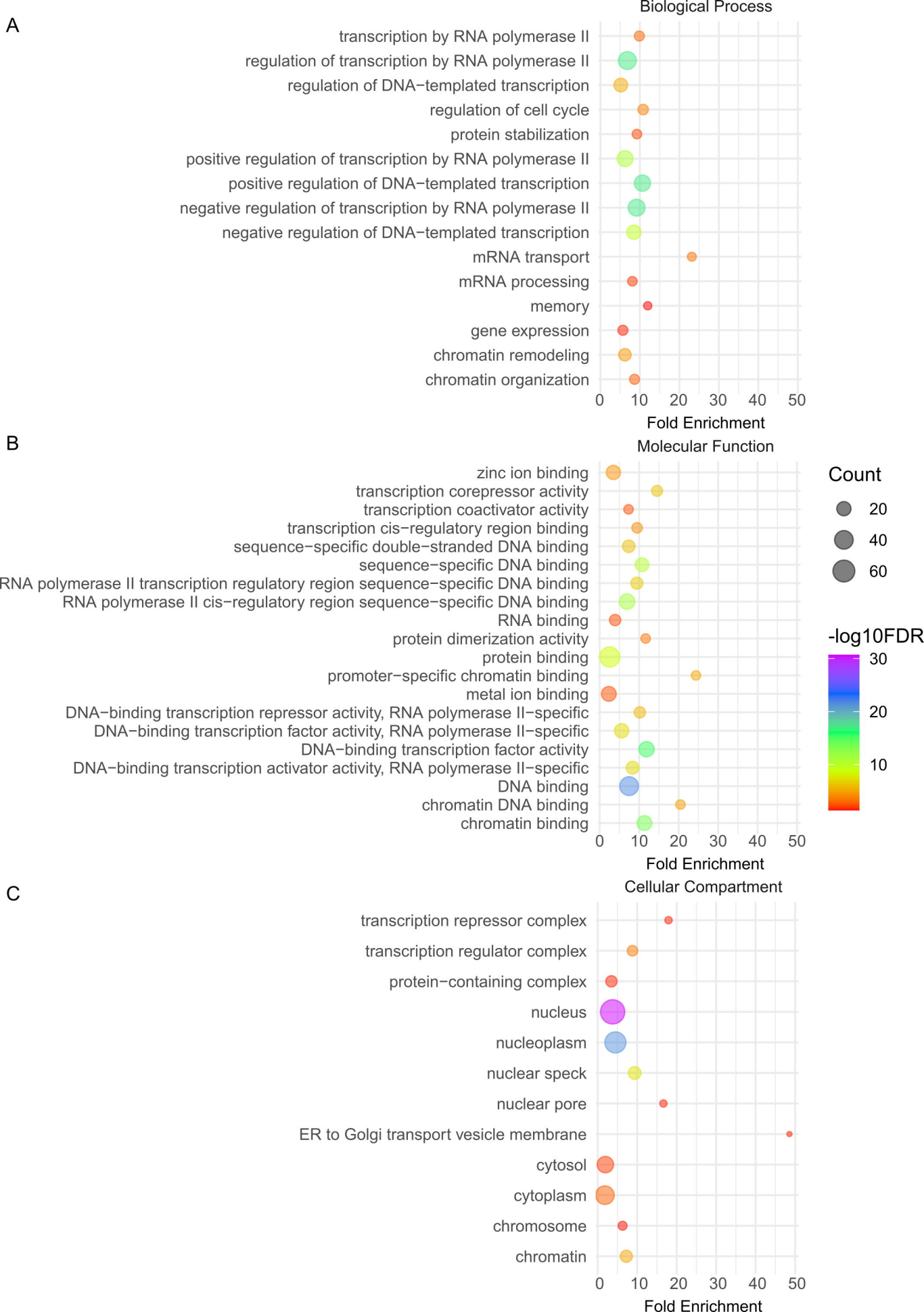
A
Biological Process
transcription by RNA polymerase II
regulation of transcription by RNA polymerase II
regulation of DNA−templated transcription
regulation of cell cycle
protein stabilization
positive regulation of transcription by RNA polymerase II
positive regulation of DNA−templated transcription
negative regulation of transcription by RNA polymerase II
negative regulation of DNA−templated transcription
mRNA transport
mRNA processing
memory
gene expression
chromatin remodeling
chromatin organization
0 10 20 30 40 50
Fold Enrichment
B
Molecular Function
zinc ion binding
transcription corepressor activity
transcription coactivator activity
transcription cis−regulatory region binding
sequence−specific double−stranded DNA binding
sequence−specific DNA binding
RNA polymerase II transcription regulatory region sequence−specific DNA binding
RNA polymerase II cis−regulatory region sequence−specific DNA binding
RNA binding
protein dimerization activity
protein binding
promoter−specific chromatin binding
metal ion binding
DNA−binding transcription repressor activity, RNA polymerase II−specific
DNA−binding transcription factor activity, RNA polymerase II−specific
DNA−binding transcription factor activity
DNA−binding transcription activator activity, RNA polymerase II−specific
DNA binding
chromatin DNA binding
chromatin binding
0 10 20 30 40 50
Fold Enrichment
Count
20
40
60
-log10FDR
30
20
10
C
Cellular Compartment
transcription repressor complex
transcription regulator complex
protein−containing complex
nucleus
nucleoplasm
nuclear speck
nuclear pore
ER to Golgi transport vesicle membrane
cytosol
cytoplasm
chromosome
chromatin
0 10 20 30 40 50
Fold Enrichment

A

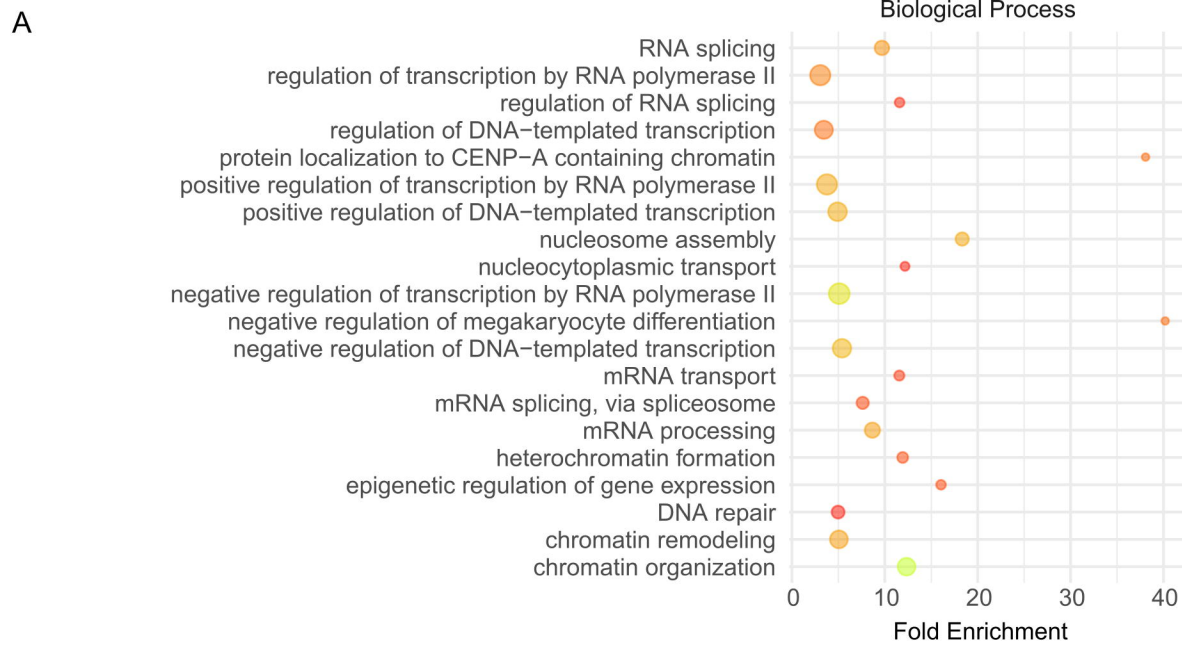
Biological Process
RNA splicing
regulation of transcription by RNA polymerase II
regulation of RNA splicing
regulation of DNA−templated transcription
protein localization to CENP−A containing chromatin
positive regulation of transcription by RNA polymerase II
positive regulation of DNA−templated transcription
nucleosome assembly
nucleocytoplasmic transport
negative regulation of transcription by RNA polymerase II
negative regulation of megakaryocyte differentiation
negative regulation of DNA−templated transcription
mRNA transport
mRNA splicing, via spliceosome
mRNA processing
heterochromatin formation
epigenetic regulation of gene expression
DNA repair
chromatin remodeling
chromatin organization
0
10
20
30
40
Fold Enrichment

B

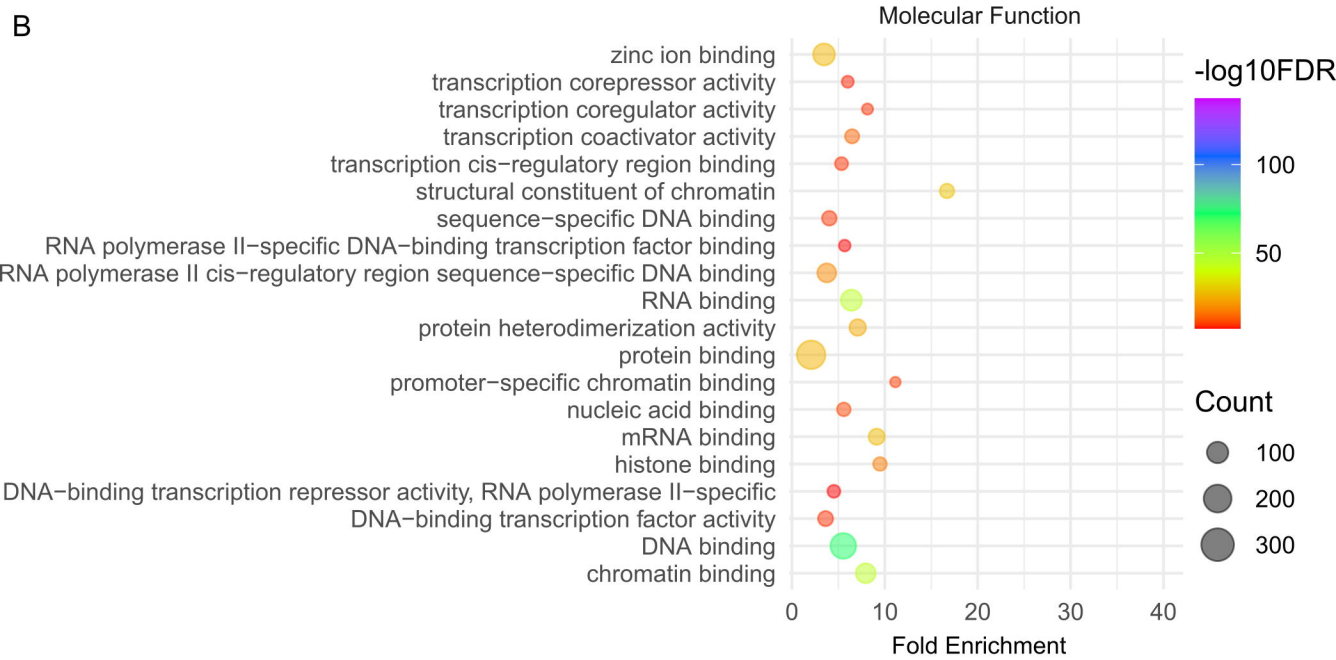
Molecular Function
zinc ion binding
transcription corepressor activity
transcription coregulator activity
transcription coactivator activity
transcription cis−regulatory region binding
structural constituent of chromatin
sequence−specific DNA binding
RNA polymerase II−specific DNA−binding transcription factor binding
RNA polymerase II cis−regulatory region sequence−specific DNA binding
RNA binding
protein heterodimerization activity
protein binding
promoter−specific chromatin binding
nucleic acid binding
mRNA binding
histone binding
DNA−binding transcription repressor activity, RNA polymerase II−specific
DNA−binding transcription factor activity
DNA binding
chromatin binding
0
10
20
30
40
Fold Enrichment
-log10FDR
100
50
Count
100
200
300

C

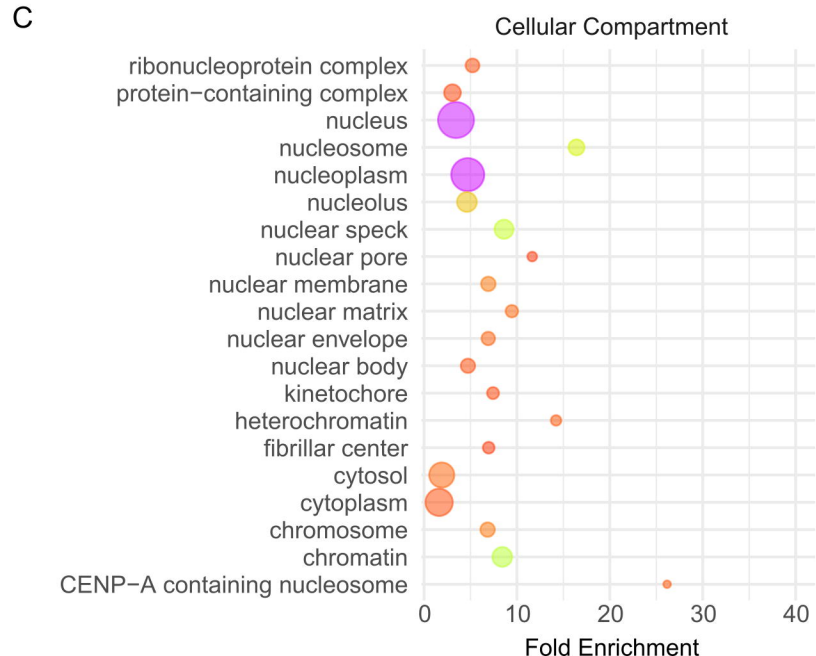
Cellular Compartment
ribonucleoprotein complex
protein−containing complex
nucleus
nucleosome
nucleoplasm
nucleolus
nuclear speck
nuclear pore
nuclear membrane
nuclear matrix
nuclear envelope
nuclear body
kinetochore
heterochromatin
fibrillar center
cytosol
cytoplasm
chromosome
chromatin
CENP−A containing nucleosome
0
10
20
30
40
Fold Enrichment

D

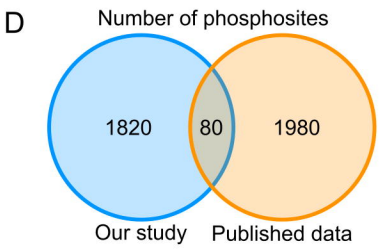
Number of phosphosites
1820
80
1980
Our study
Published data

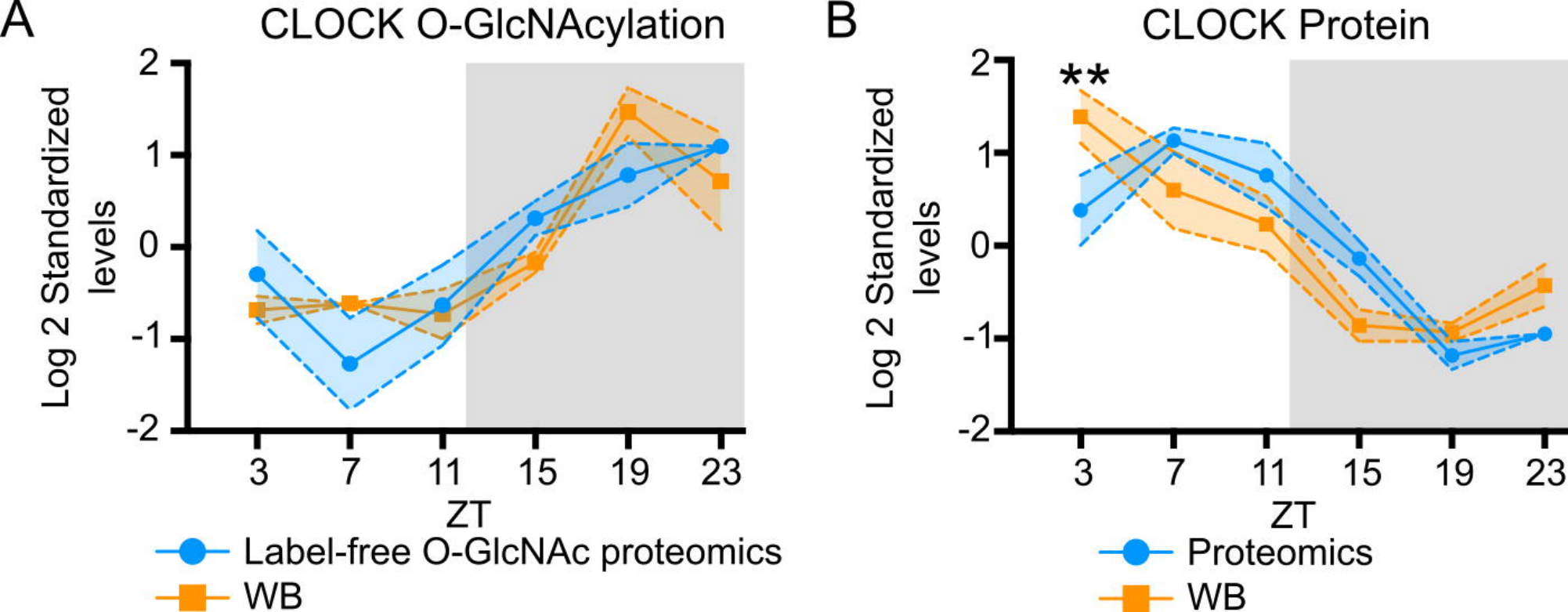
A
CLOCK O-GlcNAcylation
Log 2 Standardized levels
2
1
0
-1
-2
3
7
11
15
19
23
ZT
Label-free O-GlcNAc proteomics
WB
B
CLOCK Protein
**
Log 2 Standardized levels
2
1
0
-1
-2
3
7
11
15
19
23
ZT
Proteomics
WB

A

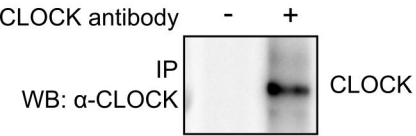
CLOCK antibody
-
+
IP
WB: α-CLOCK
CLOCK

B

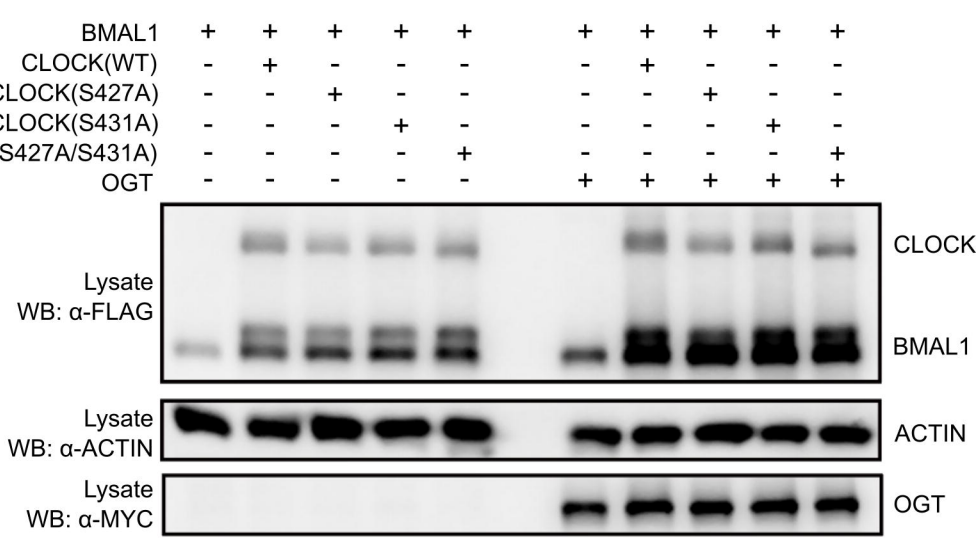
BMAL1 + + + + + + + + + +
CLOCK(WT) - + - - - - + - - -
CLOCK(S427A) - - + - - - - + - -
CLOCK(S431A) - - - + - - - - + -
CLOCK(S427A/S431A) - - - - + - - - - +
OGT - - - - - + + + + +
Lysate
WB: α-FLAG
CLOCK
BMAL1
Lysate
WB: α-ACTIN
ACTIN
Lysate
WB: α-MYC
OGT

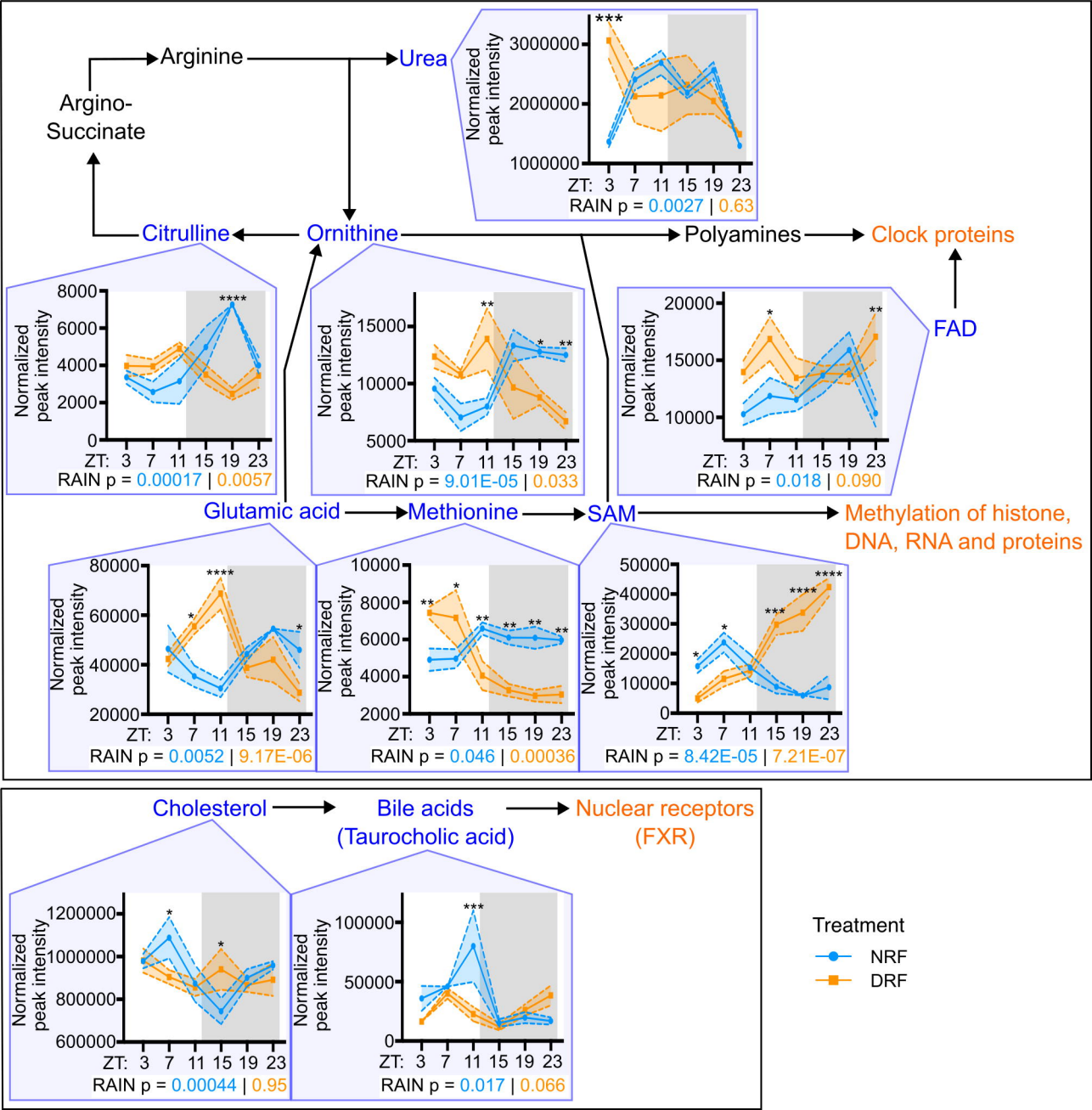
Argino-Succinate
Arginine
Urea
Citrulline
Ornithine
Polyamines
Clock proteins
FAD
Glutamic acid
Methionine
SAM
Methylation of histone, DNA, RNA and proteins
Cholesterol
Bile acids (Taurocholic acid)
Nuclear receptors (FXR)
Normalized peak intensity
ZT: 3 7 11 15 19 23
RAIN p = 0.0027 | 0.63
RAIN p = 0.00017 | 0.0057
RAIN p = 9.01E-05 | 0.033
RAIN p = 0.018 | 0.090
RAIN p = 0.0052 | 9.17E-06
RAIN p = 0.046 | 0.00036
RAIN p = 8.42E-05 | 7.21E-07
RAIN p = 0.00044 | 0.95
RAIN p = 0.017 | 0.066
Treatment
NRF
DRF